Geochronology of pallasite meteorites: First in situ Lu–Hf ages and Pu fission track methodology refinements

Thesis submitted in accordance with the requirements of the University of Adelaide for an Honours Degree in Geology

Thomas David Burke

October 2021

THE UNIVERSITY of ADELAIDE

GEOCHRONOLOGY OF PALLASITE METEORITES: FIRST IN-SITU LU-HF AGES AND PU FISSION TRACK METHODOLOGY REFINEMENTS

LU–HF AND PU FISSION TRACK PALLASITE GEOCHRONOLOGY

ABSTRACT

Pallasite meteorites are stony-iron meteorites that are generally accepted to have originated from the core-mantle boundary of a planetesimal. With only 141 pallasite meteorites discovered on Earth, it is uncertain if they were sourced from a single planetary body or multiple planetoids. Constraining absolute ages would aid our understanding of this, yet few have been determined. This is due to historical age methodologies involving time consuming, challenging analytical processes, that usually result in whole-rock ages and complete sample destruction. This study develops an analytical workflow using micro-X-ray fluorescence spectrometry, scanning electron microscopes, electron probe micro-analysis and Laser ablation inductively coupled plasma-mass spectrometry to identify and date phosphate minerals in pallasites. The main advantages of the approach are: (1) no destructive sample preparation requirements, (2) high spatial resolution, and (3) large quantities of data can be collected in a short time span. Using this workflow, the first *in situ* Lu–Hf ages and Pu fission track analyses for phosphate crystals in pallasites are presented. The Lu-Hf ages for Springwater (4564±91Ma) and Seymchan (4560±67Ma) pallasites are in good agreement with the timing of solar system formation. The presented Pu fission track data demonstrate the initial $^{244}Pu/^{238}U$ ratio used in published work (0.015) is flawed and a more appropriate minimum initial ratio of 0.019-0.029 was calculated for stanfieldite phosphates within Springwater, Sericho and NWA10023. These new methods have wide application to rapidly obtain age constraints for the formation and thermal evolution of not only pallasites, but potentially any phosphate-bearing meteorites, enabling new insights into the evolution of the solar system.

KEYWORDS

Geochronology, Lu–Hf, Pu fission-track, planetesimal, merrillite, stanfieldite

TABLE OF CONTENTS

LIST OF FIGURES AND TABLES

INTRODUCTION

Pallasite meteorites are stony-iron meteorites that represent some of the oldest known examples of planetary differentiation and provide an insight into the formational processes of the solar system (Buseck, 1977; Buseck and Holdsworth, 1977; Scott 1977). It has generally been accepted that the protolith to pallasites formed within the core-mantle boundary region of extinct planetary bodies (Figure 1) (e.g., Buseck, 1977; McKibbin et.al, 2019). Recent studies have highlighted number of formational mechanisms, including: (1) deep impact mixing, (Scott, 2007; Yang et. al., 2010), (2) quiet core-mantle boundary evolution, (Boesenberg et.al, 2012), or (3) surficial mixing, (Bryson et. al., 2015). These studies have led to further investigation of planetesimal formation processes, with suggestions that pallasite meteorites discovered on Earth, may have originated from several different parental bodies (e.g., Clayton and Mayeda 1996; Greenwood et. al., 2015).

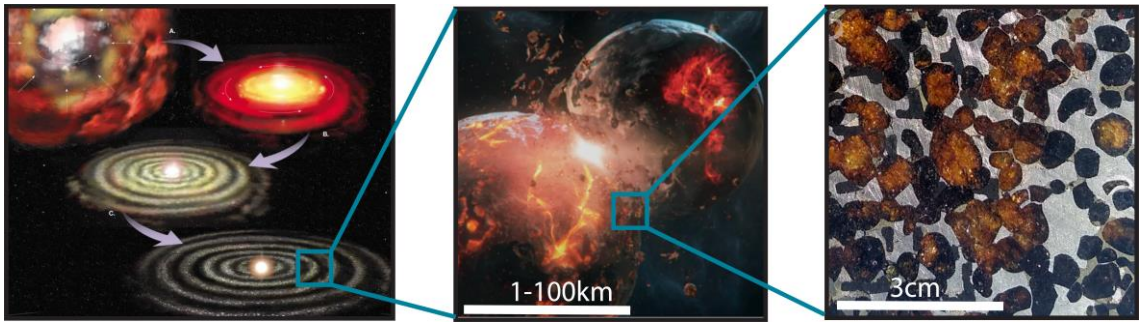

Figure 1 (a) artistic interpretation of early solar system accretion (University of Plymouth, Plymouth, UK, 2021), (b)artistic interpretation of early planetesimal extinction event (NASA/JPL-Caltech), (c)Example of polished Sericho pallasite meteorite rock slice from this study.

Time constraints on the formation and history of pallasites are severely limited, however. This is due to age determination of meteoritic samples usually requiring destructive, time consuming and, challenging analytical processes, such as (1) sample irradiation at a nuclear facility for ^{244}Pu fission track analysis (Bondar and Perelygin,

2001, 2003, 2005), or (2) whole-rock analysis techniques, such as calcium-aluminium-inclusion (CAI) formation ages determined through internal ^{182}Hf–^{182}W ratios (Markowski et. al., 2007; Homma et. al., 2019), or ^{26}Al–^{26}Mg deficit dating (Baker et. al., 2012). The ^{244}Pu fission track method additionally relies on several assumptions, such as the initial $^{244}Pu/^{238}U$ ratio of the solar system (Bondar & Perelygin, 2001, 2003, 2005). Furthermore, fission tracks can anneal at low temperatures, suggesting published ^{244}Pu fission track ages might be cooling ages or mixing ages between the time of formation and a subsequent thermal event. The ^{182}Hf–^{182}W and ^{26}Al–^{26}Mg methods use a combination of different pallasite samples (or other meteorites of their same respective classification) to constrain ages, assuming they all formed at the same time. In addition, latter methods are essentially short-decay systems that constrain the timing of pallasite protolith formation since the solar system formation.

Out of over 65,000 meteorites recognised by the International Society for Meteoritics and Planetary Science, only 141 are classified as pallasites (The Meteoritical Society, 2021). Hence, given the tiny pallasite archive on Earth, the development of analytical techniques for absolute age calculations that involve minimal sample destruction is clearly important. Furthermore, constraining age information for individual pallasites tests the hypothesis that individual pallasites on Earth were derived from different parental bodies (Mckibbin et. al., 2019) and that they may have independently experienced different thermal histories. In addition it potentially provides valuable constraints on models for the formation of pallasites in general. This includes any thermal perturbation they may have experienced throughout their histories such as shock metamorphism.

This study applies a novel approach using a recently developed *in situ* Lu–Hf dating method (Simpson et.al., 2021). In contrast to the methods above, radioactive decay from Lu to Hf has a long half-life (~37 billion years, Scherer et. al., 2001), allowing calculation of an absolute age rather than an age since solar system formation. The *in situ* approach affords the opportunity to (1) date individual pallasites, without solar system age assumptions, (2) significantly expand the geochronological archive for pallasites in a short timeframe, while (3) simultaneously maintaining textural integrity, as the method is minimally destructive compared to more traditional methods.

This work documents a time-efficient workflow for *in situ* Lu–Hf geochronology that targets pallasite phosphate minerals. The workflow incorporates phosphate mineral identification using a combination of micro-XRF, scanning electron microscope (SEM), and electron probe micro analysis (EPMA). Subsequently, appropriate phosphate phases are targeted using Laser Ablation Inductively Coupled Plasma-Mass Spectrometry (LA-ICP-MS/MS) for *in situ* Lu-Hf isotope analysis to rapidly determine absolute ages. In addition, this study develops a modified ^{244}Pu fission track analytical method, which involve direct *in situ* measurement of U concentrations. This study demonstrates the main assumption associated with the method, the initial ^{244}Pu–^{238}U ratio used in published work, is flawed, and uses acquired fission track data to produce more accurate initial ^{244}Pu–^{238}U ratios. These new methods have wide application to rapidly obtain ages in not only pallasites, but potentially any phosphate-bearing meteorites, and therefore expand the inventory of tools to explore the early evolution of the solar system.

BACKGROUND

Pallasite petrography and mineralogy

Pallasite petrography and geochemistry has been well studied. For recent reviews on petrological and geochemical data from pallasites, see Boesenberg et, al., (2012) and McKibbin et. al., (2019). These studies show pallasites are predominantly comprised of olivine crystals and Fe-Ni metals. However they also contain varying amounts of accessory phosphates, sulphides, phosphides, and chromites (e.g., Buseck, 1977; Boesenberg et. al, 2012; McKibbin et. al., 2019). The vast majority of pallasites have similarities in their petrography, geochemistry, and isotopic compositions. These are classified as "main group" pallasites (PMG; Wasson and Choi, 2003). However, as identified by Boesenberg et. al., (2012), this classification does not form a singular, coherent grouping and subsequent sub-groups of PMG have been suggested, which are differentiated by olivine composition: (1) "Low-MnO PMG", with MnO in olivine of less than ~0.25 wt%, (2) "common PMG" with MnO in olivine of ~0.30 wt%, (3) PMG-as with anomalous high FeO in silicate, and (4) "anomalous transitional" containing grains of common and Low-MnO PMGs, denoting transitional histories (McKibbin et. al., 2019). The Eagle-Station pallasite (PES) forms the basis of a second grouping of the same name, (Scott, 1977). The few remaining pallasites are classified into individual sample categories due to the lack of similarities with any other pallasites. This study focussed on samples obtained from the main group pallasites (table 1).

Phosphate minerals in pallasites are the only realistic reservoirs for Lu to provide an avenue for Lu-Hf geochronology, as well as the only transparent mineral that can be readily analysed for fission tracks to provide age data. Phosphate presence has been typified as peripheral to olivine, occurring along interstices, junctures and filling

narrow, parallel-walled veinlets between silicate minerals (Buseck and Holdsworth 1977). Buseck and Holdsworth (1977) strengthen this observation by suggesting the phosphates were likely still liquid after olivine crystallisation, and thus represent solidified droplets on the boundary of olivine grains with the metallic exposed sides acting as a meniscus. table 1 summarises phosphate occurrences across the samples in this study from literature. Phosphates occur as three main types in pallasites: (1) Merrilite, a high temperature refractory Ca-rich phosphate (Ando 1958), previously named whitlockite, with chemical composition ($Ca_9Na[Fe,Mg][PO_4]_7$; Mckibbin et. al., 2019), (2) stanfieldite, a Ca-Mg phosphate ($Ca_4[Mg,Fe]_5[PO_4]_6$; Mckibbin et. al., 2019) that also may occur as a solid solution (Fuchs, 1967), and (3) farringtonite, a Mg-rich endmember ($Mg_3[PO_4]_2$; Mckibbin et. al., 2019), and the least abundant of the three. Having only been identified in 8 pallasites (Fowler-Gerace et. al., 2013), farringtonite is volumetrically abundant (several vol%) in only 2 pallasites, Krasnojarsk and Springwater (Buseck and Clark 1984). Ando (1958) indicated that merrillite is a high-temperature refractory phosphate, whilst stanfieldite can crystalise through consumption of merrillite and Mg-rich phosphate melt. In addition, Ando (1958) suggested the eutectic of a Ca-Mg phosphate phase diagram lies between farringtonite and stanfieldite. This was furthered by Fuchs (1967) who suggested meteorites containing both Ca- and Mg- endmembers should be in disequilibrium hinting to a transitional formational history. Merrilite and stanfieldite have been typically reported to occur in contact of one another, however not all boundaries suggest merrillite consumption (Buseck and Holdsworth 1977).

Olivine itself has three distinct morphologies in pallasites, which are usually attributed to different formational environments (Buseck, 1977; Scott, 1977; Boesenberg et. al.,

2012; McKibbin et. al, 2019): (1) highly angular, irregular grains adjacent to each other described to be in "textural equilibrium" of up to 25mm diameter; (2) rounded euhedral grains of ~5-15mm in diameter that are partly isolated; and (3) highly angular fragmental grains of widely varying size formed through intragranular fracturing (table 1).

Table 1: Literature summary of PMG subgroupings with associated olivine textures, phosphate presence and age calculations

Sample	Grouping[a]	Olivine texture[a]	Phosphate presence[b]	Phosphate appearance[b]
Admire	Common-PMG	AF	Merrillite	50-1000μm grains
Albin	Common-PMG	F	Merrillite	100-500μm interstitial grains
Brahim	Low-MnO	ARF	Stanfieldite	_[d]
Brenham	Low-MnO	R	Merrillite	_[d]
			Stanfieldite	_[d]
			Farringtonite	_[d]
Esquel	Common-PMG	A	Merrillite	_[d]
Fukang	Common-PMG	AR	Merrillite	Grains up to mm size
Glorieta Mountain	Common-PMG	A	_[c]	_[d]
Huckitta	Common-PMG	F	_[d]	_[d]
Imilac	Common-PMG	AF	Stanfieldite	50 - 1000μm grains
			Merrillite	200 - 500μm grains with extensive fracturing
NWA 10023	_[d]	_[d]	Stanfieldite	_[d]
NWA 2957	_[d]	_[d]	_[c]	_[d]
Sericho	Low-MnO	AR	_[c]	_[d]
Seymchan	Anomalous Transitional	ARF	_[d]	_[d]
Springwater	PMG-as	R	Merrillite	30 x 100μm
			Stanfieldite	1000μm
			Farringtonite	Grains up to 1500μm

(a) PMG Grouping and Olivine textures are classified according to McKibbin et. al., (2019) where: A=Angular, R=Rounded, F=Fragmental

(b) Summary of identified phosphates data from: Buseck (1977); Buseck and Holdsworth (1977); Scott (1977b); Wasson and Choi (2003); Boesenberg et al. (2012); Boesenberg et al. (2018); Mckibbin et. al (2019); Chernonozhkin et. al., (2021)

(C) Not observed within studied samples

(d) No available literature

Additional to olivine and phosphates, the Ni-phosphide schreibersite, - ($[Fe,Ni]_3P$) is also common , usually encased within the metallic phase (McKibbin et. al., 2019). Opposed to other phosphates, which are closely linked to olivine petrogenesis, several studies (e.g., Clark and Goldstein 1978; Yoshikawa and Matseuda, 1992) suggest that

schreibersite is likely the result of exsolution from the metal phase at lower temperatures. The metallic phase within pallasites is considered to have considerable similarities to that of iron meteorites, consisting of kamacite and taenite intergrowths forming a widmanstätten lamellae texture (Buseck, 1977). The iron sulphide, Troilite (FeS), is also in abundances of several weight percent across all pallasites (e.g., Buseck 1977; McKibbin et. al., 2019). Chromite has been identified throughout most pallasite samples in scarce quantities of euhedral grains (~60um), however larger millimetre-sized grains have been noted within the Sericho PMG (Boesenberg et. al., 2018).

Pallasite geochronology

Historically, age determination of pallasites and other meteorites has generally revolved around the calculation of an age relative to calcium-aluminium-inclusion (CAI) ages (henceforth referred to as a 'post CAI age'). This assumption is based on the premise that CAIs are from the oldest dated soils from carbonaceous chondrites and are thus commonly accepted to define the age of the solar system (e.g., Amelin et. al., 2010; Connelly et. al., 2012). Homma et. al., (2019) calculated model ages of -0.30 ± 1.43 to 0.31 ± 1.74 Myrs after CAI formation for 4 main group pallasites (Imilac, Seymchan, Esquel, and Brahim). This was achieved through crushing and dissolution of the metal phases to determine ^{182}Hf–^{182}W ratios. Baker et. al., (2012) digested olivine grains to calculate ^{26}Al–^{26}Mg deficit model ages of 1.24 (+0.40, -0.28) Myrs after CAI formation from 4 pallasites (Admire, Brenham, Esquel and Molong). The ^{26}Al–^{26}Mg system also relies on the assumption of a uniform ^{26}Al distribution.

FISSION TRACK GEOCHRONOLOGY AND METHODOLOGY

An alternative age calculation involves ^{244}Pu fission track analysis. ^{244}Pu is extinct (half live ≈ 81.7 Myr; Fields et. al., 1966), however, fission tracks provide a fossil archive of radiometric ^{244}Pu decay during early solar system evolution. Hence, the relative proportion of ^{244}Pu fission tracks compared to ^{238}U fission tracks (= a long-lived decay system) can be used to calculate pallasite fission track ages. The application of this method has been well documented by Bondar and Perelygin (2001, 2003, 2005), reporting ^{244}Pu fission track ages for Brahim (4.6 ± 0.02Ga), Brenham (4.21 ± 0.02Ga), Krasnoyarsk (4.18 ± 0.03Ga), Marjalahti (4.37 ± 0.02Ga), and Omolon (4.37 ± 0.02 Ga). Fission track analysis requires experimental determination of fission track densities and ^{238}U concentrations in phosphates (Fleischer et. al., 1975), such as stanfieldite and merrillite (Buseck 1977). Traditionally, the ^{238}U concentration is determined via irradiation at a nuclear facility to stimulate ^{235}U fission (e.g., Bondar and Perelygin 2001A, 2001B, 2003, 2005). Using the resulting induced fission tracks, the ^{238}U concentration can be calculated, assuming natural ^{238}U/^{235}U abundance. However, this is a time-consuming process, and poor records of nuclear parameters such as irradiation time and total neutron flux, can lead to erroneous calculations, especially for very low U concentrations as those typically observed in meteorites (~1-100ppb) (Fleischer et. al., 1975; Chernonozhkin et. al., 2021).

There are 4 different sources that can contribute fission tracks: (1) iron group nuclei of galactic cosmic rays (GCR), (2) induced fission of heavy nuclei through the influence of cosmic ray bombardment (CRI), (3) spontaneous fission of ^{238}U, and (4) spontaneous fission of ^{244}Pu (Fleischer et. al., 1967). Heavy iron group nuclei of GCR contributions can be calculated by observing track densities in adjacent uranium-poor olivine grains

and this is identified as a negligible contribution to model age calculations (Bondar and Perelygin, 2000). The contribution of fission tracks from spontaneous fission of ^{238}U can be calculated using equation (1), which assumes the uranium concentration and sample age to be known (Kothari and Rajan 1982). Alternatively, a maximum contribution can be calculated if sample age is not known by using the maximum established solar system age of 4.6Ga (Pellas et. al., 1982).

$$\rho_{\mathrm{U}} = \frac{C_{\mathrm{U}} N_0}{A} \frac{R}{2} \frac{\lambda_{\mathrm{fU}}}{\lambda_{\mathrm{DU}}} d[\exp(\lambda_{\mathrm{DU}}\, t_0) - 1] \qquad (1)$$

Where $\rho_{U} = {}^{238}U$ fission track density, N_0 = Avagadro`s number, A = atomic wt (g), C_U = concentration of U (g), R = mean etchable ^{235}U fission track length (cm), d = density of studied sample (3.2 g/cm^3 for Stanfieldite), λ_{DU} = total decay constant of ^{238}U, and λ_{fU} = spontaneous fission decay constant of ^{238}U. Historically, ^{238}U concentration determination is done indirectly through irradiation in a nuclear reactor (Fleischer et. al., 1975). This methodology involves complete annealing of all natural fission tracks through heating above the assumed fission track retention temperature (500°C for 1 hour, Bondar and Perelygin, 2000), followed by inducing ^{235}U fission by applying a known thermal neutron dose from a thermal reactor. Induced ^{235}U tracks can then be counted, with a direct relationship proportional to U concentration (Fleischer et. al., 1975).

Contributions via induced fission of heavy nuclei through the influence of cosmic ray bombardment (CRI) is estimated by comparing the curve of the total cosmic-ray-

induced fission rate against the depth below the lunar surface (Damm et. al., 1978). This is shown in equation (2).

$$\rho_{\mathrm{cri}} = \frac{1}{2} N_v R T \cos m, \tag{2}$$

Where ρ_{CRI} = density of fission tracks due to cosmic ray bombardment, N_v = total cosmic ray induced fission rate, and T_{cos} = cosmic exposure age. Once the GCR and CRI contributions are known and subtracted from the observed total fission track density, the fission track age can be calculated by rearranging the relationship of track density with age in equation (3) (Durrani, 1981):

$$\frac{\rho_{\mathrm{f\,Pu}}}{\rho_{\mathrm{f\,U}}} = \frac{\lambda_{\mathrm{f\,Pu}}}{\lambda_{\mathrm{DPu}}} \frac{\lambda_{\mathrm{DU}}}{\lambda_{\mathrm{f\,U}}} \cdot \left(\frac{Pu}{U}\right)_0 \frac{\exp(-\lambda_{\mathrm{DPu}}\Delta t) - \exp(-\lambda_{\mathrm{DPu}} t_0)}{\exp(-\lambda_{\mathrm{DU}}\Delta t) - \exp(-\lambda_{\mathrm{DU}} t_0)}, \tag{3}$$

Where ρ_{Pu} and ρ_U are the observed fission track densities due to ^{244}Pu and ^{238}U decay respectively, $\lambda_{f\,Pu} = 1.06 \times 10^{-11}\ yr^{-1}$ (Jaffey et. al., 1971), $\lambda_{DPu} = 8.48 \times 10^{-9}\ yr^{-1}$ (Fields et. al., 1966), $\lambda_{f\,U} = 7.03 \times 10^{-17} yr^{-1}$ (Roberts et. al., 1968) and $\lambda_{DU} = 1 : 552 \times 10^{-10}\ yr^{-1}$ (Jaffey et. al., 1968) are the spontaneous decay constants of ^{244}Pu and ^{238}U; t_0 is the formational age of the sample; $\triangle t$ = is the time difference between formational age t_0 and cooling below track retention temperature; $(^{244}Pu/^{238}U)_0$ is the initial ratio of ^{244}Pu to ^{238}U at time, t_0. When $(^{244}Pu/^{238}U)_0$ and t_0 are treated as knowns, the above relationship can be rearranged into equation (4) (Green et. al., 1978), to determine the model fission track age.

$$\Delta t = 1.198 \times 10^8 \ln\left[\frac{5371}{\rho_{\mathrm{f\,Pu}}/\rho_{\mathrm{f\,U}}}(\mathrm{Pu/U})_0\right]. \tag{4}$$

The above method used by Bondar and Perelygin makes critical assumptions on (1) the solar system initial Pu/U ratio, $(^{244}Pu/^{238}U)_0$, (2) similarities between pallasite meteorites and lunar surface conditions for cosmic ray bombardment contributions, (3) the solar system formation age, and (4) the accuracy of obtained ^{238}U concentrations using indirect measurements. The $(^{244}Pu/^{238}U)_0$ value has the largest impact on the model fission track age, of which there is presently no consensus. Bondar and Perelygin (2000, 2001, 2003, 2005) use a value of 0.015 (Burnett, 1982), however experimental values ranging between 0.0060 and 0.113 have been reported (e.g., Burnett, 1982; Kuroda, 1991; Kuroda & Myers, 1992; Nakashima et. al., 2021), highlighting how poorly this parameter is constrained.

LU–HF GEOCHRONOLOGY AND METHODOLOGY

The Lu–Hf decay system has been extensively applied to garnet and to lesser extent to apatite systems (e.g., Vervoot, 2014; Bird et. al., 2013; Ibanez-Mejia et. al., 2018). We still have a limited understanding of Lu–Hf thermal robustness and derived ages may therefore represent the last thermal perturbation event in meteorites (e.g. impactor shock metamorphism) instead of formation age. This is still a valuable and highly applicable system however, as identification of differing pallasite thermal histories aids our understanding of their formation.

Conventional age determinations using the Lu–Hf analysis require time-consuming chemical separation process (Vervoot, 2014). Although the use of chemical separation enables high precision data, it lacks the ability to (1) readily obtain spatially precise data, (2) to acquire large datasets in a rapid timeframe, and (3) maintain sample integrity as it generally requires complete sample dissolution (Johnson et. al., 2015; Schmidt et. al., 2015). The application of an i*n situ* laser-ablation inductively-coupled-plasma mass-

spectrometry (LA-ICP-MS) approach has been hindered by the presence of isobaric interferences of ^{176}Lu and ^{176}Yb on ^{176}Hf (Zack and Hogmalm, 2015) within the plasma stream. However, Simpson et. al. (2021) developed a novel Lu–Hf method using LA-ICP-MS/MS, and two quadrupole mass analysers on either side of a reaction cell (Agilent, 2016) that can filter Lu from Hf. This novel method takes advantage of mass-filtering procedures to enable high-order reaction products of ^{176}Hf, ^{175}Lu and ^{178}Hf to be measured free from isobaric interferences. In this method, measured ^{175}Lu and ^{178}Hf are used as proxies for ^{176}Lu and ^{177}Hf, respectively. Consequently, isotopic ratios of ^{176}Hf/^{177}Hf and ^{176}Lu/^{177}Hf can be accurately determined, which are used to calculate absolute Lu-Hf ages (Simpson et. al., 2021).

METHODS

Pallasite Samples

14 main group pallasites were analysed as part of this study: Admire, Albin, Brahim, Brenham, Esquel, Fukang, Glorietta Mountain, Huckitta, Imilac, NWA 10023, NWA 2957, Sericho, Seymchan, and Springwater. Huckitta and Springwater samples were acquired from the Tate Museum at the University of Adelaide and Museum of Ontario respectively. The remainder were purchased from commercial meteorite dealers, with the assumption provided provenance claims are valid. Admire, Albin, Brahim, Esquel, Benham, Glorietta, Huckitta, Imilac, and Springwater samples were studied in both polished rock slices, as well as whole rock mounted epoxy discs, cut from the same rock slice. Samples of Fukang, Sericho, Seymchan, and NWA 10023 were studied in polished rock slices only.

Phosphate identification and sample selection

Phosphate grains are scarce (< 2 volume %) and range between 30-500μm in size. Phosphate target identification was completed in three stages (Figure 2). Firstly, qualitative elemental micro-X-ray fluorescence (Micro-XRF) maps were created of whole samples using a Bruker M4 Tornado micro-XRF spectrometer at Adelaide Microscopy. This was used as a reconnaissance tool to identify regions of high P. Analysis time per sample approximated 4 hours. Subsequent regions of interest were mapped via scanning electron microscopy (SEM) with mineral liberation analysis capability, to create refined qualitative high-resolution mineral maps of all phosphate regions. This was completed on either a FEI Quanta MLA-600 scanning electron microscope or a Hitachi SU3800 Automated Mineralogy Scanning Electron Microscope at Adelaide Microscopy. Each sample region approximated 1-4 hours analysis time. Electron probe micro analysis (EPMA) was conducted on a Wavelength Dispersive Spectrometers (WDS) with a CAMECA SXFive Electron Microprobe instrument to quantify elemental concentrations and identify the types of phosphates using stoichiometric abundances.

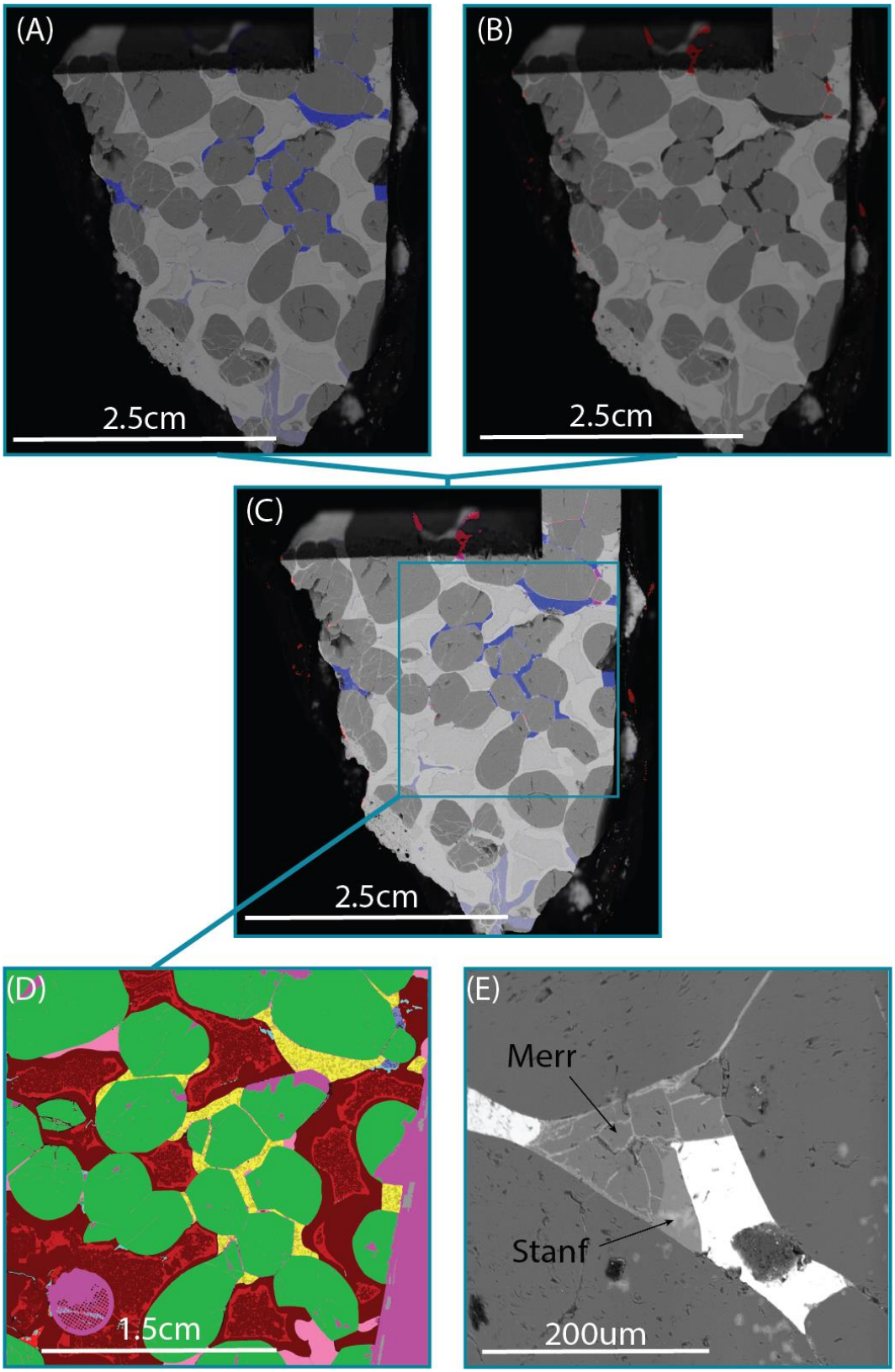

Figure 2 Phosphate identification workflow. (a)Micro-XRF image of Springwater rock slice with P in blue, (b)Micro-XRF image of Springwater rock slice with Ca in red. (c)Composite micro-XRF image of Springwater rock slice overlaying P(blue) with Ca(red) with subsequent SEM target region, (d) SEM AMICS map of Springwater with olivine (green), metallic matrix (reds), Farringtonite (yellow) and stanfieldite (blue), (e) EMPA image of Seymchan with merrillite (Merr) and stanfieldite (Stanf) interaction.

In-situ geochronology

LA-ICP-MS/MS

All phosphate grains were analysed via La-ICP-MS/MS to identify their Lu-Hf isotopic ratios. Analyses were conducted using a RESOlution 193 nm excimer laser ablation system with a S155 sample chamber, coupled to an Agilent 8900 ICP-MS/MS at Adelaide Microscopy, following analytical procedures by Simpson et. al. (2021). National Institute of Standards and Technology 610 (NIST610) glass was used as a primary standard (analysed every 10 unknowns), alongside Olympic Dam 306 (OD306) apatite as a secondary standard to correct for matrix-induced fractionation. 19589 Harts Range (19589-HR) and 215 Ødegårdens Verk (215-OV) apatite were additionally analysed for the purpose of accuracy confirmation. The pallasite phosphates were analysed in three separate sessions with method refinements occurring between sessions. To find the best possible sensitivity, a variety of spot sizes were used across sessions and phosphate minerals, as shown in Table 2. See appendix 2 for OD306 secondary standard corrections, and 19589-HR and 215-OV accuracy confirmations. Post-analysis data reduction was conducted using LADR software (Norris & Danyushevsky, 2018) to calculate background subtracted ratios and correct for instrument mass-bias and drift. OD306 analyses was processed a second time with the addition of a common Hf correction, as detailed by Simpson et. al. (2021). The Lu–Hf ratios were then corrected for matrix-induced fractionation against reference apatite OD306 (U-Pb age:1597±7; Thompson et. al., 2016). Subsequently, ISOPLOTR was used to plot isochrons and weighted mean ages (Vermeesch, 2018). As the samples are expected to originate from the initiation of the solar system, the literature value for the

bulk solar system initial (BSSI) 176Hf–177Hf ratio of 0.279781±0.000018 (Iizuka et. al., 2015) was used to anchor isochrons.

^{244}PU FISSION TRACK ANALYSIS

Merrillite and stanfieldite grains from samples of NWA10023, Sericho, and Springwater were etched for fission track dating. Each sample was etched for 50 seconds in 0.25% HNO3. When etching was completed, Stanfieldite grains were approaching a bulk etch state, whilst merrillite grains remained slightly under-etched. To maintain sample integrity, only stanfieldite grains were used for fission track analysis.

To enable track counting, the etched samples were imaged using a Hitachi SU3800 SEM, as well as optically using a Zeiss AXIO Imager M2m Autoscan System with a magnification of x1000. As rock slices and discs were used for analysis, only reflected light was useable for track observation and counting. SEM imagery was used as a reference for track confirmation. Fission tracks were manually counted within the TrackWorks fission track software (Melbourne University Fission Track Group, 2021) to determine fission track densities.

In contrast to previous studies, uranium concentrations were measured directly by LA-ICP-MS, using a RESOlution 193 nm excimer laser ablation system with a S155 sample chamber coupled to an Agilent 8900 ICP-MS/MS without the use of a reaction gas. Data reduction was conducted using LADR software (Norris and Danyushevsky, 2018), using NIST610 as primary standard to obtain trace element concentrations.

^{238}U concentration measurements in conjunction with fission track count data were used to calculate track source contributions from (1) iron group nuclei of galactic cosmic rays (GCR), (2) induced fission of heavy nuclei through cosmic ray bombardment, (3) from

spontaneous fission of ^{238}U, and (4) spontaneous fission of ^{244}Pu, following Bondar & Perelygin (2005). GCR influence was rendered negligible given the observations by Bondar & Perelygin (2005). The cosmic ray bombardment track density contribution was calculated as per equation (2), using a maximum exposure age of 178Ma (Reedy, 1982), and applied to each sample independently. Variance in cosmic exposure ages was later determined to be negligible to model age calculations. ^{238}U track contributions were calculated as per equation (1) using measured ^{238}U concentrations and a maximal t_0 of 4.56Ga. For samples with *in-situ* Lu-Hf ages calculated in this study, this age was substituted for their t_0. The ^{244}Pu fission track densities were then calculated as the difference of the total track densities and the sum of all other contributions (Bondar & Perelygin, 2005).

RESULTS

Phosphate identification

Micro-XRF and SEM imagery combined with EPMA identified the scarce isolated merrillite grains ranging 30-600μm in Admire, Albin, Fukang, Glorieta Mountain, Imilac and Huckitta, (figures 3-4). Fukang was only analysed by micro-XRF due to sample size limitations, and thus mineral identification was confirmed instead through LA-ICP-MS/MS (figure 4). Stanfieldite was identified as the most abundant in Springwater, Seymchan, Sericho and NWA10023, commonly appearing alongside merrillite in Seymchan and ranging 30-500μm in size (figures 2d,3-5). Stanfieldite was most abundant in junctures and filling veinlets between olivine grains that stretched for several millimetres. Farringtonite was identified only in Springwater epoxy mount, in

roughly equal abundance with stanfieldite (figure 2d,4f). Appendix 1 reports expanded micro-XRF, SEM and, EMPA imagery and data.

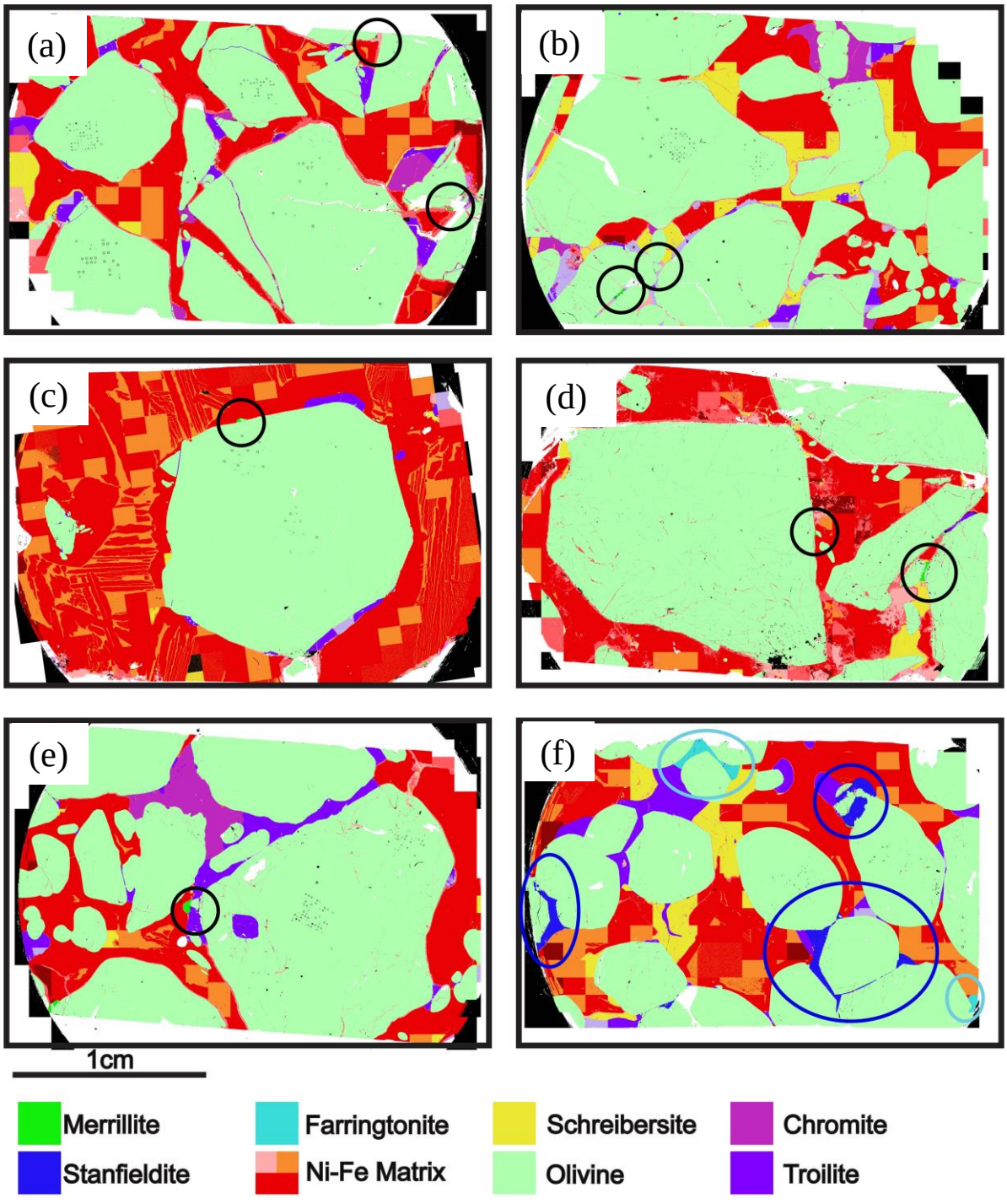

Figure 3: SEM MLA imagery of identified phosphate grains in mounted epoxy discs. Black circles note merrillite grains, dark blue denote stanfieldite and teal denotes farringtonite. (a)Admire, (b)Albin, (c)Glorieta Mountain, (d)Imilac, (e)Huckitta, (f)Springwater. See Appendix 1 for detailed imagery.

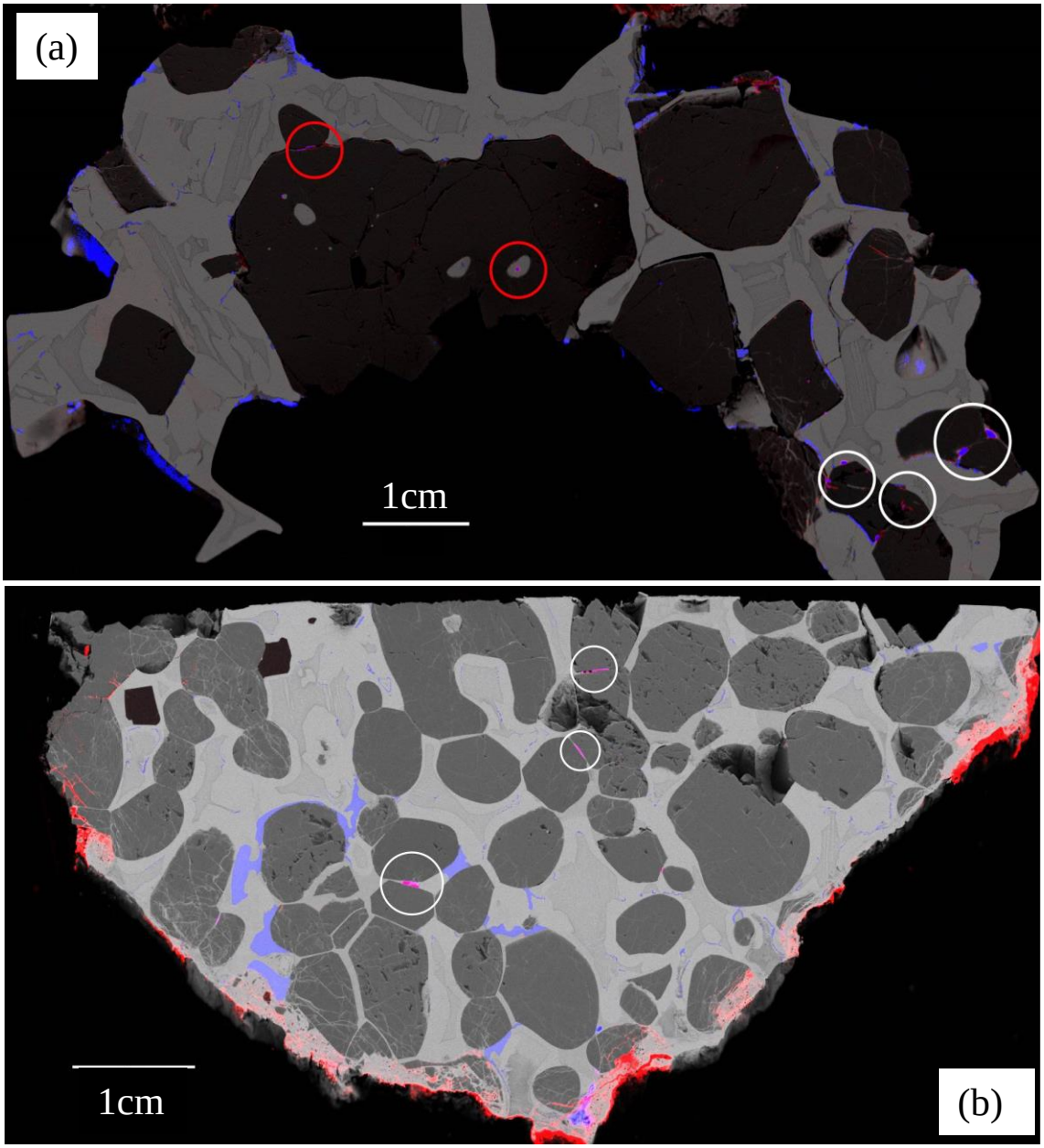

Figure 4 Composite micro-XRF imagery of phosphate identification in (a)Fukang and (b) Sericho. Blue = P, red = Ca, white circles represent later confirmed phosphate grains via LA-ICP-MS/MS, red circles represent false elemental overlap

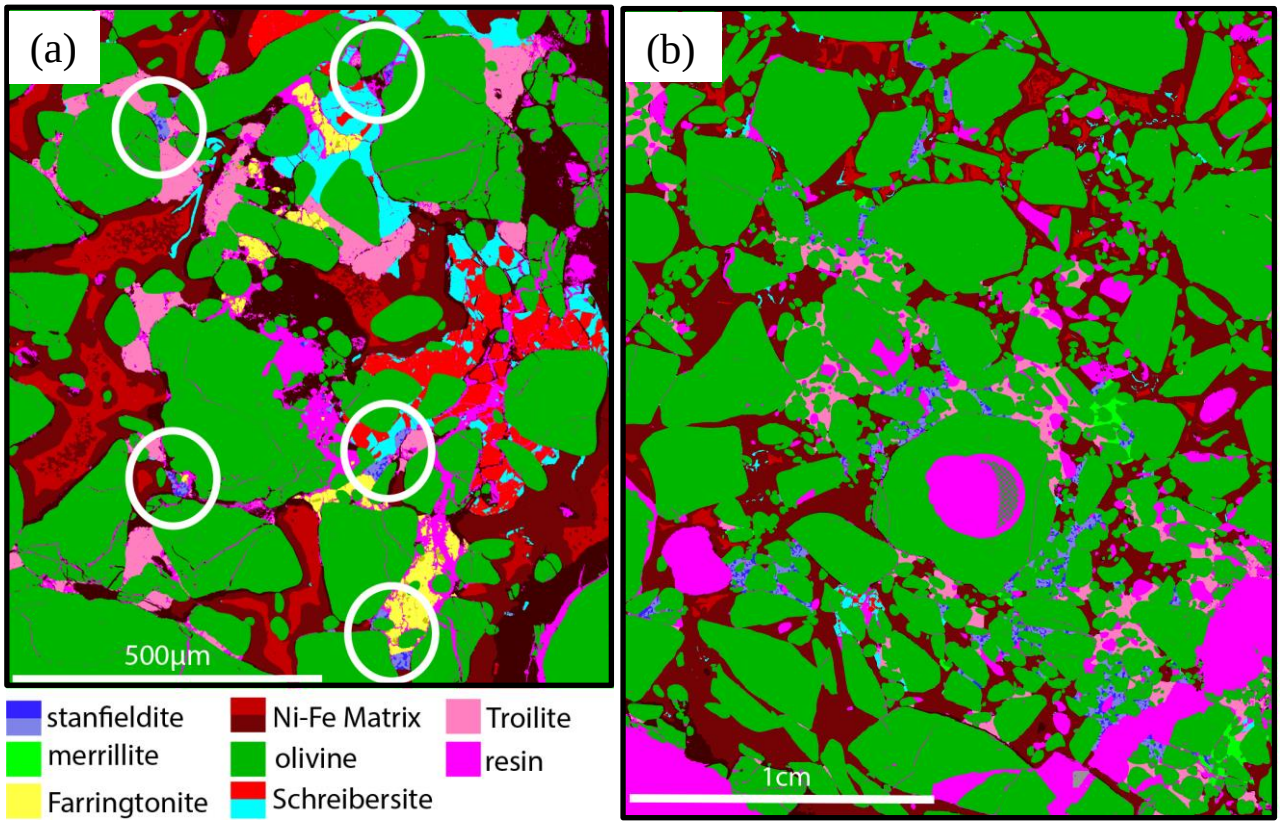

Figure 5 SEM AMICS imagery of identified phosphate regions of (a)NWA10023 and (b)Seymchan. White circles highlight isolated regions of phosphates within NWA10023, whilst Seymchan displays interconnected juncture formations of stanfieldite and merrillite.

Lu–Hf Geochronology

A total of 45 phosphate grains of >110μm in surface area were selected for analysis with LA-ICP-MS/MS. The limited amount of analysable phosphate only permitted statistically defendable Lu-Hf isochron regressions and associated Lu–Hf age calculations for NWA10023 (4374±327Ma), Seymchan (4560±67Ma) and Springwater (4564± 91) (Fig.7a,b,c). The remainder of the samples either only produced imprecise 2-point isochrons with the initial Hf anchor (Glorietta Mountain, Huckitta and, Imilac), had phosphates that could only be analysed with laser spot sizes too small to generate enough sensitivity for age calculations (Albin, Admire, Fukang), or didn't have large enough phosphate grains for laser targeting (Sericho). Table 2 summarises all age and LA-ICP-MS/MS data. See Appendix 3 for extended LA-ICP-MS/MS datasets and isochrons for Glorieta Mountain, Huckitta and Imilac and Fukang.

Table 2 In-situ Lu–Hf LA-ICP-MS/MS analysis summary and isochron age calculation. Merr refers to merrillite and stanf refers to stanfieldite analysis. Laser ablation spots and sizing are in micron by circular diameter. Isotopic ratio range and concentration reported from processed LA-ICP-MS/MS dataset of sessions 2 and 3 only using LADR processing software. Isotopic ratio range and concentration data reported within 10% uncertainty.

Sample	Minerals Analysed	No. Grains Analysed	Laser ablation spots and sizing						Age (Ma) 95% conf.	Isotopic ratio range				Isotopic concentration (ppm)		
			session 1		session 2		session 3			$^{176}Lu/^{177}Hf$		$^{176}Hf/^{177}Hf$		^{176}Hf	^{176}Lu	^{177}Hf
			Spots	Size	Spots	Size	Spots	Size		min	max	min	max			
High-quality Isochrons																
Seymchan	Merr	14	-	-	12	173µm	32	173µm	4560±67	0.88	4.60	0.35	0.73	0.062	0.66	0.033
	Stanf	14	-	-	20	257µm	12	257µm		0.71	2.74	0.34	0.55	0.037	0.3	0.024
Springwater	Stanf	5	7	110µm	6	257µm	27	257µm	4564± 91	38.23	81.74	3.73	8.57	0.008	0.175	0.00005
NWA10023	Stanf	4	-	-	6	173µm	-	-	4374±327	2.1	2.2	0.47	0.49	0.06	0.44	0.04
2-Point isochrons																
Glorietta	Merr	1	7	67µm	2	173µm	-	-	4609 ± 222	5.12	5.57	0.74	0.79	0.16	2.29	0.06
Huckitta	Merr	2	9	67µm	1	173µm	-	-	4798 ± 369	5.20	-	0.79		0.10	1.33	0.03
Imilac	Merr	1	25	67µm	6	173µm	-	-	4558 ± 160	2.1	2.18	0.47	0.49	0.22	1.90	0.13
Insufficient sensitivity																
Albin	Merr	3	7	67µm	-	-	-	-	4807 ± 1294	-	-	-	-	-	-	-
Admire	Merr	1	2	67µm	-	-	-	-	4606 ± 1580	-	-	-	-	-	-	-
Fukang	Merr	3	23	67µm	-	-	-	-	4698 ± 515	-	-	-	-	-	-	-

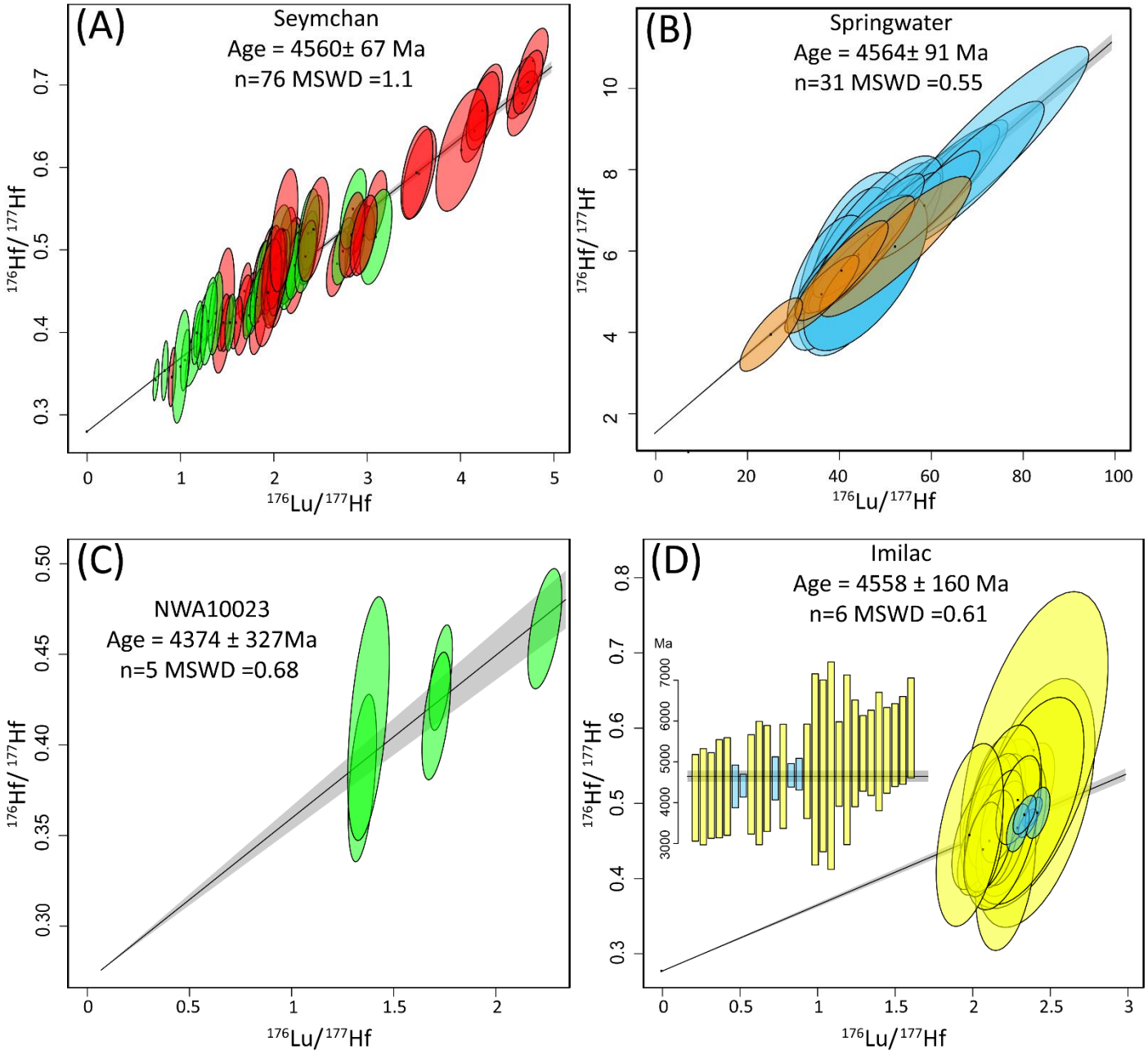

Figure 6 : Lu-Hf Isochrons for (a) Seymchan, (b)Springwater, (c) NWA10023, and (d) Imilac. All isochrons are anchored to the BSSI value of 0.279781 (Iizuka et. al., 2015). Red = merrillite, green = stanfieldite, yellow = analyses from session 1, blue = analyses from session 2 and orange = analyses from session 3. N= total number of analysis, MSWD = Mean square weighted deviation, denoting the goodness of fit. Values <1 show analytical uncertainties overestimated, >1 show analytical uncertainties underestimated, and values of 1 shows the data represents a univariate normal distribution. All uncertainty is reported at 2σ

Fission Track Analysis

Uranium concentration determinations and fission track imagery.

The first column denotes the average uranium concentration across all measured Stanfieldite grains for each sample with an average detection limit of 0.01ppb, achieved via LA-ICP-MS. Uncertainties for pooled data are reported as the standard error of the mean, calculated by dividing the standard deviation by the square root of the number of grains analysed. The second through fifth columns describe the total track densities from all possible sources: ρCRI = CRI track density, $\rho U = {}^{238}U$ fission track density, and $\rho Pu = {}^{244}Pu$ fission track density. Using equation (2), the maximal induced fission rate identified by Reedy (1981), $N_v = 2.2 \times 10^{-7}$ s^{-1} cm^{-3} and maximum cosmic exposure ages from Megrue (1968), $T_{cos\ m} = 178 \times 10^6$ yr, a ρ_{CR} value of 8.95×10^5 cm^2 was calculated. However, the curve of total cosmic-ray-induced fission rate against the depth below the lunar surface that equation (2) derives from assumes a uranium concentration of lunar proportions (~1000ppb). Therefore, this ratio was reduced by multiplying individual analysis by their ratio of experimentally determined ^{238}U to lunar ^{238}U concentration from each sample (U_{exp}/U_{lunar}). This resulted in ratios ranging from 0.002 and 0.014. Consequently, the mean track density due to CRI ranges between 3.3 - 5.1 x 10^3 cm^2 and was hence determined to be insignificant. Track densities attributed to fission of ^{238}U were calculated using equation (1) using the measured uranium concentrations with t_0 =4.56 Ga for NWA10023 and Sericho pallasites, and 4.53 Ga for Springwater. Fission track densities attributed to GCR are not reported, as they treated as negligible (Bondar and Perelygin, 2005). ^{244}Pu fission track density was calculated by subtracting all other sources from the total density. The sixth column denotes model fission track Δt ages, calculated from equation (4) for Springwater, Sericho and

NWA10023. The resulting pooled model fission track ages are -47.52±0.98, -80.05±3.96 and -28.05±1.28, respectively. Uncertainties were calculated using equation (5).

$$\delta(\Delta t) = \Delta t * \sqrt{(\frac{1}{\sum N_i}) + \delta(C_U)^2} \quad (5)$$

The seventh column rearranges equation (4) to instead solve for $(^{244}Pu/^{238}U)_{t0}$ using a near zero Δt (0.00001) calculating a minimum initial $^{244}Pu/^{238}U$ ratio, assuming no fission track age disturbance (i.e. no thermal annealing) after solar system formation. The uncertainty on this ratio was calculated using equation (6).

$$\delta(Pu/U)_0 = (Pu/U)_0 * \sqrt{(\frac{1}{\sum N_i}) + \delta(C_U)^2} \quad (6)$$

Table 3: Fossil track densities, uranium concentration, pallasite fission-track age and re-calculated initial Pu/U ratio.

Sample	grain	^{238}U (ppb ± 2σ)			Track Density (10^6 cm^{-2})				Δt (Ma ± 1σ)			(^{244}Pu/^{238}U)t_0 ± 1σ		
					ρtot	ρCR	ρU	ρPu						
Springwater	1	6.45	±	0.35	1.5460	0.0058	0.0213	1.5189	14.54	±	5.31	0.0133	±	0.0048
	2	8.50	±	0.40	1.8580	0.0076	0.0280	1.8223	25.76	±	10.51	0.0121	±	0.0049
	3	5.77	±	0.20	2.7048	0.0052	0.0190	2.6806	-66.94	±	13.72	0.0262	±	0.0054
	4	4.91	±	0.30	2.4764	0.0044	0.0162	2.4558	-75.81	±	22.89	0.0282	±	0.0085
	5	11.31	±	0.26	2.5691	0.0101	0.0373	2.5217	21.08	±	5.65	0.0126	±	0.0034
	6	6.54	±	0.19	3.1583	0.0059	0.0216	3.1308	-70.43	±	14.38	0.0270	±	0.0055
	7	10.53	±	0.25	2.8538	0.0094	0.0348	2.8096	-0.39	±	0.10	0.0150	±	0.0040
	8	8.76	±	0.29	2.5507	0.0078	0.0289	2.5140	-9.16	±	2.80	0.0162	±	0.0049
	9	4.73	±	0.15	2.2909	0.0042	0.0156	2.2711	-70.75	±	11.75	0.0271	±	0.0045
	10	6.00	±	0.34	2.2478	0.0054	0.0198	2.2227	-39.82	±	13.91	0.0209	±	0.0073
	11	4.25	±	0.26	2.3420	0.0038	0.0140	2.3242	-86.38	±	25.32	0.0308	±	0.0090
	12	2.78	±	0.31	2.7205	0.0025	0.0092	2.7088	-155.44	±	50.08	0.0549	±	0.0177
	13	3.31	±	0.27	2.2234	0.0030	0.0109	2.2095	-110.26	±	30.58	0.0377	±	0.0104
	14	6.20	±	0.22	2.2880	0.0055	0.0204	2.2620	-38.02	±	8.76	0.0206	±	0.0047
	15	4.55	±	0.26	2.2669	0.0041	0.0150	2.2479	-74.35	±	21.15	0.0279	±	0.0079
	16	3.60	±	0.40	1.7436	0.0032	0.0119	1.7285	-70.98	±	29.11	0.0271	±	0.0111
	17	3.93	±	0.28	2.5054	0.0035	0.0130	2.4890	-104.07	±	30.89	0.0358	±	0.0106
	18	6.30	±	0.26	1.9985	0.0056	0.0208	1.9720	-19.52	±	5.42	0.0177	±	0.0049
	19	4.83	±	0.33	1.6475	0.0043	0.0159	1.6272	-28.43	±	9.73	0.0190	±	0.0065
	20	4.99	±	0.37	2.3268	0.0045	0.0165	2.3058	-66.12	±	25.12	0.0260	±	0.0099
	Pooled	5.44	±	0.01	2.1743	0.0049	0.0180	2.1515	-47.52	±	0.98	0.0223	±	0.0005
Sericho	1	4.68	±	0.46	2.235	0.0042	0.0155	2.2154	-69.03	±	34.41	0.0267	±	0.0133
	2	4.23	±	0.46	2.017	0.0038	0.0140	1.9992	-68.89	±	33.45	0.0267	±	0.0129
	3	4.23	±	0.39	1.434	0.0038	0.0140	1.4162	-27.59	±	11.63	0.0189	±	0.0080
	4	4.21	±	0.39	2.072	0.0038	0.0139	2.0543	-72.68	±	29.57	0.0275	±	0.0112
	5	4.21	±	0.39	2.412	0.0038	0.0139	2.3943	-91.02	±	36.78	0.0321	±	0.0130
	6	3.68	±	0.29	1.91	0.0033	0.0122	1.8945	-79.02	±	24.52	0.0290	±	0.0090
	7	3.68	±	0.29	2.094	0.0033	0.0122	2.0785	-90.13	±	28.20	0.0318	±	0.0100
	8	3.23	±	0.26	2.423	0.0029	0.0107	2.4095	-123.61	±	36.00	0.0421	±	0.0123
	9	2.31	±	0.24	1.267	0.0021	0.0076	1.2573	-86.10	±	23.16	0.0308	±	0.0083
	10	2.31	±	0.24	1.872	0.0021	0.0076	1.8623	-133.17	±	37.22	0.0456	±	0.0127
	Pooled	3.68	±	0.03	1.9228	0.0033	0.0121	1.9074	-80.05	±	3.96	0.0293	±	0.0014
NWA10023	1	13.64	±	0.66	2.069	0.0122	0.0450	2.0118	70.60	±	47.15	0.0083	±	0.0056
	2	4.65	±	0.32	2.526	0.0042	0.0154	2.5065	-84.59	±	30.39	0.0304	±	0.0109
	3	3.38	±	0.27	1.994	0.0030	0.0111	1.9798	-94.81	±	27.71	0.0331	±	0.0097
	4	13.64	±	0.66	1.851	0.0122	0.0450	1.7938	84.34	±	56.31	0.0074	±	0.0050
	5	3.38	±	0.27	2.055	0.0030	0.0111	2.0408	-98.44	±	27.91	0.0341	±	0.0097
	6	5.16	±	0.30	1.95	0.0046	0.0170	1.9283	-40.69	±	13.44	0.0211	±	0.0070
	7	5.48	±	0.41	1.582	0.0049	0.0181	1.5590	-8.21	±	3.46	0.0161	±	0.0068
	8	5.48	±	0.41	1.606	0.0049	0.0181	1.5830	-10.04	±	4.19	0.0163	±	0.0068
	9	4.65	±	0.32	2.371	0.0042	0.0154	2.3515	-76.94	±	26.71	0.0285	±	0.0099
	10	3.38	±	0.27	2.13	0.0030	0.0111	2.1158	-102.77	±	30.44	0.0354	±	0.0105
	11	3.38	±	0.27	1.973	0.0030	0.0111	1.9588	-93.53	±	26.80	0.0327	±	0.0094
	12	3.38	±	0.27	1.729	0.0030	0.0111	1.7148	-77.59	±	22.42	0.0287	±	0.0083
	13	5.00	±	0.28	2.623	0.0045	0.0165	2.6020	-80.43	±	24.75	0.0294	±	0.0090
	Pooled	5.74	±	0.04	1.9517	0.0051	0.0189	1.9276	-28.05	±	1.28	0.0190	±	0.0009

DISCUSSION

Phosphate availability and sample representation

A comparison of tables 1 and 3 show a general consistency of phosphate availability between literature and this study. Although phosphates were not identified across all samples, it is a safe assumption that the remainder of their host meteorites do. The lack of identified phosphates is likely a by-product of available sample size for analysis (tables 2-3, figures 3-5). This has been discussed by numerous authors with Brahim, Brenham, and Esquel being examples with well documented phosphates (e.g., Buseck, 1977; Buseck and Holdsworth, 1977; Scott 1977; Mckibbin et. al., 2019), yet none were identified within this study. Similarly, Admire, Albin, Huckitta, Fukang, Glorieta Mountain, and Imilac have well documented phosphate abundance, yet the samples analysed in this study did not contain enough for robust age dating.

In-situ Lu–Hf age interpretations and discussion of the variation in Lu-Hf ratios

With absolute temporal information on pallasites being limited, as well as protoplanetary accretion suggested to have occurred over only a few million years (Baker et. al., 2012), it is difficult to resolve a robust pallasite history. Even with significant leaps of method refinement that rapidly increased precision between sessions as evidenced by figure 6d, due to the nature of already using 257μm laser spot sizes on stanfieldite, and 173μm spots on merrillite (table 2), it seems unlikely that sample precision can increase beyond the ~1.5-2%, obtained in this study. Additional observations of targetable phosphate scarcity often resulting in 2-point isochron ages

with greater uncertainty complicate this further (table 2). The Lu-Hf data for individual samples from this study do not reveal different pallasite histories that are distinguishable with the available analytical uncertainties and it is therefore not possible to robustly test this hypothesis.

This study, however, successfully dates several pallasite meteorites for the first time. The presented Lu-Hf ages, with <2% uncertainties, for Seymchan (4560±67Ma) and Springwater (4564±91) (Table 2) agree within uncertainty to the solar system formation ages of U-Pb in CAI's of 4567.3±0.16 Ma (Connelly et. al., 2012). These ages agree with the ~10Myr post solar system formation cooling ages suggested by Mn-Cr isotope closure systematics (Lugamair and Shukolyukov, 1998). Likewise, the initial differentiation of silicate within PMG and separation from aluminous melt is recorded to initiate ~1.24Myrs after solar system formation (Baker et. al., 2012).

Given the Lu-Hf data for individual samples from this study do not reveal independent pallasite histories, an assumption could be made that PMGs originated from the same parental body as suggested by Mckibbin et. al., (2019). If we agree with this suggestion, all obtained data could be used to produce a single Lu-Hf isochron for the PMGs. A combined isochron for the Lu-Hf data from Seymchan, NWA10023, Springwater, Huckitta, Glorieta Mountain and Imilac is presented in figure 7, which reveals a Lu-Hf age of 4560 ± 50Ma, with an MSWD of 1.00. Table 2 and figure 7 also illustrate that there are two distinct ranges of ^{176}Lu-^{177}Hf ratios, with the ratios in the Stanfieldite-dominated Springwater being roughly an order of magnitude greater compared to the other samples. This could be rationalised for Springwater by the exposure to a prolonged interaction between silicate and metal reservoirs, such as at genuine core-mantle boundary zones (McKibbin et. al., 2019). In agreement with McKibbin et. al.,

(2019), this prolonged interaction is evidenced in Springwater by its large, rounded olivine morphologies that are suggested to have been generated through silicate melt removal at peak temperatures. The larger presence of farringtonite supports this interpretation as it also reflects a primary metallic liquid phosphorus source being mineralized during back-reactions post-silicate melt removal (McKibbin et. al., 2019). Additionally, as LREE-MREE are incompatible in metal liquid-silicate liquid systems, preferentially going into the silicate liquid, it is assumed that HREE will behave in the same manner (Faure et. al., 2021). Therefore, although subsequent mineralization from a silicate melt removed system would be expected to be depleted in Lu relative to less evolved samples (as evidenced in Table 2). Remaining Lu reservoirs would therefore be concentrated within the silicate derived phosphate mineralisation, generating the larger ratios we observe.

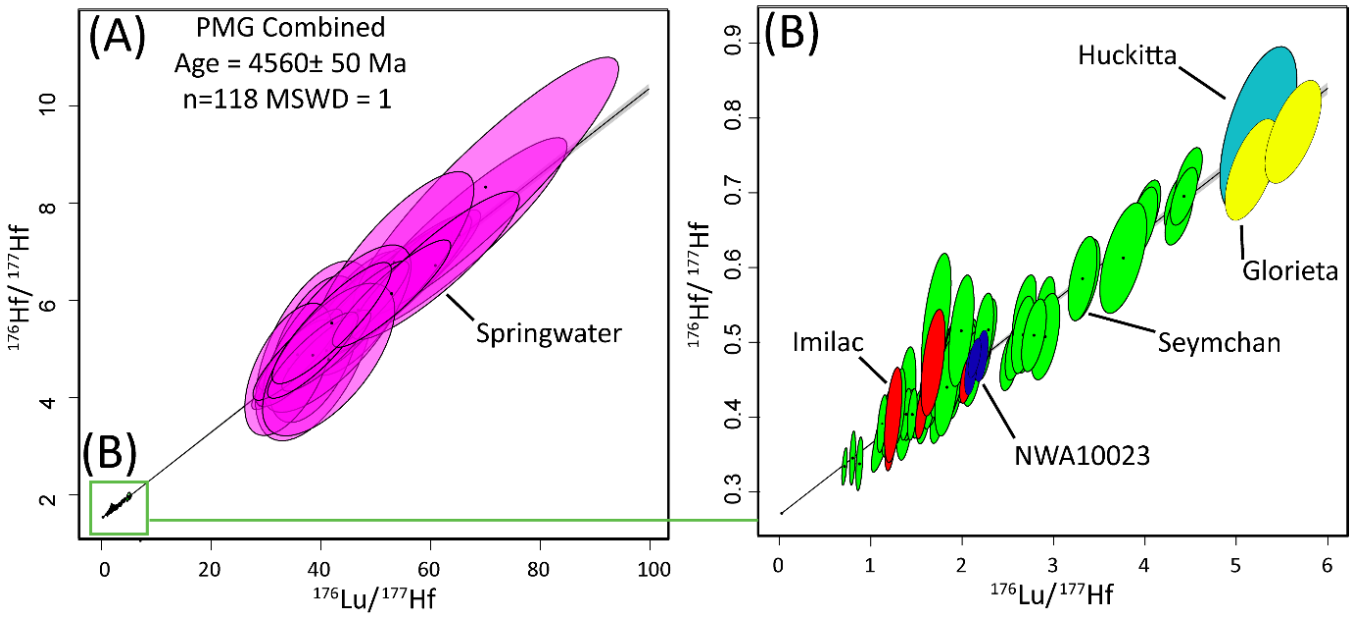

Figure 7: (a)Combined isochron of all data with (b) magnification of low ratio samples. N= total number of analysis included in calculation, MSWD = Mean square weighted deviation, denoting the goodness of fit. Values <1 show analytical uncertainties overestimated, >1 show analytical uncertainties underestimated, and values of 1 shows the data represents a univariate normal distribution. All uncertainty is reported at 2σ

This study shows Seymchan is the only other sample that shows significant variation in 176Lu–177Hf ratios between individual analyses (Table 2; Figure 7), producing one of the most precise Lu-Hf ages in this study. However, the lack of ^{176}Lu–^{177}Hf variations in other samples may be partly a consequence of phosphate scarcity. The heterogeneity in ^{176}Lu–^{177}Hf ratios between grains of Seymchan could be attributed to progressive stages of stanfieldite replacement of merrillite throughout. SEM imagery (figure 5) reveals that when merrillite and stanfieldite appears within the same sample, merrillite rarely does so without a textural relationship to stanfieldite, whilst stanfieldite occurs independent of merrillite (figures 3-5). As stanfieldite is the dominant phosphate mineral observed in Seymchan, lower overall ^{176}Lu–^{177}Hf ratios can be attributed to fractional crystallization of a primary silicate liquid source lower temperatures with a less evolved melt (McKibbin et. al., 2019).

Fission track interpretations and methodological revisions

As noted above, prior fission track studies revealed model ^{244}Pu fission track retention ages of ~4.16 – 4.60 Ga (Bondar and Perelygin, 2000, 2001, 2003, 2005). These fission track ages are consistent with post solar system formational ages (Connelly et. al., 2012) and interpreted as cooling ages associated with the last heat or shock event the pallasite samples experienced (Bondar and Perelygin, 2000, 2001, 2003, 2005). However, this work has revealed that several assumptions in the methodology applied in previous ^{244}Pu fission track studies by Bondar and Perelygin are inappropriate. As shown by Table 3, the Δt (= time since solar system formation) values obtained in this study yield incompatible mean negative ages of -25 to -80Ma. To reconcile this observation, the differences between the approach of Bondar and Perelygin (2000, 2001, 2003, 2005) and the method used in this study are summarized below.

Fleischer et. al., (1967) identified four track contributions in extra-terrestrial samples as noted prior. As both GCR and CRI are calculated in this study in the same manner as Bondar and Perelygin (2000, 2001, 2003, 2005), and contributions from the spontaneous decay of ^{244}Pu are calculated by a method of elimination (i.e., as the difference between total observed tracks and the combined total of other contributions), the GCR and CRI assumptions are exempt from immediate scrutiny. This leaves the contributions from the spontaneous decay of ^{238}U to be considered. Contributions via spontaneous decay of ^{238}U are calculated via equation (1), for which the ^{238}U concentration is the only variable (all other parameters are constants). Hence, differing methods for determining U concentration is the focus for comparison. As described above, , Bondar and Perelygin (2000) use the indirect method of sample irradiation in a nuclear reactor. The total neutron fluence received by the samples (expressed as the number of neutrons per cm^{-2} at a given time, Fleischer et. al., 1975) is a function of a number of parameters, including sample location within the reactor, combined with total exposure time. If these operating conditions are not controlled and quantified properly, induced fission tracks from ^{232}Th, or other nuclides could be created, leading to a statistically significant deviation from true ^{238}U concentration (Fleischer et. al., 1975). The exact irradiation parameters are not presented in previous ^{244}Pu fission track studies by Bondar and Perelygin (2000, 2001, 2003, 2005), and therefore, it is impossible to quantify the presence of such deviations. It is likely however, that to generate enough fission for a countable number of tracks in samples with low concentrations of U, either a long irradiation time (enabling fast neutron interactions) or position close to the reactor (stimulating ^{232}Th fission) would have been used. Therefore, a statistically

significant amount of induced ^{232}Th fission, or fast neutron interaction could have occurred during irradiation.

Fleischer (1975) observed that Th/U ratios within phosphates are also known to deviate considerably from the expected range of ~3.6-4. More generally, U and Th concentrations in pallasites are only scantly reported. Chernonozhkin et. al., (2021), presented a more comprehensive geochemical dataset of trace elements from *in situ* LA-ICP-MS analysis for stanfieldite and merrillite grains in the Brahin, CMS04071, Esquel, and Seymchan pallasites (summarised in Table 4). Table 4 shows Th/U ratios obtained by Chernonozhkin et. al., (2021) denote a clear, non-systematic deviation from expected ranges reported in Fleischer et. al. (1975). This observation suggests that pallasite U concentrations are more heterogeneous than initially reported. It further suggests that induced fission of ^{232}Th might indeed have caused a greater contribution to the total track counts than previously considered.

Conversely, this study has directly quantified ^{238}U concentrations through high precision *in situ* LA-ICP-MS analysis, obtaining sub-ppb uncertainties and detection limits, with comparable concentrations to that of Chernonozhkin et. al., (2021). Table 4 summarises and compares U concentrations from Bondar and Perelygin (2000, 2001, 2003, 2005), Chernonozhkin et. al (2021), and this study.

The mean U concentrations measured in this study as well as those observed by Chernonozhkin et. al (2021) are roughly an order of magnitude lower than those indirectly measured by Bondar and Perelygin (2000,2001,2003,2005). This discrepancy is attributed to a contribution of ^{232}Th fission to the total induced fission track count used for the indirect U concentration measurement approach. Further *in situ* LA-ICP-

MS analysis of U and Th of phosphates in pallasites however, would be required to strengthen this interpretation.

Table 4 Summary comparison of literature U concentration from Chernonozhkin et. al., (2021), Bondar and Perelygin (2000, 2001, 2003, 2005) and this study. Thermal neutron flux is reported for indirect radiation determination methods. Stanf represents stanfieldite, merr represents merrillite and farr represents farringtonite

Study					
Chernonozhkin et. al (2021)	**Th (ppb)[a]**	**U ppb[a]**		**Th/U ratio**	
Brahim (stanf)	1110	7		158.57	
CMS04071 (stanf)	3100	5		620.00	
	360	6		60.00	
	19	2		9.50	
Esquel (merr)	83	16		5.19	
	127	16		7.94	
	70	13		5.38	
	36	17		2.12	
	47	21		2.24	
	44	20		2.20	
	58	26		2.23	
Seymchan (merr)	43	31		1.39	
	41	11		3.73	
	430	4		107.50	
	450	6		75.00	
	580	6		96.67	
	171	13		13.15	
	240	5		48.00	
Bondar and Perelygin 2000, 2001 [b]	**U ppb (2σ)**				**Thermal Neutron Flux (cm^2)[c]**
Brahim (stanf)	98.00	±	13.00		$1.34x10^{17}$
Bondar and Perelygin 2003	**U ppb (1σ)**				**Thermal Neutron Flux (cm^2)[c]**
Marjalahti (merr)	51	±	8		
Brahin (stanf)	98	±	13		
Krasnoyarsk (farr)	22	±	5		10^{17} - 10^{18}
Omolon (stanf)	67	±	10		
Brenham (merr)	39	±	10		
Bondar and Perelygin 2005	**U ppb (1σ)**				**Thermal Neutron Flux (cm^2)[c]**
Marjalahti (merr)	50	±	7		$1.5x10^{16}$ - $1.8x10^{18}$
This Study	**U ppb (2σ)[d]**				
Springwater (stanf)	5.44	±	0.01		
Sericho (stanf)	3.68	±	0.03		
NWA10023 (stanf)	5.74	±	0.04		

(a)uncertainty reported as 3-20%

(b) The same dataset is used for U concentration determination across both studies

(c) reported uncertainty as ±10%

(d)mean analytical values displayed. See table 2 for detailed results

Another area for contention is the assumed initial Pu/U ratio, which is used as part of Δt calculation in equation (4). Bondar and Perelygin (2000, 2001, 2003, 2005) use a recommended ratio from a review by Pellas (1982) of 0.015, however there is no overarching consensus amongst researchers on this value. Based on the fission track data from this study, it is suggested that a value closer to 0.019-0.029 would be more appropriate as a minimum constraint (see table 3, where equation (4) was rearranged to solve for initial Pu/U ratio, assuming a Δt at the time of solar system formation). This value is in good agreement with theoretical computations by Schramm (1982), who investigated ratios of actinide isotope contents at the formation of the solar system.
The most probable reason for such a large variance in reported initial Pu/U ratios, is the process of chemical fractionation. In more detail, the heterogeneous solidification of elements throughout the thermal evolution of the solar systems formation (Krot et. al., 2014). I therefore suggest that a true initial Pu/U ratio of the solar system is more likely to resemble a value closer to 0.006, as derived from unfractionated chondritic CAIs (Fleischer et al., 1975). Evidence for chemical fractionation has been documented in St Severin chondrite meteorite, where a whole rock initial Pu/U ratio was calculated at 0.013, whilst for merrillite a ratio of 0.033 was obtained (Pellas et. al., 1979). Similarly, CAIs of Allende meteorite have been calculated at anomalously high initial ratio 0.087, further suggesting chemical fractionation. This highlights the requirement for mineral dependant initial Pu/U ratio to be constrained for a more robust age calculation.
The chemical fractionation and Pu enrichment in phosphates relative to U can be rationalised when taking fractional crystallization models for pallasites into account (Boesenberg et. al., 2012; McKibbin et. al., 2019; Chernonozhkin et. al., 2021). These show that Pu is enriched in Ca rich-phases relative to U (by up to a factor of 40;

Fleischer et. al., 1975), generating the observed highly anomalous ratios. This is caused by the high mobility of U within residual mineralisation of phosphate phases at their respective formational temperatures (e.g. merrillite at peak, involving silicate melt or subsequent eutectic formation of stanfieldite).

Taking chemical fractionation into account, the initial Pu/U ratio of 0.019-0.029, calculated in this study, can serve as a suitable minimum constraint for stanfieldite within pallasites which is in suitable agreement with the chemically fractionated merrillite in chondrites.

CONCLUSIONS

This study developed and applied an efficient workflow for phosphate identification and dating in pallasite meteorites. A total of two pallasites were, for the first time, dated in this study, using a newly developed rapid, *in situ*, minimally destructive approach, involving LA-ICP-MS/MS Lu–Hf geochronology (after Simpson et. al., 2021). Two pallasite samples were dated with statistically defendable analytical precision and uncertainties of <2% using this approach: Seymchan (4560±67Ma) and Springwater (4564± 91). These ages are consistent with post CAI solar system formational ages (4567.3±0.16; Connelly et. al., 2012). Due to similar age determination, analytical precision was insufficient to differentiate pallasite formational ages or thermal perturbation histories. Unless further evidence becomes available, a singular PMG parental body is suggested in alignment with recent advances in our understanding of pallasite petrogenesis from McKibbin et. al., (2019). The recent introduction of reaction-cell technology to multi-collector-inductively coupled plasma mass spectrometry (MC-ICPMS/MS) might pose an opportunity to shed new light on this hypothesis in the future.

Nonetheless, the analytical workflow of rapid identification through to minimally destructive *in situ* analysis has demonstrated its viability for widespread application of campaign-style analysis, catered to phosphate-bearing extra-terrestrial, or otherwise exceptionally finite material.

Fission track retention age determination was conducted on a further 3 pallasites: Springwater, Sericho, and NWA10023. Using previously published assumptions, the resulting ages are not feasible, calculating negative fission track cooling ages. From the observations made in this thesis, historical indirect U concentration measurements are likely too high estimates of the true U concentration by an order of magnitude.

Furthermore, the initial Pu/U ratio of the solar system is poorly understood due to chemical fractionation. Based on the data from this thesis, a value range of 0.019-0.029 is suggested as the minimum constraint for the initial Pu/U of stanfieldite in pallasites. This value differs from previous estimations, which are based on whole-rock data, likely due to the different partitioning properties of Pu relative to U during fractional crystallization of phosphate minerals.

In summary, with appropriate phosphate availability, absolute age dating using *in situ* Lu-Hf and/or fission track methods has the capability to improve our understanding of the evolution of the solar system, including the early differentiation process of parental bodies for PMGs.

ACKNOWLEDGMENTS

I would like to thank my supervisors, Stijn Glorie and Martin Hand for their support, guidance, patience throughout the entirety of 2021. I would also like to acknowledge Martin Hand for the provision of samples for analysis, along with the Tate museum and Museum of Ontario. Sarah Gilbert, Aoife McFadden, and Benjamin Wade along with the team at Adelaide Microscopy are also thanked for their expert guidance throughout the project. I acknowledge funding from the Institute of Mineral and Energy Resources that enabled the project to be carried out. I am grateful to the Geological Society of Australia and Playford Trust for their personal financial assistance that has allowed me to focus on my studies.

REFERENCES

AMELIN Y., et al. 2010 U–Pb chronology of the Solar System's oldest solids with variable 238U/235U, Earth and Planetary Science Letters, vol. 300, no. 3, pp. 343-350.
ANDO J. 1958 Phase Diagrams of Ca3(PO4)2-Mg3(PO4)2 and Ca3(PO4)2-CaNaPO4 Systems, Bulletin of the Chemical Society of Japan, vol. 31, no. 2, pp. 201-205.
BAKER J., SCHILLER M. & BIZZARRO M. 2012 26Al– 26Mg deficit dating ultramafic meteorites and silicate planetesimal differentiation in the early Solar System?, Geochimica Et Cosmochimica Acta - GEOCHIM COSMOCHIM ACTA, vol. 77.
BARNES C. A., et al. 1982 Essays in nuclear astrophysics: presented to William A. Fowler, on the occasion of his seventieth birthday. Cambridge University Press, Cambridge [Cambridgeshire] ;.
BIRD A. F., et al. 2013 Lu–Hf and Sm–Nd dating of metamorphic garnet: evidence for multiple accretion events during the Caledonian orogeny in Scotland, Journal of the Geological Society, vol. 170, no. 2, pp. 301-317.
BOESENBERG J. S., DELANEY J. S. & HEWINS R. H. 2012 A petrological and chemical reexamination of Main Group pallasite formation, Geochimica et Cosmochimica Acta, vol. 89, pp. 134-158.
BONDAR J. V. & PERELYGIN V. P. 2001 Cosmic history of the Bragin pallasite: evidence from the fission-track analysis, Radiation measurements, vol. 34, no. 1, pp. 391-396.
BONDAR Y. & PERELYGIN V. 2003 Cosmic history of some pallasites based on fossil track studies, Radiation Measurements - RADIAT MEAS, vol. 36, pp. 367-373.
BONDAR Y. V. & PERELYGIN V. P. 2001 Fission Track Age of the Brahin Pallasite, Solar system research, vol. 35, no. 4, pp. 299-306.
--- 2005 Fission-track analysis of meteorites: Dating of the Marjalahti pallasite, Radiation measurements, vol. 40, no. 2, pp. 522-527.
BRYSON J. F. J., et al. 2015 Long-lived magnetism from solidification-driven convection on the pallasite parent body, Nature, vol. 517, no. 7535, pp. 472-475.
BUSECK P. R. 1977 Pallasite meteorites—mineralogy, petrology and geochemistry, Geochimica et cosmochimica acta, vol. 41, no. 6, pp. 711,723-721,740.
BUSECK P. R. & CLARK J. 1984 Zaisho—a pallasite containing pyroxene and phosphoran olivine, Mineralogical Magazine, vol. 48, no. 347, pp. 229-235.
BUSECK P. R. & HOLDSWORTH E. 1977 Phosphate minerals in pallasite meteorites, Mineralogical Magazine, vol. 41, no. 317, pp. 91-102.
CHERNONOZHKIN S. M., et al. 2021 New constraints on the formation of main group pallasites derived from in situ trace element analysis and 2D mapping of olivine and phosphate, Chemical Geology, vol. 562, p. 119996.
CLARKE R. S. & GOLDSTEIN J. I. 1976 Schreibersite Growth and Its Influence on the Metallography of Coarse-Structured Iron Meteorites.
CLAYTON R. N. & MAYEDA T. K. 1996 Oxygen isotope studies of achondrites, Geochimica et Cosmochimica Acta, vol. 60, no. 11, pp. 1999-2017.
CONNELLY J. N., et al. 2012 The Absolute Chronology and Thermal Processing of Solids in the Solar Protoplanetary Disk, Science, vol. 338, no. 6107, pp. 651-655.

DAMM G., THIEL K. & HERR W. 1978 Cosmic-ray-induced fission of heavy nuclides: Possible influence on apparent 238U-fission track ages of extraterrestrial samples, Earth and planetary science letters, vol. 40, no. 3, pp. 439-444.
DURRANI S. A. 1981 Track Record in Meteorites, Proceedings of the Royal Society of London. Series A, Mathematical and physical sciences, vol. 374, no. 1757, pp. 239-251.
FLEISCHER R. L., PRICE P. B. & WALKER R. M. 1975 Nuclear tracks in solids : principles and applications. University of California Press, Berkeley.
FLEISCHER R. L., et al. 1967 Origins of fossil charged-particle tracks in meteorites, Journal of Geophysical Research (1896-1977), vol. 72, no. 1, pp. 331-353.
FOWLER-GERACE N. A. & TAIT K. T. 2015 Phosphoran olivine overgrowths: Implications for multiple impacts to the Main Group pallasite parent body, American Mineralogist, vol. 100, no. 10, pp. 2043-2052.
FUCHS LOUIS H. 1967 Stanfieldite: A New Phosphate Mineral from Stony-Iron Meteorites, Science, vol. 158, no. 3803, pp. 910-911.
GREEN P. F., BULL R. K. & DURRANI S. A. 1978 The fission track records of the Estherville, Nakhla and Odessa meteorites, Geochimica et cosmochimica acta, vol. 42, no. 9, pp. 1359-1366.
GREENWOOD R. C., et al. 2015 Geochemistry and oxygen isotope composition of main-group pallasites and olivine-rich clasts in mesosiderites: Implications for the “Great Dunite Shortage” and HED-mesosiderite connection, Geochimica et Cosmochimica Acta, vol. 169, pp. 115-136.
HOMMA Y., IIZUKA T. & ISHIKAWA A. 2019 Hf-W dating of main-group pallasites, Japan Geoscience Union.
HSU W. 2005 Mn-Cr systematics of pallasites, Geochemical Journal - GEOCHEM J, vol. 39, pp. 311-316.
IBANEZ-MEJIA M., BLOCH E. M. & VERVOORT J. D. 2018 Timescales of collisional metamorphism from Sm-Nd, Lu-Hf and U-Pb thermochronology: A case from the Proterozoic Putumayo Orogen of Amazonia, Geochimica et Cosmochimica Acta, vol. 235, pp. 103-126.
JAFFEY A. H., et al. 1971 Precision measurement of half-lives and specific activities of U235 and U238, Physical review. C, Nuclear physics, vol. 4, no. 5, pp. 1889-1906.
JOHNSON T. A., et al. 2018 Constraints on the timing and duration of orogenic events by combined Lu–Hf and Sm–Nd geochronology: An example from the Grenville orogeny, Earth and Planetary Science Letters, vol. 501, pp. 152-164.
KURODA P. K. 1992 Plutonium-244 in the early solar system and the Pre-Fermi natural reactor, Geochemical Journal, vol. 26, pp. 1-20.
KURODA P. K. & MYERS W. A. 1991 Plutonium-244 dating I. Initial ratio of plutonium to uranium in the allende meteorite, Journal of Radioanalytical and Nuclear Chemistry, vol. 150, no. 1, pp. 35-51.
MARKOWSKI A., et al. 2007 Hafnium–tungsten chronometry of angrites and the earliest evolution of planetary objects, Earth and Planetary Science Letters, vol. 262, no. 1, pp. 214-229.
MCKIBBIN S. J., et al. 2016 Rapid cooling of planetesimal core-mantle reaction zones from Mn-Cr isotopes in pallasites, Geochemical Perspectives Letters, vol. 2, pp. 68-77.
MCKIBBIN S. J., et al. 2019 Petrogenesis of main group pallasite meteorites based on relationships among texture, mineralogy, and geochemistry, Meteoritics & Planetary Science, vol. 54, no. 11, pp. 2814-2844.
METTA D., et al. 1966 Decay Properties of Plutonium-244, and Comments on its Existence in Nature, Nature (London), vol. 212, no. 5058, pp. 131-134.
PELLAS P., et al. 1979 PU-244/U-238 Ratios in Whitlockites of Ordinary Chondrites: a Possible Chronological Tool, Meteoritics, vol. 10 pp. 969-971.
PELLAS P., et al. 1983 Fission track age and cooling rate of the Marjalahti pallasite, Earth and planetary science letters, vol. 64, no. 3, pp. 319-326.
REEDY R. 1982 Cosmic-Ray Stable Nuclides: Various Production Rates and Their Implications, Proc. Lunar Planet. Sci., vol. 12, pp. 1809-1823.
ROBERTS J. H., GOLD R. & ARMANI R. J. 1968 Spontaneous-fission decay constant of U238, Physical review, vol. 174, no. 4, pp. 1482-1484.
SCHERER E., MÜNKER C. & MEZGER K. 2001 Calibration of the Lutetium-Hafnium Clock, Science, vol. 293, no. 5530, pp. 683-687.
--- 2001 Calibration of the Lutetium-Hafnium Clock, Science, vol. 293, no. 5530, pp. 683-687.
SCHMIDT A., et al. 2015 Lu–Hf geochronology on cm-sized garnets using microsampling: New constraints on garnet growth rates and duration of metamorphism during continental collision (Menderes Massif, Turkey), Earth and Planetary Science Letters, vol. 432, pp. 24-35.

SCOTT E. 2007 Impact Origin for Pallasites.
SCOTT E. R. D. 1977 Pallasites—metal composition, classification and relationships with iron meteorites, Geochimica et Cosmochimica Acta, vol. 41, no. 3, pp. 349-360.
SIMPSON A., et al. 2021 In-situ LuHf geochronology of garnet, apatite and xenotime by LA ICP MS/MS, Chemical Geology, vol. 577, p. 120299.
THOMPSON J., et al. 2016 Matrix effects in Pb/U measurements during LA-ICP-MS analysis of the mineral apatite, Journal of analytical atomic spectrometry, vol. 31, no. 6, pp. 1206-1215.
VERMEESCH P. 2018 IsoplotR: A free and open toolbox for geochronology, Geoscience Frontiers, vol. 9, no. 5, pp. 1479-1493.
VERVOORT J. 2013 Lu-Hf Dating: The Lu-Hf Isotope System. In RINK W. J. & THOMPSON J. eds. Encyclopedia of Scientific Dating Methods. pp. 1-20. Dordrecht: Springer Netherlands.
WASSON J. & CHOI B.-G. 2003 Main-group pallasites: Chemical composition, relationship to IIIAB irons, and origin, Geochimica et Cosmochimica Acta, vol. 67, pp. 3079-3096.
WEISBERG M. K., MCCOY T. J. & KROT A. N. 2006 Systematics and evaluation of meteorite classification. Univ. of Arizona Press.
YANG J., GOLDSTEIN J. I. & SCOTT E. R. D. 2010 Main-group pallasites: Thermal history, relationship to IIIAB irons, and origin, Geochimica et Cosmochimica Acta, vol. 74, no. 15, pp. 4471-4492.
YOSHIKAWA M. & MATSUEDA H. 1992 Texture, chemical composition and genesis of schreibersite in iron meteorite, Journal of the Faculty of Science, Hokkaido University, Series 4: Geology and mineralogy, vol. 23, no. 2, pp. 255-280.

APPENDIX 1: XRF IMAGERY AND EMPA RESULTS

Complete composite XRF imagery of rock slices. Blue = P, Red = Ca, Green = Ni.

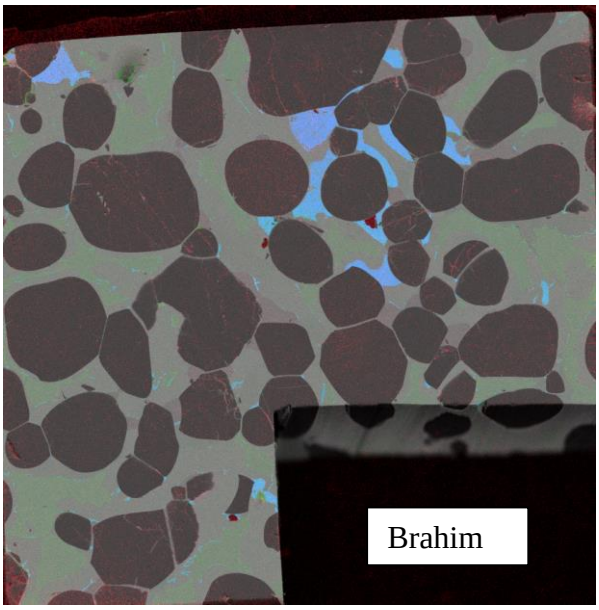

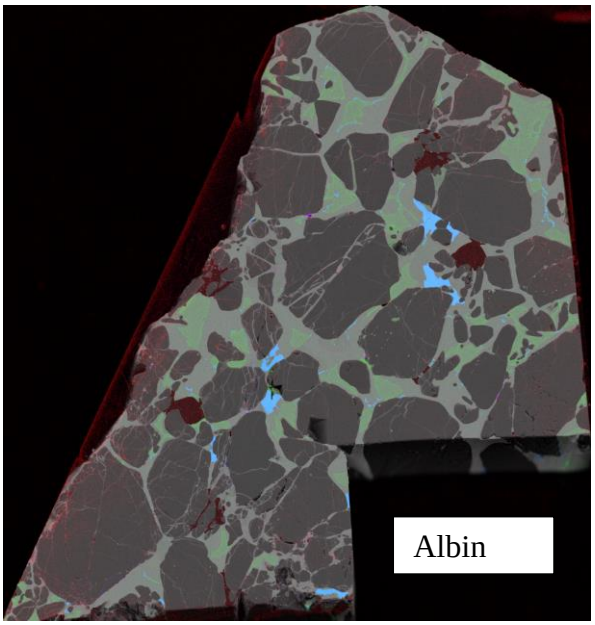

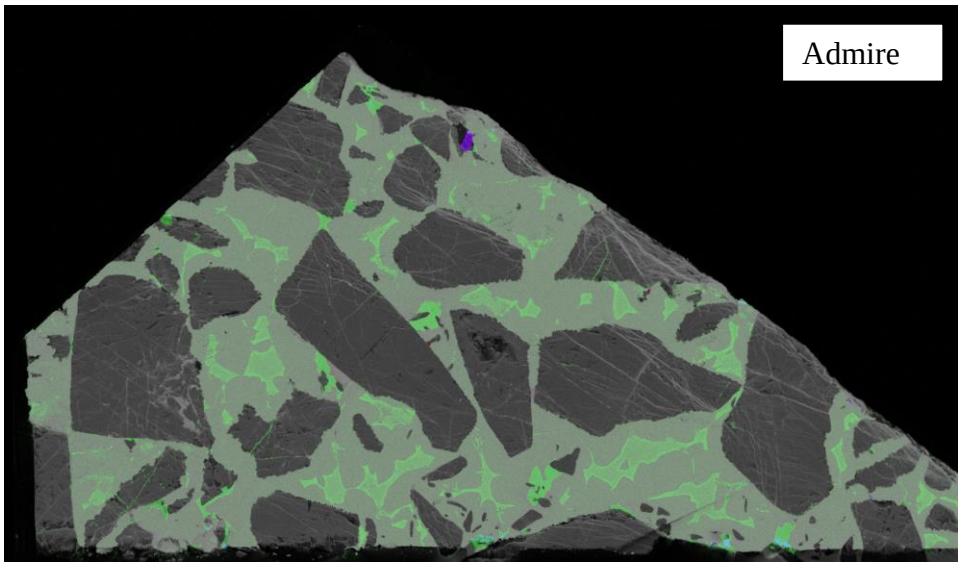

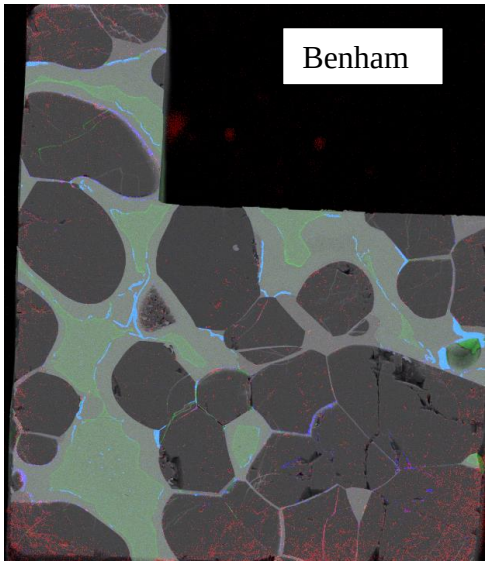
Benham

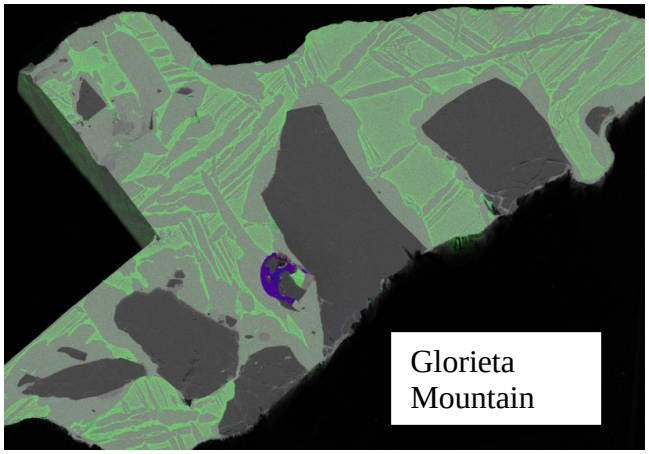
Glorieta
Mountain

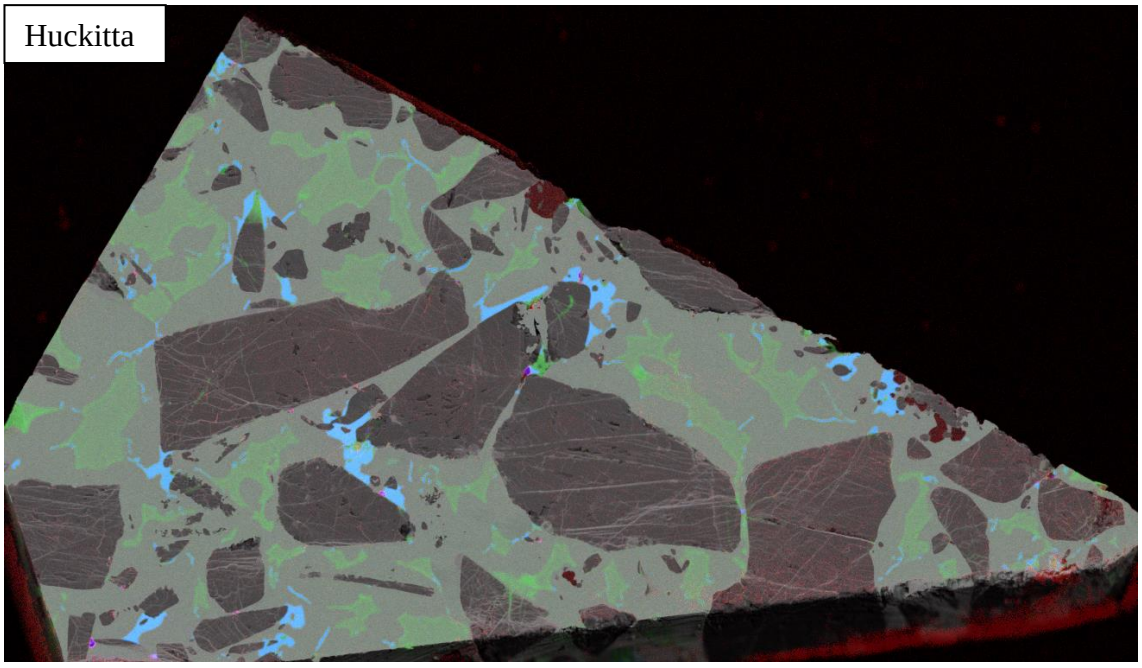
Huckitta

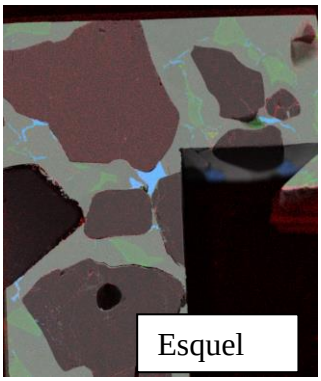
Esquel

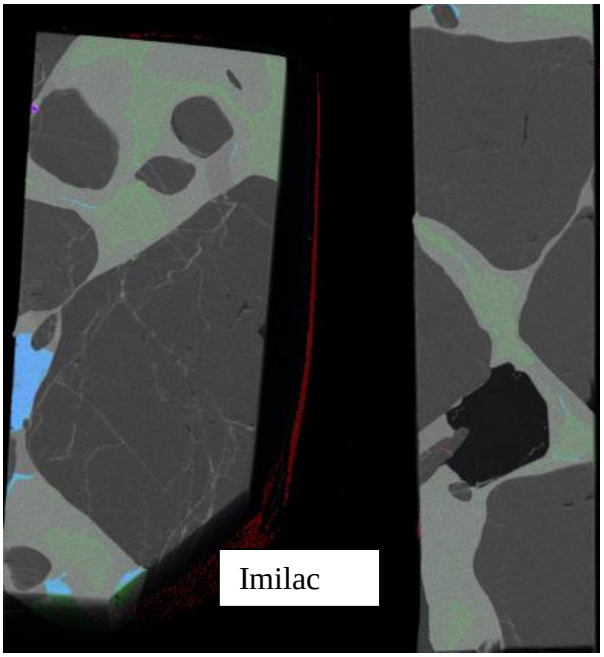
Imilac

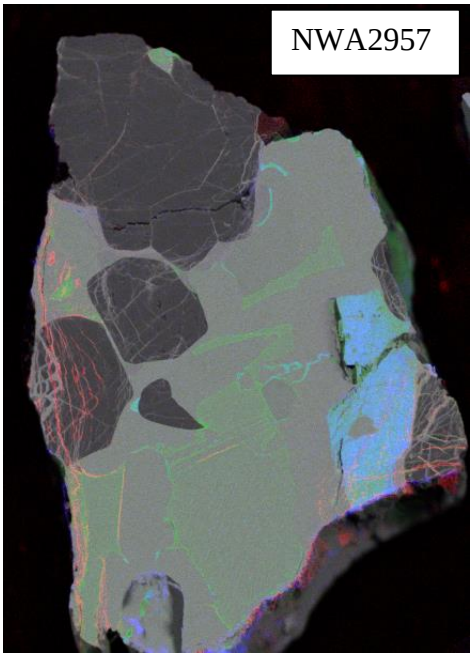
NWA2957

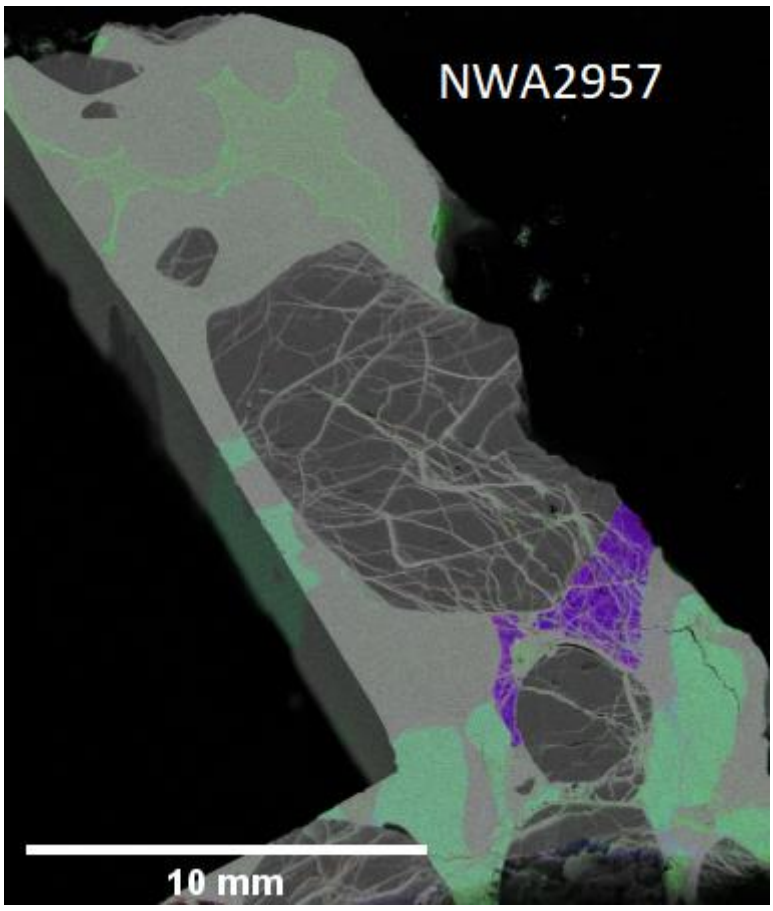
NWA2957
10 mm

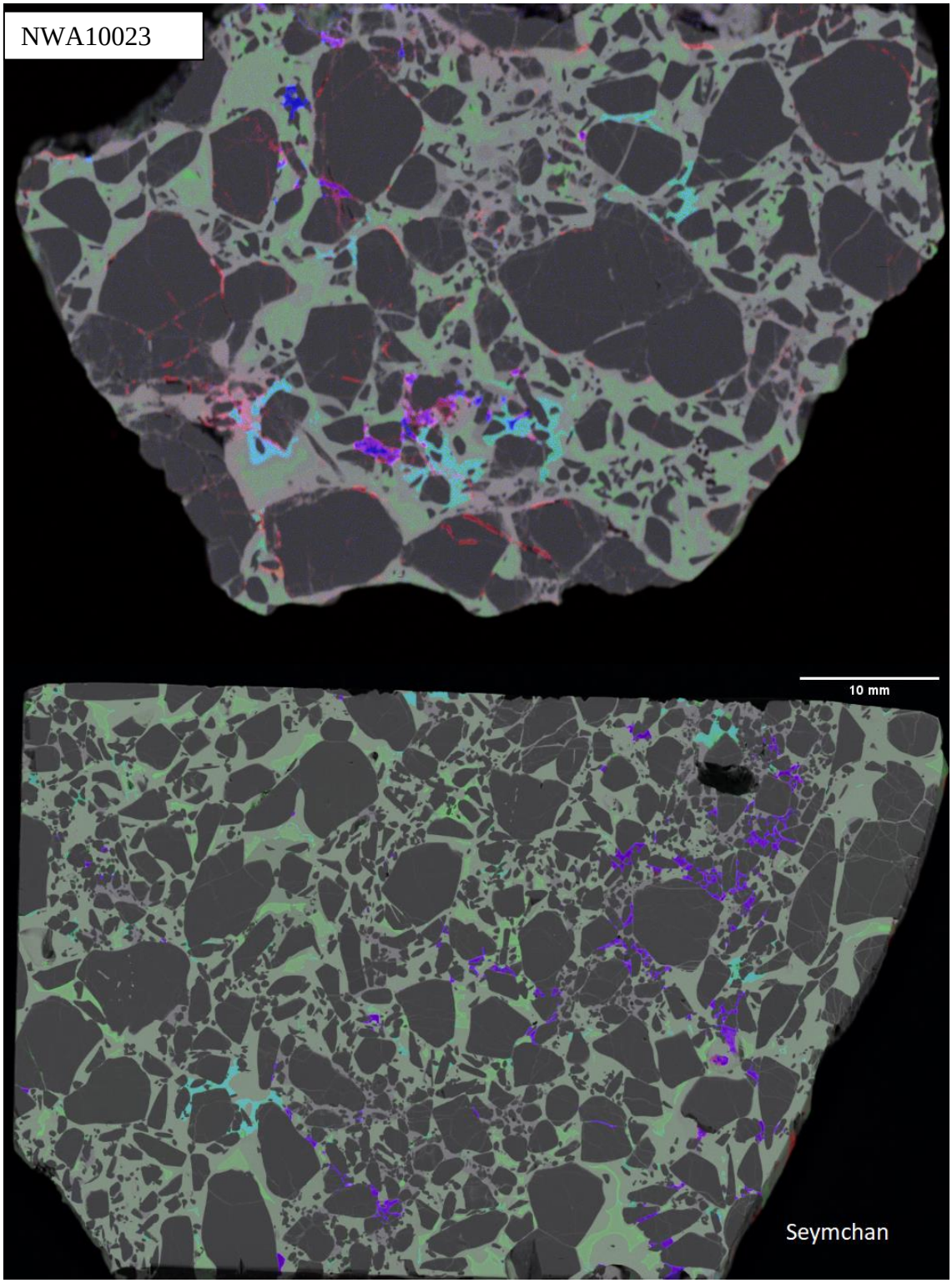
NWA10023
10 mm
Seymchan

EMPA session 1 elemental abundances

SAMPLE	Interpreted mineral	TOTAL	Cl	CaO	K2O	BaO	F	TiO2	P2O5	Na2O	SiO2
Sericho	Merrilite	100.302	0	46.3738	0.135895	0	0.062012	0	46.1418	2.56817	0.014007
Sericho	Olivine	100.999	0.005423	0.02962	0	0	0.041807	0	0	0.001448	39.8208
Sericho	stanfieldite	93.3575	0.014332	22.6886	0	0	0.063747	0	46.1065	0	0.00977
Sericho	stanfieldite	101.122	0.005831	26.0199	0	0	0.068944	0	49.5967	0.019898	0.00659
Sericho	stanfieldite	101.627	0.015165	26.1848	0	0.004184	0.034826	0	49.7685	0	0.01435
Sericho	stanfieldite	100.817	0.002579	25.9945	0	0.012898	0.080367	0	49.4329	0.018578	0
Sericho	stanfieldite	101.605	0	25.6033	0	0	0.065498	0	49.7716	0	0.009142
Sericho	stanfieldite	101.783	0.001058	25.6906	0	0	0.056133	0.003682	50.0192	0.021988	0.003059
Sericho	stanfieldite	99.9823	0.012853	25.8004	0	0	0.09011	0.003578	48.6686	0.004697	0.008904
Sericho	stanfieldite	101.249	0	25.4962	0	0	0.063613	0	49.489	0	0.014112
Sericho	stanfieldite	101.478	0.005243	26.2515	0.008372	0	0.05713	0	49.5418	0.003545	0.033706
Sericho	stanfieldite	100.05	0.028412	24.109	0	0	0.058024	0	47.9802	0.017599	0.043634
Sericho	Olivine	102.663	0.007189	0.002758	0	0.017928	0.045622	0	0	0.007302	41.1785
Unknowns											
Seymchan	Merrilite	99.2297	0.021719	48.3123	0.046097	0	0.086635	0	45.9928	0.544187	0.003212
Seymchan	Merrilite	99.8216	0.010672	48.2796	0.047947	0	0.074738	0	46.1028	0.538394	0.072256
Seymchan	Merrilite	98.7879	0.017198	47.5909	0.027676	0	0.112703	0	44.9951	0.52483	0.068717
Seymchan	Merrilite	100.532	0.015905	48.6318	0.028508	0	0.054122	0.0046	46.784	0.549636	0.025328
Seymchan	Merrilite	100.524	0.005802	48.5932	0.031853	0	0.013028	0.006091	46.6982	0.531496	0.023973
Seymchan	Merrilite	99.7923	0.000974	48.5349	0.030198	0	0.05334	0	45.9774	0.561339	0.046441
Seymchan	Merrilite	99.7709	0.007062	47.6335	0.033769	0	0.064008	0	46.5136	0.617452	0.094626
Seymchan	Merrilite	99.6633	0	48.3502	0.034032	0	0.074195	0	45.755	0.578805	0.011857
Seymchan	Merrilite	96.0704	0.026409	43.1221	0.064897	0	0.18265	0	41.218	0.490556	0.200388
Seymchan	Merrilite	100.484	0.005706	48.3888	0.024737	0	0.077627	0	46.4827	0.589099	0.02091
Seymchan	Merrilite	99.4844	0.004445	48.4085	0.028209	0	0.091993	0	46.2135	0.55316	0.00251

Seymchan	Merrilite	99.5565	0	48.7325	0.017026	0	0.053698	0	46.0218	0.55752	0.011295
Seymchan	Merrilite	99.5208	0.011956	48.4238	0.030218	0	0.079837	0	45.9998	0.561854	0.042576
Seymchan	Merrilite	99.0487	0.000458	48.1707	0.022013	0	0.056242	0	45.8281	0.540282	0.01867
Seymchan	Merrilite	99.1783	0.003445	48.2691	0.023597	0	0.090208	0	45.6467	0.522249	0.028779
Seymchan	Merrilite	99.245	0.011563	48.1368	0.022478	0	0.076419	0	45.9443	0.54918	0.020938
Seymchan	Merrilite	99.1106	0.015829	48.2608	0.034674	0	0.065924	0	45.7216	0.489872	0.017825
Seymchan	Merrilite	99.2367	0.009388	48.2711	0.053732	0	0.088719	0	45.7747	0.552645	0.054844
Seymchan	Merrilite	99.8396	0.000196	48.4908	0.015413	0	0.077897	0.003513	46.0681	0.571245	0.045948
Seymchan	Merrilite	98.9753	0.007029	48.1454	0.019164	0	0.055167	0	45.0952	0.40067	0.026804
Seymchan	Merrilite	99.8875	0.00579	48.1791	0.022912	0	0.069662	0	46.7442	0.593154	0.023235
Seymchan	Merrilite	99.6879	0	48.6199	0.035889	0	0.086416	0	46.0509	0.521603	0.0267
Seymchan	Merrilite	99.5084	0.009063	48.3018	0.035734	0	0.061275	0	46.1027	0.538979	0.01484
Seymchan	Merrilite	99.9181	0.002353	48.592	0.016115	0	0.082473	0	46.4521	0.569407	0.005066
Seymchan	Merrilite	99.6506	0.004394	48.5244	0.017511	0	0.057463	0	46.181	0.564752	0.003625
Seymchan	Merrilite	98.8952	0.007986	48.5766	0.029063	0	0.061758	0	45.4649	0.413861	0.01198
Seymchan	Merrilite	99.9833	0	48.8575	0.014235	0.009956	0.042129	0	46.1228	0.524692	0.021332
Seymchan	Merrilite	98.4578	0.024001	47.1274	0.068656	0	0.079734	0	44.9437	0.554476	0.192785
Seymchan	Merrilite	99.1643	0.004452	48.2624	0.013286	0	0.086903	0	45.9246	0.576036	0.020757
Seymchan	Merrilite	99.8313	0.0062	48.5873	0.030717	0.002473	0.088334	0.002901	46.3825	0.517223	0.016329
Seymchan	Merrilite	99.8232	0.005396	48.1071	0.011046	0	0.085516	0	46.7691	0.548021	0.032331
Seymchan	Merrilite	99.7765	0.007086	46.7477	0.058997	0	0.077087	0	45.6281	0.544841	0.061339
Seymchan	Merrilite	100.215	0	48.4165	0.018713	0	0.080601	0	46.3829	0.543515	0.053031
Seymchan	Merrilite	99.7774	0	48.3247	0.032752	0	0.114583	0	46.1469	0.56507	0.028145
Seymchan	Merrilite	99.0067	0.007867	48.283	0.031094	0	0.099783	0	46.1317	0.425771	0.014031
Seymchan	Merrilite	99.9337	0	48.3902	0.019324	0	0.071722	0	46.5524	0.576498	0.011944
Seymchan	Merrilite	99.8978	0	48.375	0.036935	0	0.10287	0	46.3123	0.516312	0.021989
Seymchan	Merrilite	100.002	0.005204	48.6296	0.014213	0	0.070229	0	46.3583	0.506532	0.005556
Seymchan	Olivine	99.9266	0.068869	0.016124	0.091243	0	0.056091	0.007492	0.021785	0.010872	39.5034

Seymchan	Olivine	100.545	0.017992	0.089056	0.040793	0	0.070399	0	0.092151	0.0295	40.3286
Seymchan	Olivine	101.118	0.018563	0.023184	0.022425	0	0.048895	0.003659	0	0.001123	40.8085
Seymchan	stanfieldite	100.958	0.103972	25.7573	0.159373	0	0.071789	0	49.5761	0.092185	0.084213
Seymchan	stanfieldite	100.897	0.009306	26.2786	0.006456	0	0.107472	0	49.5489	0.067699	0.042528
Seymchan	stanfieldite	100.086	0.00689	26.3857	0.010747	0	0.054548	0	48.9315	0.027548	0.032522
Seymchan	stanfieldite	100.308	0.003817	26.4222	0.010281	0	0.068165	0	49.3025	0	0.009224
Seymchan	stanfieldite	100.008	0.004219	26.3665	0.015753	0	0.078571	0	48.9353	0.011179	0.00706
Seymchan	stanfieldite	100.613	0.006079	26.2583	0.003228	0	0.087725	0	49.6513	0.015538	0.026417
Seymchan	stanfieldite	100.205	0.014854	26.5723	0.022835	0	0.075008	0	49.2412	0.028875	0.052052
Seymchan	stanfieldite	101.969	0.006595	26.4721	0.013282	0.006746	0.080866	0	50.0843	0.030777	0.042244
Seymchan	stanfieldite	101.013	0.010355	26.3826	0.016667	0	0.064015	0	49.3045	0.041695	0.023755
Seymchan	stanfieldite	99.8226	0.00643	26.3746	0.019474	0	0.056607	0	48.957	0.031707	0.026167
Seymchan	stanfieldite	100.771	0.007163	26.6757	0.004271	0.010848	0.097019	0	49.5675	0.019249	0.026298
Seymchan	stanfieldite	101.185	0	26.51	0.011759	0.007717	0.087756	0	49.8177	0.037948	0.033427
Seymchan	stanfieldite	100.664	0.002143	26.4695	0.012047	0	0.048354	0	49.0556	0.058365	0.021294
Seymchan	stanfieldite	100.761	0	26.5673	0.001661	0	0.055272	0	49.5597	0.022424	0.018523
Seymchan	stanfieldite	100.305	0.005528	26.4696	0.01067	0	0.055425	0	49.3072	0	0.040384
Seymchan	stanfieldite	100.061	0.000328	26.415	0.011943	0	0.080405	0	49.09	0.034875	0.033806
Seymchan	stanfieldite	99.8797	0.012225	26.2485	0.028853	0	0.085821	0	49.0328	0.037967	0.022152
Seymchan	stanfieldite	100.49	0.009645	26.3714	0.008386	0	0.073288	0	49.1941	0.047235	0.033869
Seymchan	stanfieldite	101.529	0.006084	26.2682	0.02216	0.00561	0.057468	0	49.9972	0.047854	0.023953
Seymchan	stanfieldite	100.823	0.02016	26.3488	0.015264	0	0.071775	0.007335	49.534	0.026724	0.022267
Seymchan	stanfieldite	100.78	0.004801	26.4021	0.009764	0	0.081532	0	49.4217	0.015657	0.019394
Seymchan	stanfieldite	101.045	0.00297	26.2249	0.019092	0	0.07307	0.001506	49.6747	0.035714	0.032551
Seymchan	stanfieldite	100.756	0.004778	26.3445	0.013187	0	0.059158	0	49.538	0.033937	0.043653
Seymchan	stanfieldite	101.317	0.006589	26.2376	0.015579	0	0.066235	0	49.9502	0.036958	0.055601
Seymchan	stanfieldite	101.75	0.003908	26.6192	0.012286	0	0.074934	0.005542	49.6677	0.017645	0.020403
Seymchan	stanfieldite	101.41	0.00486	26.5263	0.026749	0	0.067299	0	49.9333	0.017818	0.037406

Seymchan	stanfieldite	100.535	0.002091	26.4396	0.012185	0	0.097267	0	49.1656	0.051126	0.042709
Seymchan	stanfieldite	101.139	0.03563	26.4521	0.066933	0	0.045801	0	49.5107	0.089	0.064902
Seymchan	stanfieldite	99.9483	0	26.5031	0.012667	0.016066	0.08276	0	49.0491	0.017457	0.018439
Seymchan	stanfieldite	101.12	0.001245	26.5395	0.025421	0	0.086018	0	49.3959	0.031987	0.044713
Seymchan	stanfieldite	100.607	0.003368	26.4942	0.010961	0	0.064328	0	49.2059	0.040886	0.036407
Seymchan	stanfieldite	100.04	0.039713	26.0961	0.07218	0	0.119882	0.000853	49.0617	0.08145	0.056856
Seymchan	stanfieldite	100.759	0	26.4312	0.012016	0	0.068367	0	49.4434	0.004412	0.045843
Seymchan	stanfieldite	100.456	0.03015	26.2102	0.087811	0	0.092131	0	49.0053	0.139643	0.098839
Seymchan	stanfieldite	100.357	0.272582	26.1593	0.359591	0	0.089482	0	48.9248	0.038462	0.010255
Seymchan	stanfieldite	100.601	0.043288	26.3348	0.027535	0	0.079275	0	49.2273	0.064237	0.031057
Seymchan	stanfieldite	100.315	0.00415	26.2738	0.016092	0.001703	0.097945	0	49.1626	0.018341	0.026339
Seymchan	stanfieldite	100.853	0.009469	26.2844	0.020564	0	0.06608	0	49.548	0.033699	0.028719
Seymchan	stanfieldite	101.125	0	26.3915	0.022091	0	0.058587	0	49.4924	0.023696	0.036175
Seymchan	stanfieldite	100.27	0.004328	26.1645	0.016872	0	0.042518	0	49.0978	0.030949	0.014547
Seymchan	stanfieldite	100.292	0.00765	26.2556	0.012625	0	0.051317	0	49.1113	0.016276	0.03984
Seymchan	stanfieldite	99.7806	0.010823	26.1425	0.008171	0	0.063995	0	49.0218	0.035888	0.052321
Seymchan	stanfieldite	101.313	0	26.4289	0.038304	0	0.063469	0	49.8728	0.040067	0.028607
Seymchan	stanfieldite	100.52	0.01435	26.2219	0.017889	0	0.146427	0.002672	49.1579	0.014536	0.038664
Seymchan	stanfieldite	101.369	0.004798	26.4525	0.00305	0	0.090801	0	49.6237	0.014713	0.071053
Seymchan	stanfieldite	100.787	0.028043	26.1588	0.043634	0	0.040847	0	49.3969	0.054186	0.068136
Seymchan	stanfieldite	100.904	0.00082	26.2197	0.031453	0	0.056069	0	49.6241	0.049373	0.047209
Seymchan	stanfieldite	99.7726	0.006679	26.7444	0.021923	0.001655	0.089614	0	48.5123	0.066439	0.070055
Seymchan	stanfieldite	100.595	0.014133	26.5344	0.027904	0	0.052481	0	49.3612	0.072244	0.056248
Seymchan	stanfieldite	100.338	0.004617	26.1159	0.016829	0.002818	0.052946	0	49.2379	0.026534	0.036515
Seymchan	stanfieldite	101.705	0.003028	26.6301	0.00951	0	0.047317	0	49.8587	0.041281	0.021126
Seymchan	stanfieldite	100.912	0.007411	26.1009	0.023577	0	0.095589	0	49.4719	0.025828	0.042063
Seymchan	stanfieldite	100.128	0.012547	26.378	0.014122	0	0.104838	0	48.9304	0.025725	0.052391
Seymchan	stanfieldite	101.012	0.011242	26.3773	0.015061	0	0.070979	0	49.4976	0.033816	0.058054

Seymchan	stanfieldite	101.2	0.021112	26.101	0.017427	0	0.065331	0	49.8304	0.041309	0.06617
Seymchan	stanfieldite	99.7175	0.008207	26.2701	0.026905	0	0.030302	0	48.6956	0.01967	0.041759
Seymchan	stanfieldite	100.624	0.005202	26.2845	0.03166	0	0.070913	0.004538	49.4384	0.043355	0.058438
Seymchan	stanfieldite	100.028	0.012478	26.1994	0.008245	0.025012	0.068769	0	49.1276	0.041966	0.063267
Seymchan	stanfieldite	101.563	0.000853	26.2958	0.028516	0	0.057089	0	50.1009	0.063802	0.095712
Seymchan	stanfieldite	100.894	0.014707	26.3919	0.027216	0	0.062268	0	49.0536	0.039907	0.054744
Seymchan	stanfieldite	100.35	0.011258	26.5086	0.021779	0.013778	0.087254	0.008389	49.2098	0.022864	0.030957
Seymchan	stanfieldite	100.443	0.002368	26.4535	0.012369	0.002018	0.089536	0	48.8601	0.019458	0.037826
Seymchan	stanfieldite	100.356	0.002475	26.4299	0.017867	0.013301	0.087875	0	49.1476	0.018756	0.044181
Seymchan	stanfieldite	99.4311	0.026921	26.0383	0.065823	0	0.091145	0.001283	48.5883	0.081649	0.053676
Seymchan	stanfieldite	99.9218	0.020991	26.1399	0.037134	0	0.07837	0	48.6567	0.034058	0.059965
Seymchan	stanfieldite	98.0378	0.18843	26.2094	0.09618	0	0.033593	0	47.9139	0.212636	0.031343
Seymchan	stanfieldite	97.9063	0.010622	26.222	0.021685	0.004058	0.101008	0	48.0241	0.05043	0.024766
Seymchan	stanfieldite	99.4714	0.384931	25.5431	0.39013	0	0.095755	0	48.246	0.180415	0.09384
Seymchan	stanfieldite	100.201	0.047475	26.2084	0.068514	0	0.094687	0	48.9421	0.032661	0.067071
Seymchan	stanfieldite	99.9505	0.024462	26.2966	0.023653	0.002299	0.072173	0.001803	48.8179	0.033076	0.071806
Seymchan	stanfieldite	99.4607	0.008875	26.2126	0.01962	0	0.062617	0	48.5271	0.038792	0.047836
Seymchan	stanfieldite	99.0658	0.017806	26	0.042259	0	0.06113	0	48.2362	0.031056	0.41714
Seymchan	stanfieldite	100.216	0.018598	26.2975	0.019048	0.000326	0.095804	0	49.2619	0.047104	0.040012
Seymchan	stanfieldite	98.9656	0.008999	26.0359	0.012442	0	0.035401	0	48.346	0.03103	0.063159
Seymchan	stanfieldite	99.6053	0.00278	26.2779	0.008408	0	0.095829	0	48.535	0.026797	0.035475
Seymchan	stanfieldite	100.249	0	26.4365	0.007691	0.017227	0.114388	0	49.1284	0.025897	0.051744
Seymchan	stanfieldite	98.6731	0.074366	26.1736	0.050631	0	0.087161	0	48.0913	0.070066	0.032661
Seymchan	stanfieldite	99.5742	0.011544	26.0579	0.034444	0	0.078576	0.004993	48.2988	0.040118	0.081914
Seymchan	stanfieldite	99.8091	0.01108	25.8448	0.014799	0	0.083385	0	48.7523	0.053297	0.120287
Seymchan	stanfieldite	99.8466	0.016813	25.9379	0.023604	0	0.082754	0	48.469	0.037203	0.097251
Seymchan	stanfieldite	99.6741	0.000958	26.0339	0.010363	0	0.062616	0	48.4936	0.019657	0.012612
Seymchan	stanfieldite	100.663	0.014284	26.1233	0.030241	0	0.079789	0	49.2409	0.059992	0.111738

Seymchan	stanfieldite	100.295	0.013123	26.1651	0.013193	0.004839	0.101346	0	48.6601	0.008221	0.060683
Seymchan	stanfieldite	100.797	0.024742	26.1216	0.019938	0	0.079686	0	49.0646	0.044552	0.074522
Seymchan	stanfieldite	99.9525	0.016399	25.69	0.022715	0	0.082889	0	48.7474	0.011679	0.115565
Seymchan	stanfieldite	100.414	0.006197	26.1091	0.028536	0	0.076682	0	48.9043	0.031112	0.055643
Seymchan	stanfieldite	99.7685	0.025088	25.7479	0.046572	0	0.127345	0	48.451	0.082321	0.096931
Seymchan	stanfieldite	100.175	0.002634	25.6597	0.013452	0	0.064128	0	48.535	0.017703	0.044896
Seymchan	stanfieldite	99.126	0.022179	25.4327	0.030447	0	0.075045	0	47.7953	0.028042	0.114209
Seymchan	stanfieldite	91.3892	0.208347	22.5379	0.431241	0	0.166447	0	43.4466	0.415451	0.76297
Seymchan	stanfieldite	99.5426	0.012071	24.1688	0.067223	0.020908	0.10607	0	47.379	0.035375	0.020193
Seymchan	stanfieldite	99.3044	0.040476	24.7143	0.03971	0	0.083504	0	46.9525	0.05748	0.062534
Seymchan	stanfieldite	97.4678	0.009613	22.9233	0.056886	0	0.099236	0	46.1653	0.048909	0.063695
Seymchan	stanfieldite	94.8156	0.02946	20.1344	0.093708	0	0.161041	0	40.0356	0.187683	0.295988

EMPA session 1 continued

SAMPLE	MgO	Al2O3	FeO	MnO	Cr2O3	NiO	ZnO	SO3	O	TOTAL
Sericho	3.83424	0.415731	0.711018	0.030387	0.000872	0	0	0.013955	0	100.302
Sericho	49.224	0	11.6345	0.198633	0	0.006045	0	0.036508	0	100.999
Sericho	21.9597	0.050016	2.24152	0.205932	0	0	0	0.017399	0	93.3575
Sericho	22.3814	0	2.64639	0.348374	0.009024	0	0	0.01901	0	101.122
Sericho	22.5142	0	2.70134	0.375842	0.005885	0.006095	0.001985	0	0.000004	101.627
Sericho	22.198	0	2.72722	0.319315	0.023847	0	0	0.00724	-0.00001	100.817
Sericho	22.8262	0.003347	2.7796	0.515933	0.022283	0.005928	0	0.002223	0	101.605
Sericho	22.8655	0	2.78675	0.334761	0	0	0	0.000254	0	101.783
Sericho	22.2272	0	2.86203	0.301706	0	0.002197	0	0	0	99.9823
Sericho	22.7431	0.002615	2.91428	0.512132	0	0	0	0.014109	0.000004	101.249
Sericho	22.2373	0	2.95564	0.366744	0.000749	0	0	0.016085	0.000004	101.478
Sericho	21.3777	0.007698	5.93771	0.408539	0.027477	0.019221	0	0.03472	0	100.05
Sericho Unknowns	49.1853	0.024591	11.9043	0.23112	0.026604	0	0.021639	0.010012	0.000004	102.663

Seymchan	3.73323	0	0.276489	0.155819	0.02593	0	0	0.031199	0.000004	99.2297
Seymchan	3.74177	0	0.710793	0.190161	0.014383	0.027099	0	0.010991	0	99.8216
Seymchan	3.83084	0	1.3685	0.165082	0.021277	0	0.014209	0.050761	0.000008	98.7879
Seymchan	3.90872	0.003244	0.404075	0.083648	0.013882	0.006173	0	0.01787	0	100.532
Seymchan	3.95791	0	0.535444	0.078359	0.0274	0.000637	0	0.020892	0.000004	100.524
Seymchan	3.99057	0	0.455006	0.09406	0	0.039629	0.003858	0.004552	0.000008	99.7923
Seymchan	3.98419	0	0.6413	0.086306	0.033886	0	0.005641	0.055614	0.000008	99.7709
Seymchan	3.83798	0	0.866062	0.108488	0.016517	0	0	0.030147	0.000004	99.6633
Seymchan	3.57706	0.0457	6.38585	0.102458	0.026125	0.432131	0.042913	0.15314	0	96.0704
Seymchan	4.081	0	0.627176	0.135582	0.013624	0.022124	0	0.014701	0.000015	100.484
Seymchan	3.71165	0	0.284227	0.134014	0.037227	0.001022	0	0.013915	0	99.4844
Seymchan	3.67537	0.006101	0.309381	0.141931	0.02357	0	0	0.006333	0.000004	99.5565
Seymchan	3.73009	0.008036	0.420549	0.16379	0.02795	0	0	0.020318	0	99.5208
Seymchan	3.6946	0.009537	0.44712	0.163006	0.015262	0.033128	0	0.049603	-0.00001	99.0487
Seymchan	3.82533	0	0.498785	0.099219	0.009864	0.005661	0	0.155382	-0.00001	99.1783
Seymchan	3.79534	0	0.50982	0.160199	0.017964	0	0	0	0.000008	99.245
Seymchan	3.7512	0.027947	0.491779	0.156908	0.035977	0.011353	0	0.028889	0.000004	99.1106
Seymchan	3.69379	0.008917	0.504475	0.140694	0.036719	0.000938	0.025147	0.020927	0	99.2367
Seymchan	3.79117	0	0.566989	0.166099	0.02594	0.010602	0.005685	0	0.000004	99.8396
Seymchan	3.81305	0.003411	1.22517	0.091797	0.026771	0.020309	0	0.045335	0	98.9753
Seymchan	3.9131	0	0.206652	0.108461	0.013998	0.004828	0	0.002464	0	99.8875
Seymchan	3.86972	0	0.321848	0.134679	0.020309	0	0	0	0	99.6879
Seymchan	3.81373	0.032994	0.421785	0.08886	0.048215	0	0	0.038356	0	99.5084
Seymchan	3.86155	0	0.223131	0.113887	0	0	0	0	0	99.9181
Seymchan	3.87822	0	0.230072	0.13186	0.034807	0.002368	0	0.0201	0	99.6506
Seymchan	3.54622	0	0.653159	0.054039	0.021813	0.032746	0	0.021077	0	98.8952
Seymchan	3.80656	0	0.384694	0.150249	0.025805	0.020929	0	0.002421	0	99.9833
Seymchan	3.70923	0.024835	1.33715	0.134043	0.064668	0.105746	0.008821	0.082607	0.000004	98.4578

Seymchan	3.7913	0	0.249635	0.190983	0.02052	0	0.023413	0	0	99.1643
Seymchan	3.74866	0	0.294777	0.139926	0	0	0.001116	0.012907	0.000004	99.8313
Seymchan	3.80436	0	0.264683	0.149877	0.017411	0	0	0.028222	0.000004	99.8232
Seymchan	3.64183	0	2.55893	0.116974	0.052901	0.157319	0	0.123371	0.000011	99.7765
Seymchan	3.79942	0	0.695994	0.187256	0	0.012359	0	0.024362	0.000004	100.215
Seymchan	3.80789	0	0.61782	0.133237	0	0	0.002337	0.003968	0.000004	99.7774
Seymchan	3.69552	0	0.215175	0.074596	0.013968	0	0	0.014164	0	99.0067
Seymchan	3.76168	0	0.371428	0.133848	0.043818	0	0	0.000854	0	99.9337
Seymchan	3.68273	0	0.692608	0.109928	0.02746	0	0	0.019734	0.000004	99.8978
Seymchan	3.81136	0	0.451731	0.114239	0.000077	0.01839	0	0.016731	0.000004	100.002
Seymchan	48.6037	0.009516	11.2658	0.221195	0	0	0	0.050586	0.000004	99.9266
Seymchan	48.7054	0.017589	10.8325	0.256599	0	0	0.020039	0.04478	0	100.545
Seymchan	48.9636	0.000093	10.9394	0.263747	0.01114	0	0	0.013894	0.000008	101.118
Seymchan	22.2044	0.030534	2.32921	0.472249	0.007381	0.025315	0	0.043756	0.000004	100.958
Seymchan	21.9699	0	2.41297	0.41508	0.012253	0.015431	0	0.009907	0.000008	100.897
Seymchan	21.7782	0.001501	2.41813	0.410528	0.011583	0.002579	0	0.013452	0	100.086
Seymchan	21.6863	0	2.43185	0.358264	0	0	0	0.015526	-0.00001	100.308
Seymchan	21.806	0	2.4352	0.343332	0.000451	0	0	0.004346	0	100.008
Seymchan	21.6502	0	2.43705	0.457419	0	0.006213	0.013209	0	0	100.613
Seymchan	21.2886	0	2.43764	0.414176	0.012843	0	0	0.04503	0.000004	100.205
Seymchan	22.3585	0	2.46538	0.377508	0.000972	0.015819	0	0.014234	0	101.969
Seymchan	22.123	0	2.47275	0.56777	0	0.003091	0	0.00227	0	101.013
Seymchan	21.4132	0.010835	2.47373	0.411405	0.012593	0	0	0.028837	0	99.8226
Seymchan	21.4078	0	2.47824	0.436272	0.025307	0	0	0.01561	0.000004	100.771
Seymchan	21.7506	0	2.48276	0.421023	0.01283	0	0.011953	0	0	101.185
Seymchan	22.0424	0	2.49012	0.394209	0.018493	0.005557	0.031935	0.013643	0.000004	100.664
Seymchan	21.6035	0	2.4927	0.412576	0	0	0	0.027695	0	100.761
Seymchan	21.4868	0	2.49429	0.398259	0.01029	0.026843	0	0	0.000004	100.305

Seymchan	21.4964	0.010003	2.49547	0.371624	0	0.010916	0	0.009957	0	100.061
Seymchan	21.5123	0	2.49783	0.358996	0.008437	0	0.011972	0.021721	0	99.8797
Seymchan	21.8082	0	2.50041	0.394326	0.009722	0.011467	0	0.027754	0	100.49
Seymchan	22.1718	0	2.50484	0.389407	0.000717	0	0.004157	0.02969	0.000004	101.529
Seymchan	21.8671	0	2.51606	0.347061	0.004081	0.021955	0	0.019966	0	100.823
Seymchan	21.8618	0	2.52394	0.42078	0.011902	0	0	0.006176	0	100.78
Seymchan	21.9964	0.000561	2.52427	0.454976	0	0	0	0.004321	0.000004	101.045
Seymchan	21.7511	0	2.52591	0.370941	0	0.023565	0.027159	0.020228	0	100.756
Seymchan	21.9974	0	2.53121	0.368263	0.00753	0.013234	0.012833	0.018209	0.000008	101.317
Seymchan	22.291	0	2.53834	0.492991	0	0	0	0.005847	0	101.75
Seymchan	21.847	0	2.5422	0.359956	0.026462	0.010951	0	0.009281	0	101.41
Seymchan	21.7924	0	2.54461	0.37066	0.000642	0	0	0.016405	0	100.535
Seymchan	21.8638	0.006348	2.5474	0.371561	0	0	0	0.084406	0	101.139
Seymchan	21.2524	0	2.55469	0.375284	0.031068	0.019909	0.005524	0.009899	0	99.9483
Seymchan	21.9186	0	2.55845	0.460925	0.017297	0.023508	0	0.016396	0	101.12
Seymchan	21.7653	0	2.57224	0.3685	0.034676	0	0	0.010307	0.000004	100.607
Seymchan	21.3963	0.016227	2.59364	0.363958	0.003577	0.029967	0	0.107167	0	100.04
Seymchan	21.7581	0.004142	2.59372	0.359135	0.010668	0.011168	0	0.016347	0	100.759
Seymchan	21.6469	0.018114	2.61022	0.413131	0.028011	0.00734	0.001932	0.066463	-0.00001	100.456
Seymchan	21.449	0.001206	2.61822	0.384398	0.024068	0	0.018065	0.007226	0	100.357
Seymchan	21.709	0.028596	2.62888	0.401935	0	0	0	0.02476	0	100.601
Seymchan	21.6361	0	2.64194	0.393754	0.034242	0	0	0.008331	0.000008	100.315
Seymchan	21.7513	0	2.6602	0.376815	0.013487	0	0.049655	0.010284	-0.00001	100.853
Seymchan	21.9587	0	2.66543	0.407045	0.031415	0	0.020655	0.017598	0	101.125
Seymchan	21.7779	0	2.67108	0.412247	0.023879	0	0.001605	0.011725	0	100.27
Seymchan	21.6754	0	2.67545	0.401895	0	0	0.012226	0.031901	0.000004	100.292
Seymchan	21.3533	0	2.67614	0.349089	0.026848	0.008862	0	0.030865	0	99.7806
Seymchan	21.7301	0	2.67614	0.359676	0.033708	0	0.007101	0.034405	0	101.313

Seymchan	21.7745	0	2.70168	0.370161	0.021394	0.022156	0	0.015863	0	100.52
Seymchan	21.9949	0	2.70338	0.335575	0.02841	0.02781	0	0.018145	-0.00001	101.369
Seymchan	21.9283	0	2.70838	0.348623	0	0	0	0.011134	0	100.787
Seymchan	21.7256	0	2.70846	0.370069	0.031608	0.033382	0	0.005804	0.000004	100.904
Seymchan	21.1063	0	2.70971	0.399478	0.009757	0.017479	0.016782	0	0.000008	99.7726
Seymchan	21.2828	0	2.71524	0.425136	0.017414	0.013416	0	0.022219	0	100.595
Seymchan	21.6996	0	2.71837	0.374729	0.01338	0	0.036672	0.001513	-0.00001	100.338
Seymchan	21.9379	0	2.72607	0.369573	0.015125	0.010408	0.015617	0.018999	0.000004	101.705
Seymchan	21.9662	0	2.73218	0.383513	0.016131	0.007055	0	0.039424	0.000004	100.912
Seymchan	21.4972	0	2.73367	0.351834	0.001419	0.015249	0	0.010366	0	100.128
Seymchan	21.7523	0	2.74026	0.433844	0	0	0	0.021605	0	101.012
Seymchan	21.8088	0	2.75015	0.469192	0.005224	0	0.002086	0.021741	0.000008	101.2
Seymchan	21.4998	0	2.77183	0.330436	0	0	0	0.022942	0	99.7175
Seymchan	21.4706	0.002013	2.78679	0.357378	0.020525	0	0	0.049948	0.000004	100.624
Seymchan	21.2536	0	2.80013	0.399484	0.001131	0.009759	0.010764	0.006515	-0.00001	100.028
Seymchan	21.6956	0	2.80421	0.364848	0.020664	0.008052	0.003139	0.024125	0.000004	101.563
Seymchan	21.9608	0	2.80442	0.460178	0	0.024046	0	0	0	100.894
Seymchan	21.2292	0	2.80677	0.341334	0.001444	0	0.023236	0.033592	0	100.35
Seymchan	21.7188	0	2.8151	0.403153	0.006641	0	0	0.022456	-0.00001	100.443
Seymchan	21.3725	0	2.82038	0.336729	0.0103	0	0.021079	0.033234	0	100.356
Seymchan	21.1832	0.009028	2.82374	0.350915	0.015399	0.015437	0	0.0863	0.000008	99.4311
Seymchan	21.6647	0.002181	2.83053	0.367217	0	0	0	0.029943	0	99.9218
Seymchan	20.0349	0.007567	2.83257	0.410729	0.007159	0	0	0.059412	0.000004	98.0378
Seymchan	20.1365	0	2.83994	0.353876	0.046029	0.013166	0.003735	0.05429	0	97.9063
Seymchan	21.0928	0.083559	2.84706	0.364771	0.012022	0.044803	0	0.092261	0	99.4714
Seymchan	21.4212	0.000395	2.85034	0.405355	0.031774	0	0	0.030903	0.000004	100.201
Seymchan	21.346	0	2.88809	0.313929	0.033481	0	0	0.025192	0.000004	99.9505
Seymchan	21.2262	0	2.9146	0.353263	0	0.00513	0.009843	0.034222	0	99.4607

Seymchan	20.8567	0	2.92651	0.404055	0.022205	0.009162	0	0.041516	0	99.0658
Seymchan	21.1583	0.000321	2.92982	0.325408	0	0	0	0.021792	0	100.216
Seymchan	20.9741	0	2.96831	0.370102	0.033168	0	0.009744	0.077251	0	98.9656
Seymchan	21.2045	0.010572	2.98496	0.380393	0	0	0.018275	0.024459	0	99.6053
Seymchan	20.9673	0	3.03969	0.404106	0.00091	0.028182	0	0.026501	0	100.249
Seymchan	20.5819	0	3.10406	0.337842	0.006434	0	0.006341	0.056726	-0.00001	98.6731
Seymchan	21.351	0	3.17187	0.390292	0.000905	0	0	0.051872	-0.00001	99.5742
Seymchan	21.2624	0.000902	3.17871	0.387684	0.030452	0.028842	0	0.040097	0.000004	99.8091
Seymchan	21.3272	0.019295	3.28462	0.439505	0.00852	0.027261	0.017764	0.057953	0.000004	99.8466
Seymchan	21.2302	0	3.324	0.395178	0	0	0	0.091015	0.000004	99.6741
Seymchan	21.2032	0.001105	3.37413	0.348973	0.016529	0	0	0.05873	0.000008	100.663
Seymchan	21.424	0.01224	3.41299	0.36676	0.012408	0.001668	0.001179	0.03663	0	100.295
Seymchan	21.3812	0	3.51939	0.35748	0.022822	0.028915	0	0.05743	0	100.797
Seymchan	21.2875	0.007658	3.53353	0.376415	0.016207	0	0	0.044521	0.000011	99.9525
Seymchan	21.1015	0	3.5768	0.37681	0.007101	0.013485	0	0.126378	0.000004	100.414
Seymchan	21.1655	0	3.6112	0.309256	0	0	0	0.105348	0.000004	99.7685
Seymchan	21.4524	0	3.82381	0.435254	0.034247	0	0	0.091414	0	100.175
Seymchan	20.8891	0.021586	4.27343	0.375866	0.020408	0	0	0.047772	0	99.126
Seymchan	17.4343	0.047126	4.9726	0.355424	0.009073	0.165357	0	0.436407	0	91.3892
Seymchan	20.302	0	6.65593	0.393065	0.01252	0.14081	0.02867	0.199999	0.000008	99.5426
Seymchan	20.0249	0	6.68156	0.41808	0.028778	0.058714	0	0.141782	0	99.3044
Seymchan	19.1187	0.003279	8.22504	0.392042	0.013302	0	0.019584	0.328908	0.000004	97.4678
Seymchan	15.945	0.205589	16.8402	0.251397	0.023371	0.0135	0	0.598758	0.000004	94.8156

EMPA session 2 elemental abundances

SAMPLE	Cl	CaO	K2O	BaO	F	TiO2	P2O5	Na2O	SiO2
Imilac_Merrilite_1	0.010584	48.4245	0.012151	0	0.131742	0	46.1121	0.493885	0.033575
Imilac_Merrilite_2	0	48.3202	0.008258	0	0.226041	0	46.3187	0.4514	0.01606
Imilac_Merrilite_3	0	48.0623	0.018677	0	0.150715	0	46.6281	0.495986	0.024696
Huckitta_Merrilite_1	0.052039	44.3009	0.00241	0	0.328587	0.001159	42.5954	0.499149	1.79837
Huckitta_Merrilite_2	0.012378	47.4976	0	0	0.203416	0	45.6957	0.529106	0.136322
Springwater_Stanfieldite_1	0.002917	25.0136	0.001332	0	0.119564	0	49.1767	0	0.00936
Springwater_Stanfieldite_2	0.041457	22.2297	0	0	0.55041	0	48.6938	0	0.052546
Springwater_Stanfieldite_3	0	25.1015	0	0	0.175778	0.007052	48.9896	0.004655	0.008824
Springwater_Stanfieldite_4	0.003642	25.0489	0	0	0.142397	0	48.9576	0.015767	0.036774
Springwater_Farringtonite_1	0	0.080597	0.004018	0	0.073895	0	27.8894	0	0.014141
Springwater_Stanfieldite_5	0	25.1764	0	0	0.511971	0.003867	49.5286	0.003369	0.00999
Springwater_Stanfieldite_6	0.008434	25.1238	0	0	0.354596	0	49.273	0.008761	0.023335
Springwater_Stanfieldite_7	0.000854	25.0748	0	0	0.486774	0	49.4734	0	0.09457
Glorietta_Merrilite_1	0.010338	47.3575	0.012577	0	0.243954	0.001253	43.8958	0.974663	0.122435
Glorietta_Merrilite_2	0.001114	46.6619	0.02241	0	0.313661	0	44.1274	1.08544	0.205838
Glorietta_Merrilite_3	0	46.586	0.020917	0	0.242808	0.007546	44.4924	1.11969	0.182685
Springwater_Stanfieldite_8	0	25.1369	0	0	0.114274	0	49.0535	0.007097	0.020767
Springwater_Stanfieldite_9	0.013071	23.8281	0.002455	0	0.412562	0	49.3107	0.003036	0.027463
Springwater_Stanfieldite_10	0.010598	23.9132	0.003905	0	0.89006	0	49.2436	0.005037	0.023894
Springwater_Stanfieldite_11	0.03521	20.7456	0.003551	0	0.223537	0	51.7463	0.043063	0.032455
Springwater_Stanfieldite_12	0.004625	24.4435	0.006748	0	1.02686	0	49.6974	0.012648	0.008456
Springwater_Slab_Stanfieldite_1	0.011633	23.6485	0	0	0.228157	0	49.3943	0.001244	0.026861
Springwater_Slab_Stanfieldite_2	0.009064	24.4784	0	0	0.148817	0.000528	50.2371	0	0.016278
Springwater_Slab_Stanfieldite_3	0	24.8397	0	0	0.141604	0	49.0453	0.023571	0.020777
Springwater_Slab_Farringtonite_1	0.018914	0.824248	0	0	0.138861	0	55.9743	0	0.045899
Springwater_Slab_Stanfieldite_4	0.015436	24.3915	0	0	0.269086	0	49.3764	0.015636	0.054911
Springwater_Slab_Stanfieldite_5	0.003817	25.0176	0	0	0.076467	0	48.5856	0.016793	0.016673

Springwater_Slab_Stanfieldite_6	0.022551	24.2703	0.000077	0	0.158541	0	49.0924	0.030026	0.107385
Springwater_Slab_Stanfieldite_7	0.002338	24.7741	0	0	0.09902	0	48.1998	0.002461	0.004358
Springwater_Slab_Stanfieldite_8	0.016413	24.1013	0.001326	0	0.112096	0	48.6765	0.008118	0.136437
NWA10023_Merrilite_1	0.018351	23.0256	0.008912	0	0.144755	0	48.4219	0	0.115707
NWA10023_Stanfieldite_1	0	1.77529	0	0	0.102898	0	53.7745	0.006552	0.006151
NWA10023_Merrilite_2	0	25.7192	0	0	0.150669	0	48.7118	0.028934	0.004928
NWA10023_Merrilite_3	0.000986	21.0706	0	0	0.121257	0	50.1367	0	0.016099
NWA10023_Stanfieldite_2	0	0.443777	0	0	0.118941	0	52.7776	0.009746	0.028336
NWA10023_Merrilite_4	0.003174	0.090684	0	0	0.043906	0	53.3065	0.009892	0.032995
NWA10023_Merrilite_5	0.039695	22.8397	0	0	0.133602	0	47.6093	0.006729	0.10473
NWA10023_Merrilite_6	0.005835	25.3223	0	0	0.139943	0	48.5948	0.007713	0.033632
NWA10023_Merrilite_7	0.009984	8.4227	0.006084	0	0.104165	0.00129	43.9379	0.013199	0.011836
NWA10023_Merrilite_8	0	26.0795	0	0	0.107906	0	48.8251	0.014776	0.01518
NWA10023_Merrilite_9	0	25.6657	0	0	0.114536	0	48.4552	0.008669	0.006112

EMPA session 2 continued

SAMPLE	MgO	Al2O3	FeO	MnO	Cr2O3	NiO	ZnO	SO3	O	TOTAL
Imilac_Merrilite_1	3.74063	0.012951	0.332769	0.092746	0.017614	0.035846	0	0.029355	0.000004	99.4805
Imilac_Merrilite_2	3.75532	0.004966	0.400392	0.063001	0.010567	0.01602	0	0.009264	0	99.6002
Imilac_Merrilite_3	3.76563	0.006705	0.291064	0.076462	0.024677	0	0	0.060208	0	99.6052
Huckitta_Merrilite_1	4.9805	0.083861	3.86466	0.072556	0	0.477033	0	0.140894	0.000004	99.1975
Huckitta_Merrilite_2	3.75633	0	1.11069	0.026486	0	0.086299	0	0.023117	-0.00001	99.0774
Springwater_Stanfieldite_1	21.1845	0	3.80711	0.552024	0.000373	0	0	0.004821	0	99.8723
Springwater_Stanfieldite_2	19.4532	0	5.19277	0.473467	0.005541	0	0.001294	0.421682	0	97.1159
Springwater_Stanfieldite_3	21.4484	0.003865	3.89152	0.441499	0.029177	0	0	0.141515	0	100.243
Springwater_Stanfieldite_4	21.5653	0	3.7605	0.522074	0	0.00439	0	0.03225	0.000004	100.09
Springwater_Farringtonite_1	42.9171	0.007709	3.64064	0.180395	0	0	0	0	0	74.8079
Springwater_Stanfieldite_5	21.0899	0	3.96754	0.465869	0.002107	0.007783	0	0	0	100.767

Springwater_Stanfieldite_6	20.9044	0	3.9729	0.425951	0	0.003303	0.003927	0.043541	0.000004	100.146
Springwater_Stanfieldite_7	21.4399	0	4.0019	0.45667	0	0.002895	0	0.004827	0	101.037
Glorietta_Merrilite_1	3.87014	0	0.854743	0.034479	0.020315	0.060249	0	0.035449	0.000004	97.4939
Glorietta_Merrilite_2	3.9851	0.0068	1.03875	0.050513	0.006225	0.112429	0.020774	0.092411	0	97.7307
Glorietta_Merrilite_3	3.80873	0.004214	1.02481	0.013787	0.024511	0.082826	0	0.059616	0	97.6705
Springwater_Stanfieldite_8	21.2318	0.001959	3.81771	0.532799	0.00234	0	0	0.009627	0.000004	99.9288
Springwater_Stanfieldite_9	19.9295	0	3.92072	0.481379	0.025434	0	0	0.040148	0.000004	97.9945
Springwater_Stanfieldite_10	20.9175	0	3.43227	0.537209	0.0149	0	0	0.012843	0	99.005
Springwater_Stanfieldite_11	19.4379	0.001422	4.75186	0.351157	0.003777	0	0	0.173061	0	97.5488
Springwater_Stanfieldite_12	20.3778	0	3.92173	0.504325	0.013324	0.005742	0	0.0755	-0.00001	100.099
Springwater_Slab_Stanfieldite_1	19.7772	0.004633	3.69617	0.486402	0	0	0.000332	0.051491	0	97.327
Springwater_Slab_Stanfieldite_2	20.7789	0	3.67338	0.498356	0	0.014128	0	0.038688	0	99.8937
Springwater_Slab_Stanfieldite_3	20.9712	0	3.84757	0.504569	0.026461	0.007095	0	0.059404	0	99.4872
Springwater_Slab_Farringtonite_1	37.5058	0.006229	3.26638	0.172369	0	0.011216	0	0.219194	-0.00001	98.1833
Springwater_Slab_Stanfieldite_4	21.51	0.002771	3.62051	0.481668	0.007983	0	0.012083	0.016096	0.000004	99.7741
Springwater_Slab_Stanfieldite_5	21.7073	0	3.77299	0.482635	0.007916	0.016066	0	0.006409	0.000008	99.7102
Springwater_Slab_Stanfieldite_6	21.008	0	4.17603	0.536699	0.021596	0.032499	0	0.168509	-0.00001	99.6246
Springwater_Slab_Stanfieldite_7	21.3987	0	3.49353	0.573791	0	0.006535	0	0.024068	0.000004	98.5787
Springwater_Slab_Stanfieldite_8	20.5946	0	4.51355	0.532279	0.001234	0.188197	0.000302	0.57446	0	99.4568
NWA10023_Merrilite_1	19.8945	0	2.20526	0.300786	0.003228	0.025508	0	0.277212	0.000004	94.4417
NWA10023_Stanfieldite_1	40.7727	0.007797	2.29706	0.15612	0.005516	0.001297	0	0.054993	0.000004	98.9608
NWA10023_Merrilite_2	21.7617	0	2.5298	0.370135	0	0.049478	0	0.041304	0.000004	99.368
NWA10023_Merrilite_3	19.2121	0.002846	1.9369	0.294834	0	0.012118	0	0.076999	0.000008	92.8814
NWA10023_Stanfieldite_2	43.8617	0.024261	2.34114	0.162783	0	0	0.001276	0.043389	0	99.8129
NWA10023_Merrilite_4	44.514	0.008056	2.946	0.109123	0.010711	0.022616	0	0.008353	0.000004	101.106
NWA10023_Merrilite_5	19.232	0.004314	3.71543	0.30932	0	0.13907	0	0.80433	0	94.9382
NWA10023_Merrilite_6	21.4287	0	2.37784	0.438427	0	0.02798	0.009588	0.101786	0.000004	98.4884
NWA10023_Merrilite_7	11.718	0.012887	1.79897	0.290263	0.02692	0.012104	0.039101	0.018113	0	66.4234

APPENDIX 2: LA-ICP-MS/MS WEIGHTED MEAN OF SECONDARY STANDARD

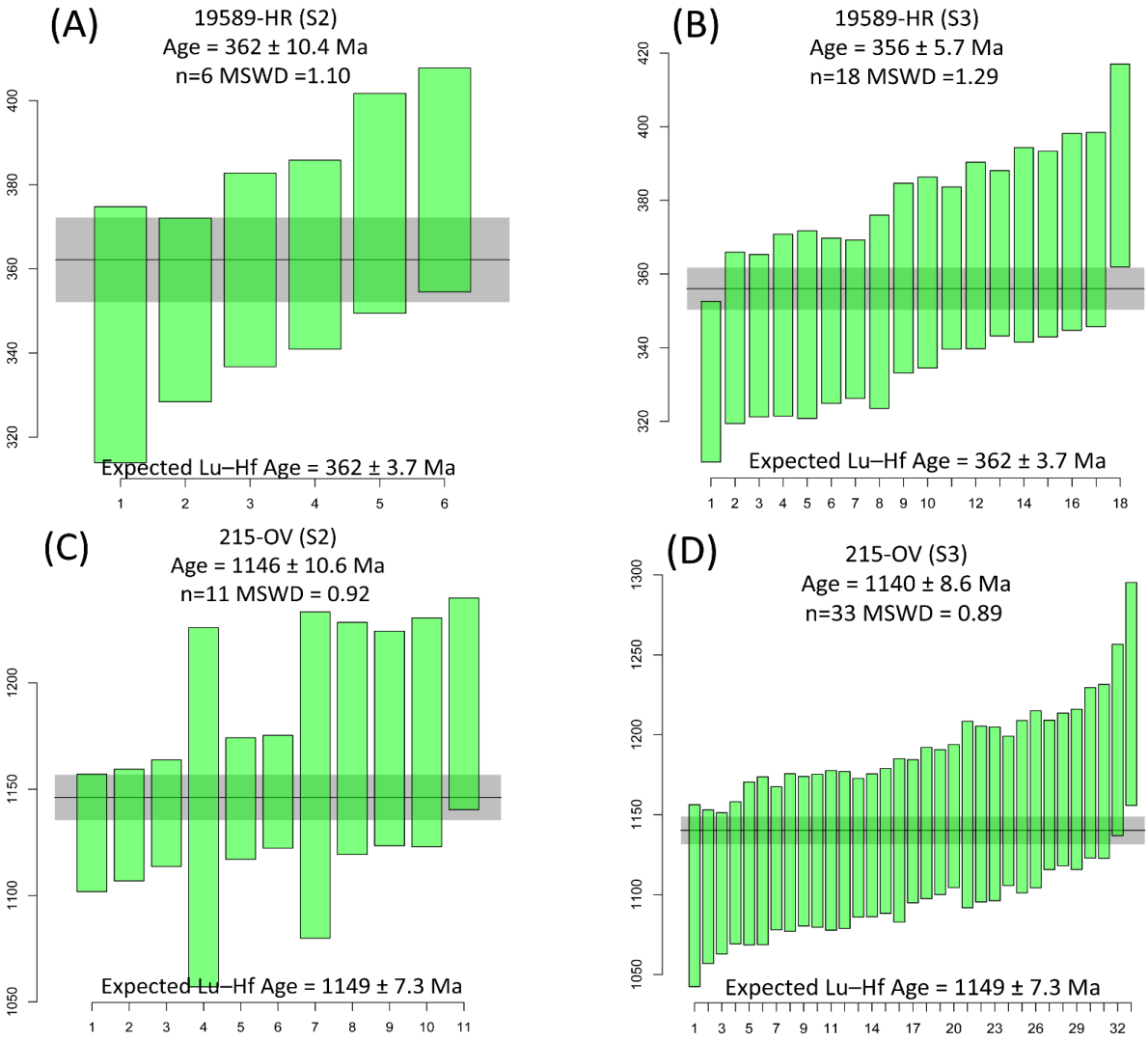

Figure 11 a-d, weighted mean ages (2σ) of 19589-HR and 215-OV with expected analytical age from Simpson et. al., (2021). N = number of samples analysed, S2 and S3 refer to laser sessions 2 and 3 respectively, MSWD = Mean square weighted deviation, denoting the goodness of fit. Values <1 = analytical uncertainties overestimated, >1 = analytical uncertainties underestimated, and 1= the data represents a univariate normal distribution.

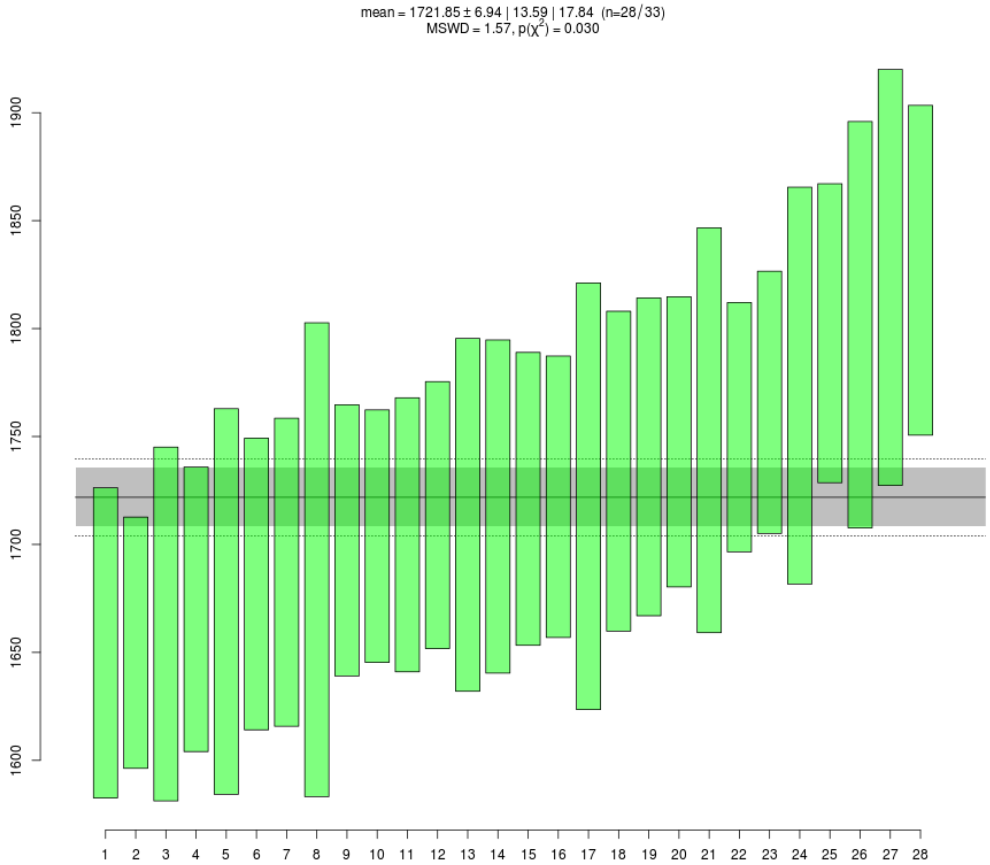

Session 2 OD306 weighted mean

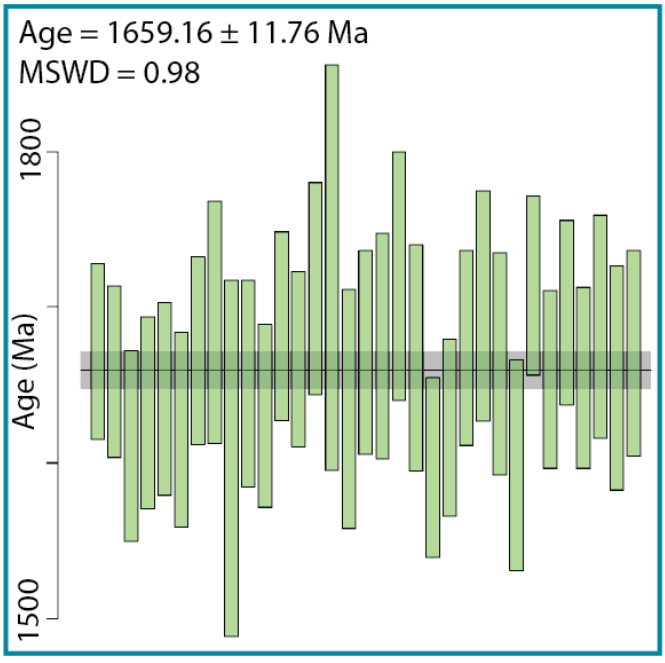

Session 3 OD306 weighted mean

LA-ICP-MS/MS LADR output data summary – Uncorrected ratios, Session 3

Sample	Uncorrected Ratios						
	176Lu/177Hf	176Lu/177Hf 2Se	176Hf/177Hf	176Hf/177Hf 2se	error correlation	176Hf/176Lu	176Hf/176Lu 2se
Session 3							
Seymchan_MerriliteG01_LuHf - 1.csv	4.472778249	0.115476514	0.696634507	0.030607473	0.587616	0.15580444	0.00575219
Seymchan_MerriliteG01_LuHf - 2.csv	4.491236497	0.123760461	0.677622824	0.032161983	0.580579	0.15131846	0.00678124
Seymchan_MerriliteG01_LuHf - 3.csv	4.108485043	0.1394893	0.678864781	0.037987235	0.606743	0.16490158	0.00794659
Seymchan_MerriliteG01_LuHf - 4.csv	4.59976801	0.120360404	0.729320445	0.032244067	0.591856	0.15872496	0.00585476
Seymchan_MerriliteG01_LuHf - 5.csv	4.547211502	0.119345315	0.703502721	0.031561018	0.585026	0.1549011	0.00583559
Seymchan_MerriliteG02_LuHf - 1.csv	1.685648188	0.063235969	0.434480732	0.031743322	0.51347	0.25842895	0.01700612
Seymchan_MerriliteG02_LuHf - 2.csv	1.625546016	0.052886481	0.450029431	0.028020304	0.522533	0.27698625	0.0156625
Seymchan_MerriliteG03 - 1.csv	0.87845126	0.031150624	0.345821508	0.029328951	0.418123	0.39405818	0.03036522
Seymchan_MerriliteG04 - 1.csv	1.613038334	0.076738965	0.421085596	0.039729574	0.504229	0.26179174	0.02232174
Seymchan_MerriliteG05_LuHf - 1.csv	1.40387347	0.092875727	0.426412927	0.062000412	0.454999	0.30448358	0.03690546
Seymchan_MerriliteG06_LuHf - 1.csv	2.760593267	0.079350893	0.501307151	0.027916636	0.516167	0.18224681	0.00995281
Seymchan_MerriliteG06_LuHf - 2.csv	2.801488481	0.072596373	0.528149317	0.025987142	0.526653	0.18904288	0.00973757
Seymchan_MerriliteG06_LuHf - 3.csv	2.974587751	0.091197226	0.553929949	0.034477891	0.492571	0.1866408	0.01142691
Seymchan_MerriliteG06_LuHf - 4.csv	2.857133795	0.083364636	0.511989761	0.033629149	0.444219	0.17940517	0.01044608
Seymchan_MerriliteG06_LuHf - 5.csv	2.772212937	0.071817054	0.52440158	0.025117168	0.540872	0.18967763	0.0080355
Seymchan_MerriliteG06_LuHf - 6.csv	2.582289782	0.090815656	0.483347366	0.032528495	0.522578	0.18776181	0.01149212
Seymchan_MerriliteG07_LuHf - 1.csv	3.996806794	0.109134496	0.644210296	0.030889149	0.56947	0.16157468	0.00696988
Seymchan_MerriliteG08_LuHf - 1.csv	1.828775678	0.050578682	0.453322925	0.024006509	0.522259	0.24824677	0.01178991
Seymchan_MerriliteG09_LuHf - 1.csv	3.426294409	0.139056574	0.592292228	0.044411523	0.541262	0.17317076	0.01229959
Seymchan_MerriliteG09_LuHf - 2.csv	3.400953241	0.131490794	0.593531439	0.04611044	0.497667	0.17499169	0.01279242

Seymchan_MerriliteG10_LuHf - 1.csv	4.080681827	0.134971535	0.668691585	0.038727074	0.571111	0.16405455	0.00867652
Seymchan_MerriliteG10_LuHf - 2.csv	3.861688857	0.214116058	0.621004714	0.060559994	0.568566	0.16073036	0.01372129
Seymchan_MerriliteG11_LuHf - 1.csv	1.537953632	0.049401092	0.411828431	0.02605868	0.507642	0.26791186	0.01634937
Seymchan_MerriliteG12_LuHf - 1.csv	1.961263154	0.08892333	0.465897261	0.048939336	0.43163	0.23743341	0.01975089
Seymchan_MerriliteG12_LuHf - 2.csv	2.158801196	0.097350572	0.477471737	0.044644248	0.48229	0.2211991	0.01908647
Seymchan_MerriliteG12_LuHf - 3.csv	2.04915036	0.090515763	0.493255844	0.047869567	0.455159	0.24051876	0.01911574
Seymchan_MerriliteG12_LuHf - 4.csv	1.792450236	0.075802317	0.468549072	0.034812929	0.56918	0.26196958	0.01739808
Seymchan_MerriliteG12_LuHf - 5.csv	2.096750349	0.097052605	0.487244214	0.0427301	0.527805	0.23262968	0.0183676
Seymchan_MerriliteG12_LuHf - 6.csv	1.86397158	0.086378787	0.474961265	0.043551235	0.505389	0.25479213	0.02328121
Seymchan_MerriliteG12_LuHf - 7.csv	1.44144602	0.052508206	0.41082158	0.027624934	0.541727	0.28630323	0.01761784
Seymchan_MerriliteG12_LuHf - 8.csv	1.40571598	0.049652058	0.4120395	0.028251165	0.51516	0.2932052	0.01889116
Seymchan_MerriliteG12_LuHf - 9.csv	1.766344833	0.073291859	0.413319275	0.03291203	0.521088	0.23447971	0.01731273
Seymchan_StanfielditeG01_LuHf - 1.csv	2.022826764	0.055965272	0.471695475	0.029895423	0.436533	0.23334046	0.01366507
Seymchan_StanfielditeG01_LuHf - 2.csv	2.277942601	0.081438123	0.502599843	0.036785357	0.488464	0.22070287	0.01530158
Seymchan_StanfielditeG01_LuHf - 3.csv	2.642398369	0.09281507	0.498386145	0.033339209	0.525087	0.18925654	0.0111571
Seymchan_StanfielditeG01_LuHf - 4.csv	2.744091153	0.107858625	0.549685389	0.039820038	0.542586	0.20055898	0.01336499
Seymchan_StanfielditeG02_LuHf - 1.csv	2.06823165	0.063641339	0.468996387	0.02858342	0.504888	0.2269766	0.01226664
Seymchan_StanfielditeG03_LuHf - 1.csv	0.801232237	0.026802465	0.353575567	0.029674576	0.398579	0.44167478	0.03529029
Seymchan_StanfielditeG03_LuHf - 2.csv	0.709743871	0.024164562	0.342323953	0.020595681	0.565898	0.48444496	0.02719604
Seymchan_StanfielditeG04_LuHf - 1.csv	1.694006509	0.040114401	0.425739564	0.01955739	0.515488	0.25172548	0.01072329
Seymchan_StanfielditeG04_LuHf - 2.csv	1.897291495	0.054193526	0.463438393	0.025205386	0.525185	0.24459924	0.01273942

Seymchan_StanfielditeG04_LuHf - 3.csv	2.287906932	0.070996821	0.496989463	0.031570208	0.488506	0.21768088	0.01173254
Seymchan_StanfielditeG05_LuHf - 1.csv	1.709725684	0.050796393	0.431344697	0.027558163	0.46503	0.25236693	0.01468793
Seymchan_StanfielditeG05_LuHf - 2.csv	1.793473744	0.053664553	0.448143198	0.025766511	0.52042	0.25033426	0.01293733
Springwater_Stanfieldite_LuHf - 01.csv	38.22782347	5.292724256	3.726839789	0.609437343	0.846665	0.09727872	0.00859747
Springwater_Stanfieldite_LuHf - 02.csv	60.80933228	11.223786	6.029616466	1.250894229	0.889689	0.09899248	0.00924646
Springwater_Stanfieldite_LuHf - 03.csv	39.87397249	5.574355093	3.815701759	0.625038712	0.853439	0.09492672	0.00870327
Springwater_Stanfieldite_LuHf - 04.csv	43.50879239	7.572388841	4.176814144	0.799376371	0.909389	0.09581131	0.00950506
Springwater_Stanfieldite_LuHf - 05.csv	52.61856673	9.205106789	5.071603095	1.00684905	0.881192	0.09641689	0.00927832
Springwater_Stanfieldite_LuHf - 06.csv	65.6070175	12.28284758	6.387845695	1.32181985	0.904755	0.09786821	0.00890836
Springwater_Stanfieldite_LuHf - 07.csv	45.21608619	10.34297727	4.457635401	1.848696233	0.551559	0.09872643	0.00816313
Springwater_Stanfieldite_LuHf - 08.csv	54.41587632	8.898995364	5.399727824	1.274562136	0.692829	0.09970951	0.00862718
Springwater_Stanfieldite_LuHf - 09.csv	51.20735968	8.42115282	5.373786717	1.002985063	0.8811	0.10526978	0.00926571
Springwater_Stanfieldite_LuHf - 10.csv	45.2323837	8.010896911	4.499078463	1.50641862	0.528944	0.09944696	0.00854993
Springwater_Stanfieldite_LuHf - 11.csv	45.03298993	9.628497973	4.3417128	0.742901564	0.800281	0.09677113	0.00840785
Springwater_Stanfieldite_LuHf - 12.csv	54.76324402	8.989136331	5.777809035	1.062435937	0.892666	0.10502689	0.00899848
Springwater_Stanfieldite_LuHf - 13.csv	62.13862971	13.55678392	6.08586985	1.472725027	0.901563	0.09878127	0.01086754
Springwater_Stanfieldite_LuHf - 14.csv	76.09393239	18.80991691	7.37209934	1.999754396	0.911279	0.0984443	0.01106919
Springwater_Stanfieldite_LuHf - 15.csv	81.7411035	23.2119796	8.574841934	2.670642175	0.911763	0.10225312	0.01302129
Springwater_Stanfieldite_LuHf - 16.csv	62.15323955	13.94897589	6.6822676	1.864470652	0.804353	0.10689833	0.01250864
Springwater_Stanfieldite_LuHf - 17.csv	49.99230936	12.90107549	5.017771093	1.719853547	0.752908	0.09982792	0.01129645
Springwater_Stanfieldite_LuHf - 18.csv	54.516557	8.834849046	5.487693484	1.003784139	0.885972	0.09979383	0.00886141
Springwater_Stanfieldite_LuHf - 19.csv	70.97907128	14.67859282	6.603851246	1.522786857	0.896834	0.09276801	0.01073598
Springwater_Stanfieldite_LuHf - 20.csv	40.94204523	6.856092781	4.151724787	0.892019983	0.779401	0.10089638	0.00927093
Springwater_Stanfieldite_LuHf - 21.csv	39.63952048	7.643465374	3.99338276	1.360388697	0.566031	0.10106807	0.01014913
Springwater_Stanfieldite_LuHf - 22.csv	41.56190062	7.801235589	4.360639658	0.935907604	0.874551	0.10440561	0.01142463

Springwater_Stanfieldite_LuHf - 23.csv	47.70677046	7.74206432	4.461927296	0.834016357	0.86821	0.09345935	0.0095799
Springwater_Stanfieldite_LuHf - 24.csv	48.1785565	11.54356681	4.23880687	1.568646898	0.647448	0.08969762	0.0100174
Springwater_Stanfieldite_LuHf - 25.csv	44.78976104	7.900130047	4.349699303	0.886416212	0.86552	0.09716993	0.01055489
Springwater_Stanfieldite_LuHf - 26.csv	61.63750834	10.31624558	5.897831295	1.103620822	0.894436	0.09540123	0.008101
Springwater_Stanfieldite_LuHf - 27.csv	48.85034586	10.3942847	5.157080418	1.247100097	0.879892	0.10581135	0.01223967

LA-ICP-MS/MS LADR output data summary – Corrected ratios, session 3

Sample	OD Corrected Ratio						
	Relative Uncert.	176Lu/177Hf	176Lu/177Hf 2Se	176Hf/177Hf	176Hf/177Hf 2se	error correlation	
Session 3							
Seymchan_MerriliteG01_LuHf - 1.csv	0.027139527	4.64687211	0.12611391	0.69663451	0.030607473	0.617703	
Seymchan_MerriliteG01_LuHf - 2.csv	0.028798205	4.666048808	0.134373831	0.67762282	0.032161983	0.606751	
Seymchan_MerriliteG01_LuHf - 3.csv	0.034967265	4.268399527	0.149254258	0.67886478	0.037987235	0.624895	
Seymchan_MerriliteG01_LuHf - 4.csv	0.027471738	4.778804691	0.13128207	0.72932045	0.032244067	0.621376	
Seymchan_MerriliteG01_LuHf - 5.csv	0.027547185	4.724202527	0.130138483	0.70350272	0.031561018	0.614033	
Seymchan_MerriliteG02_LuHf - 1.csv	0.038436042	1.751258639	0.067311451	0.43448073	0.031743322	0.526086	
Seymchan_MerriliteG02_LuHf - 2.csv	0.033593213	1.688817112	0.056732793	0.45002943	0.028020304	0.539535	
Seymchan_MerriliteG03 - 1.csv	0.036434539	0.912643202	0.033251735	0.34582151	0.029328951	0.429604	
Seymchan_MerriliteG04 - 1.csv	0.048304307	1.675822594	0.080949449	0.4210856	0.039729574	0.511967	
Seymchan_MerriliteG05_LuHf - 1.csv	0.066683743	1.45851641	0.097259334	0.42641293	0.062000412	0.458623	
Seymchan_MerriliteG06_LuHf - 1.csv	0.0299371	2.868043785	0.085860915	0.50130715	0.027916636	0.537589	
Seymchan_MerriliteG06_LuHf - 2.csv	0.027230748	2.910530763	0.07925593	0.52814932	0.025987142	0.553424	
Seymchan_MerriliteG06_LuHf - 3.csv	0.031779943	3.090367572	0.098211707	0.55392995	0.034477891	0.510584	
Seymchan_MerriliteG06_LuHf - 4.csv	0.030353635	2.968341959	0.09009997	0.51198976	0.033629149	0.462121	
Seymchan_MerriliteG06_LuHf - 5.csv	0.027223647	2.880115727	0.078407253	0.52440158	0.025117168	0.568381	
Seymchan_MerriliteG06_LuHf - 6.csv	0.036150219	2.682800197	0.096983815	0.48334737	0.032528495	0.537163	

Seymchan_MerriliteG07_LuHf - 1.csv	0.02855854	4.152374428	0.11858575	0.6442103	0.030889149	0.595604
Seymchan_MerriliteG08_LuHf - 1.csv	0.028894997	1.899957079	0.054899254	0.45332292	0.024006509	0.545634
Seymchan_MerriliteG09_LuHf - 1.csv	0.041438583	3.559656	0.147507101	0.59229223	0.044411523	0.552644
Seymchan_MerriliteG09_LuHf - 2.csv	0.039557879	3.533328477	0.139770979	0.59353144	0.04611044	0.509187
Seymchan_MerriliteG10_LuHf - 1.csv	0.034117563	4.239514126	0.144641891	0.66869159	0.038727074	0.5891
Seymchan_MerriliteG10_LuHf - 2.csv	0.056073948	4.011997297	0.224968528	0.62100471	0.060559994	0.575003
Seymchan_MerriliteG11_LuHf - 1.csv	0.033193116	1.597815371	0.053036471	0.41182843	0.02605868	0.52458
Seymchan_MerriliteG12_LuHf - 1.csv	0.046105357	2.037601361	0.093944338	0.46589726	0.048939336	0.438918
Seymchan_MerriliteG12_LuHf - 2.csv	0.045864359	2.242828173	0.102865876	0.47747174	0.044644248	0.490521
Seymchan_MerriliteG12_LuHf - 3.csv	0.044957754	2.1289094	0.095710984	0.49325584	0.047869567	0.463252
Seymchan_MerriliteG12_LuHf - 4.csv	0.043109502	1.862217742	0.08027928	0.46854907	0.034812929	0.580213
Seymchan_MerriliteG12_LuHf - 5.csv	0.047037269	2.178362122	0.102464205	0.48724421	0.0427301	0.536358
Seymchan_MerriliteG12_LuHf - 6.csv	0.047090511	1.936522909	0.091191854	0.47496127	0.043551235	0.51356
Seymchan_MerriliteG12_LuHf - 7.csv	0.037375973	1.497551396	0.055972441	0.41082158	0.027624934	0.555833
Seymchan_MerriliteG12_LuHf - 8.csv	0.036298974	1.460430636	0.053012134	0.4120395	0.028251165	0.529416
Seymchan_MerriliteG12_LuHf - 9.csv	0.042328667	1.835096239	0.077677178	0.41331928	0.03291203	0.531576
Seymchan_StanfielditeG01_LuHf - 1.csv	0.028904316	2.10156121	0.060744189	0.47169548	0.029895423	0.456058
Seymchan_StanfielditeG01_LuHf - 2.csv	0.036716743	2.366606917	0.086894097	0.50259984	0.036785357	0.501662
Seymchan_StanfielditeG01_LuHf - 3.csv	0.036108056	2.745248389	0.099125584	0.49838615	0.033339209	0.539778
Seymchan_StanfielditeG01_LuHf - 4.csv	0.040186415	2.85089936	0.114567425	0.54968539	0.039820038	0.554743
Seymchan_StanfielditeG02_LuHf - 1.csv	0.031888119	2.14873339	0.068519065	0.46899639	0.02858342	0.52322
Seymchan_StanfielditeG03_LuHf - 1.csv	0.034482035	0.832418584	0.028703487	0.35357557	0.029674576	0.410857
Seymchan_StanfielditeG03_LuHf - 2.csv	0.035059862	0.737369218	0.025852063	0.34232395	0.020595681	0.582735
Seymchan_StanfielditeG04_LuHf - 1.csv	0.02511485	1.759942292	0.044200686	0.42573956	0.01955739	0.546718
Seymchan_StanfielditeG04_LuHf - 2.csv	0.029763819	1.971139735	0.058668646	0.46343839	0.025205386	0.547252
Seymchan_StanfielditeG04_LuHf - 3.csv	0.032139512	2.376959089	0.076394306	0.49698946	0.031570208	0.505952
Seymchan_StanfielditeG05_LuHf - 1.csv	0.030865897	1.776273303	0.054826269	0.4313447	0.027558163	0.483118
Seymchan_StanfielditeG05_LuHf - 2.csv	0.031069888	1.863281087	0.057891935	0.4481432	0.025766511	0.540382

Springwater_Stanfieldite_LuHf - 01.csv	0.138704727	39.7157643	5.508764245	3.72683979	0.609437343	0.848209
Springwater_Stanfieldite_LuHf - 02.csv	0.184762953	63.17621274	11.67262364	6.02961647	1.250894229	0.890603
Springwater_Stanfieldite_LuHf - 03.csv	0.140049491	41.42598635	5.801688309	3.81570176	0.625038712	0.854966
Springwater_Stanfieldite_LuHf - 04.csv	0.174243722	45.20228427	7.876214256	4.17681414	0.799376371	0.910439
Springwater_Stanfieldite_LuHf - 05.csv	0.175140246	54.66663818	9.574328439	5.07160309	1.00684905	0.8822
Springwater_Stanfieldite_LuHf - 06.csv	0.187405368	68.16063817	12.77366946	6.3878457	1.32181985	0.905658
Springwater_Stanfieldite_LuHf - 07.csv	0.228898489	46.97603103	10.75274252	4.4576354	1.848696233	0.551927
Springwater_Stanfieldite_LuHf - 08.csv	0.163750638	56.53390442	9.257462933	5.39972782	1.274562136	0.693735
Springwater_Stanfieldite_LuHf - 09.csv	0.164664705	53.20050274	8.760245097	5.37378672	1.002985063	0.882239
Springwater_Stanfieldite_LuHf - 10.csv	0.177302869	46.99296289	8.331987133	4.49907846	1.50641862	0.529534
Springwater_Stanfieldite_LuHf - 11.csv	0.213973519	46.78580812	10.01092402	4.3417128	0.742901564	0.799669
Springwater_Stanfieldite_LuHf - 12.csv	0.164358531	56.89479271	9.351144578	5.77780904	1.062435937	0.893825
Springwater_Stanfieldite_LuHf - 13.csv	0.218330361	64.55725039	14.09480779	6.08586985	1.472725027	0.902226
Springwater_Stanfieldite_LuHf - 14.csv	0.247334945	79.05573504	19.55324587	7.37209934	1.999754396	0.911801
Springwater_Stanfieldite_LuHf - 15.csv	0.284092725	84.92271088	24.12592433	8.57484193	2.670642175	0.912159
Springwater_Stanfieldite_LuHf - 16.csv	0.224584689	64.57242889	14.50197887	6.6822676	1.864470652	0.804912
Springwater_Stanfieldite_LuHf - 17.csv	0.258196802	51.93815905	13.41026657	5.01777109	1.719853547	0.753304
Springwater_Stanfieldite_LuHf - 18.csv	0.16227393	56.63850389	9.190952611	5.48769348	1.003784139	0.887152
Springwater_Stanfieldite_LuHf - 19.csv	0.206970888	73.7417883	15.26240341	6.60385125	1.522786857	0.897568
Springwater_Stanfieldite_LuHf - 20.csv	0.167667372	42.53563166	7.131837575	4.15172479	0.892019983	0.780374
Springwater_Stanfieldite_LuHf - 21.csv	0.193005803	41.18240877	7.948443868	3.99338276	1.360388697	0.566563
Springwater_Stanfieldite_LuHf - 22.csv	0.187887993	43.17961367	8.112930946	4.36063966	0.935907604	0.87542
Springwater_Stanfieldite_LuHf - 23.csv	0.162499934	49.56366016	8.054091507	4.4619273	0.834016357	0.869363
Springwater_Stanfieldite_LuHf - 24.csv	0.239745723	50.05380952	12.00018675	4.23880687	1.568646898	0.647842
Springwater_Stanfieldite_LuHf - 25.csv	0.176580833	46.53311204	8.216855688	4.3496993	0.886416212	0.866493
Springwater_Stanfieldite_LuHf - 26.csv	0.167578607	64.03662388	10.73116825	5.8978313	1.103620822	0.895552
Springwater_Stanfieldite_LuHf - 27.csv	0.212942556	50.75174692	10.8072067	5.15708042	1.247100097	0.880572

LA-ICP-MS/MS LADR output data summary
– uncorrected ratios, session 2

Session 2 -	176Lu/177Hf	176Lu/177Hf 2Se	176Hf/177Hf	176Hf/177Hf 2se	error correlation	176Hf/176Lu	176Hf/176Lu 2se
Glorietta_LuHf_100 - 01.csv	5.122256744	0.227143006	0.739146959	0.055149188	0.594333	0.14477137	0.01073534
Glorietta_LuHf_100 - 02.csv	5.573841037	0.240212313	0.789736736	0.056043555	0.607292	0.14223077	0.00852983
Huckitta_LuHf_100 - 01.csv	5.195422223	0.337703654	0.793156172	0.090475506	0.569826	0.15193007	0.01742641
Imilac_LuHf - 1.csv	2.147136269	0.038362813	0.490649881	0.016283812	0.538352	0.22865937	0.00671957
Imilac_LuHf - 2.csv	2.118499362	0.036633619	0.476048814	0.015522608	0.53032	0.22489201	0.00651628
Imilac_LuHf - 3.csv	2.176686276	0.052174828	0.489972916	0.027861268	0.421538	0.22507711	0.01154087
Imilac_LuHf - 4.csv	2.062318478	0.048467837	0.470008807	0.026058896	0.423885	0.22824478	0.01101809
Imilac_LuHf - 5.csv	2.101634467	0.048633529	0.48739294	0.021077128	0.535114	0.2321617	0.00888359
NWA10023_LuHf_Stanfieldite - 1.csv	1.543744813	0.039303718	0.432625189	0.022556396	0.488315	0.28078711	0.01368483
NWA10023_LuHf_Stanfieldite - 2.csv	2.016532828	0.058165145	0.45817818	0.025690589	0.51442	0.22729548	0.01181455
NWA10023_LuHf_Stanfieldite - 3.csv	1.523430409	0.050333152	0.412589684	0.027288271	0.499544	0.27107063	0.01640913
NWA10023_LuHf_Whitlockite - 1.csv	1.187271346	0.050710757	0.380133585	0.035798217	0.45355	0.32066969	0.02927966
NWA10023_LuHf_Whitlockite - 2.csv	1.649159619	0.105576413	0.481124822	0.058286234	0.52844	0.2909946	0.03130307
NWA10023_LuHf_Whitlockite - 3.csv	1.215076669	0.076137907	0.411205303	0.052109745	0.494467	0.33926823	0.04283891
Seymchan_LuHf_Stanfieldite - 01.csv	2.010083284	0.087127767	0.481570577	0.044058674	0.473774	0.23938681	0.01846067
Seymchan_LuHf_Stanfieldite - 02.csv	1.423791476	0.039690218	0.411840387	0.028223713	0.406773	0.2893791	0.01931117
Seymchan_LuHf_Stanfieldite - 03.csv	1.611394442	0.045734297	0.420596003	0.023403788	0.510057	0.26142397	0.01437117
Seymchan_LuHf_Stanfieldite - 04.csv	1.742226343	0.060993798	0.471333067	0.032317383	0.510591	0.27124599	0.01600898
Seymchan_LuHf_Stanfieldite - 05.csv	2.068180801	0.071337971	0.481244198	0.033755804	0.491756	0.23356174	0.01461948
Seymchan_LuHf_Stanfieldite - 06.csv	2.871735396	0.12544518	0.515873855	0.047234276	0.477085	0.18075743	0.01576473
Seymchan_LuHf_Stanfieldite - 07.csv	2.233896398	0.085863771	0.521238529	0.037120911	0.539715	0.23329578	0.01552596
Seymchan_LuHf_Stanfieldite - 08.csv	2.200865459	0.085049939	0.520120116	0.044145367	0.455301	0.23646485	0.01656479
Seymchan_LuHf_Stanfieldite - 09.csv	2.173614217	0.082906992	0.491963583	0.035969597	0.521682	0.2259046	0.01494575
Seymchan_LuHf_Stanfieldite - 10.csv	1.881024373	0.121441916	0.481974685	0.059406847	0.523796	0.25730787	0.027805

Seymchan_LuHf_Stanfieldite - 11.csv	1.924757452	0.072915098	0.482344275	0.03460895	0.527971	0.25049054	0.01592072
Seymchan_LuHf_Stanfieldite - 12.csv	1.692209647	0.055923833	0.442507759	0.028561477	0.512015	0.2621965	0.01515733
Seymchan_LuHf_Stanfieldite - 13.csv	1.129300367	0.123486809	0.39750001	0.051431913	0.845115	0.354176	0.05094619
Seymchan_LuHf_Stanfieldite - 14.csv	1.103719089	0.033617279	0.39926726	0.023753795	0.511958	0.36251781	0.02131657
Seymchan_LuHf_Stanfieldite - 15.csv	1.27798051	0.056279888	0.422972452	0.041247336	0.451591	0.3323893	0.03025966
Seymchan_LuHf_Stanfieldite - 16.csv	1.14096112	0.040053006	0.394332976	0.032148863	0.430588	0.34567863	0.02300527
Seymchan_LuHf_Stanfieldite - 17.csv	1.09543227	0.043666907	0.399515586	0.03153306	0.50505	0.36449922	0.02780004
Seymchan_LuHf_Stanfieldite - 18.csv	0.976766873	0.036496249	0.366314741	0.030397182	0.450276	0.37521904	0.02972219
Seymchan_LuHf_Stanfieldite - 19.csv	1.210489623	0.065538571	0.413526363	0.043343564	0.516553	0.34260742	0.03257423
Seymchan_LuHf_Stanfieldite - 20.csv	0.932114303	0.068545903	0.358538257	0.056196079	0.469183	0.38670753	0.063337
Seymchan_LuHf_Whitlockite - 2.csv	2.25311727	0.121051682	0.524877978	0.05177294	0.544681	0.23285691	0.0201008
Seymchan_LuHf_Whitlockite - 04.csv	1.684890068	0.131082686	0.535503394	0.075101794	0.554735	0.31768159	0.04753823
Seymchan_LuHf_Whitlockite - 05.csv	2.632117793	0.098472723	0.518240613	0.042331115	0.458018	0.19641371	0.01393837
Seymchan_LuHf_Whitlockite - 06.csv	2.749195849	0.105546427	0.517673862	0.039820107	0.499105	0.18844578	0.01322919
Seymchan_LuHf_Whitlockite - 07.csv	1.817593733	0.068372853	0.462817733	0.033576949	0.518508	0.25524948	0.01705189
Seymchan_LuHf_Whitlockite - 08.csv	1.892621006	0.072864957	0.481678667	0.036411709	0.509297	0.25459962	0.01641834
Seymchan_LuHf_Whitlockite - 09.csv	1.835268572	0.074495968	0.478172098	0.042103128	0.461002	0.26189388	0.02029518
Seymchan_LuHf_Whitlockite - 10.csv	1.856161207	0.076747582	0.450349042	0.03695215	0.503916	0.24339715	0.01888252
Seymchan_LuHf_Whitlockite - 11.csv	1.897241735	0.068650502	0.45950814	0.032210558	0.516198	0.24268943	0.01515921
Seymchan_LuHf_Whitlockite - 12.csv	1.877419737	0.071274072	0.476951454	0.039627471	0.456928	0.254086	0.01972491
Seymchan_LuHf_Whitlockite - 13.csv	1.801037728	0.106007039	0.448210817	0.053406763	0.493967	0.2493811	0.02573795
Seymchan_LuHf_Whitlockite - 14.csv	1.957316414	0.110273414	0.52372696	0.060947581	0.484126	0.2663625	0.02623079
Springwater_LuHf_257 - 1.csv	44.94397514	10.04840751	4.687290941	1.182468154	0.886254	0.10820419	0.01354766
Springwater_LuHf_257 - 2.csv	52.97792349	13.62562498	4.884091857	1.413890261	0.888443	0.09368118	0.01323757
Springwater_LuHf_257 - 3.csv	2.459774947	0.530266152	0.549975755	0.217115856	0.546073	0.22647439	0.07767864
Springwater_LuHf_257 - 4.csv	36.82720788	6.668267985	3.709715834	0.785088259	0.855591	0.10182528	0.01165183
Springwater_LuHf_257 - 5.csv	41.18690585	8.358433143	4.293202271	1.006307922	0.865797	0.10348865	0.01243919
Springwater_LuHf_257 - 6.csv	25.6532094	5.623212041	2.717727694	0.73905792	0.806065	0.10611306	0.01734203

LA-ICP-MS/MS LADR output data summary – corrected ratios, session 2

Session 2 -	Relative Uncert.	176Lu/177Hf	176Lu/177Hf 2Se	176Hf/177Hf	176Hf/177Hf 2se	error correlation
Glorietta_LuHf_100 - 01.csv	0.045913702	5.519977367	0.253442598	0.73914696	0.055149188	0.615367
Glorietta_LuHf_100 - 02.csv	0.044709576	6.006625187	0.268553665	0.78973674	0.056043555	0.630024
Huckitta_LuHf_100 - 01.csv	0.066080855	5.598823823	0.369975064	0.79315617	0.090475506	0.5793
Imilac_LuHf - 1.csv	0.021468061	2.313851921	0.049673913	0.49064988	0.016283812	0.646857
Imilac_LuHf - 2.csv	0.020992165	2.282991485	0.047924934	0.47604881	0.015522608	0.64379
Imilac_LuHf - 3.csv	0.026761959	2.345696357	0.062775431	0.48997292	0.027861268	0.47064
Imilac_LuHf - 4.csv	0.026343415	2.222448404	0.058546881	0.47000881	0.026058896	0.475141
Imilac_LuHf - 5.csv	0.026022035	2.264817106	0.05893515	0.48739294	0.021077128	0.60174
NWA10023_LuHf_Stanfieldite - 1.csv	0.028104446	1.663609783	0.046754831	0.43262519	0.022556396	0.539035
NWA10023_LuHf_Stanfieldite - 2.csv	0.031203096	2.1731077	0.067807689	0.45817818	0.025690589	0.556491
NWA10023_LuHf_Stanfieldite - 3.csv	0.035117629	1.641718055	0.057653245	0.41258968	0.027288271	0.530967
NWA10023_LuHf_Whitlockite - 1.csv	0.044339212	1.279457725	0.056730147	0.38013359	0.035798217	0.470829
NWA10023_LuHf_Whitlockite - 2.csv	0.06511523	1.777209583	0.115723412	0.48112482	0.058286234	0.537495
NWA10023_LuHf_Whitlockite - 3.csv	0.063781258	1.309422009	0.083516582	0.4112053	0.052109745	0.503307
Seymchan_LuHf_Stanfieldite - 01.csv	0.044949623	2.166157377	0.097367958	0.48157058	0.044058674	0.491309
Seymchan_LuHf_Stanfieldite - 02.csv	0.030310794	1.534342599	0.046507143	0.41184039	0.028223713	0.442295
Seymchan_LuHf_Stanfieldite - 03.csv	0.030776232	1.736512107	0.053443299	0.420596	0.023403788	0.553088
Seymchan_LuHf_Stanfieldite - 04.csv	0.036976845	1.877502527	0.06942412	0.47133307	0.032317383	0.539289
Seymchan_LuHf_Stanfieldite - 05.csv	0.036488672	2.22876591	0.081324708	0.4812442	0.033755804	0.520206
Seymchan_LuHf_Stanfieldite - 06.csv	0.045275028	3.094712972	0.140113216	0.51587386	0.047234276	0.494476
Seymchan_LuHf_Stanfieldite - 07.csv	0.04023723	2.407348591	0.09686504	0.52123853	0.037120911	0.564997
Seymchan_LuHf_Stanfieldite - 08.csv	0.040435097	2.371752946	0.095902061	0.52012012	0.044145367	0.476406
Seymchan_LuHf_Stanfieldite - 09.csv	0.03995618	2.342385766	0.093592788	0.49196358	0.035969597	0.546489
Seymchan_LuHf_Stanfieldite - 10.csv	0.065649428	2.027077612	0.133076486	0.48197469	0.059406847	0.532621

Seymchan_LuHf_Stanfieldite - 11.csv	0.039708331	2.074206372	0.082363274	0.48234427	0.03460895	0.553414
Seymchan_LuHf_Stanfieldite - 12.csv	0.035125592	1.823602256	0.06405511	0.44250776	0.028561477	0.544207
Seymchan_LuHf_Stanfieldite - 13.csv	0.109993855	1.216985555	0.133860933	0.39750001	0.051431913	0.850106
Seymchan_LuHf_Stanfieldite - 14.csv	0.032700919	1.189418004	0.038895061	0.39926726	0.023753795	0.549656
Seymchan_LuHf_Stanfieldite - 15.csv	0.045618057	1.377210055	0.062825646	0.42297245	0.041247336	0.467792
Seymchan_LuHf_Stanfieldite - 16.csv	0.037067282	1.229551714	0.04557614	0.39433298	0.032148863	0.454662
Seymchan_LuHf_Stanfieldite - 17.csv	0.041601506	1.18048775	0.049110069	0.39951559	0.03153306	0.52708
Seymchan_LuHf_Stanfieldite - 18.csv	0.039214066	1.052608509	0.04127706	0.36631474	0.030397182	0.472567
Seymchan_LuHf_Stanfieldite - 19.csv	0.055434889	1.304478799	0.072313638	0.41352636	0.043343564	0.528886
Seymchan_LuHf_Stanfieldite - 20.csv	0.074494962	1.004488864	0.07482936	0.35853826	0.056196079	0.475288
Seymchan_LuHf_Whitlockite - 2.csv	0.055028772	2.42806188	0.133613263	0.52487798	0.05177294	0.557886
Seymchan_LuHf_Whitlockite - 04.csv	0.078704044	1.815714343	0.142904061	0.53550339	0.075101794	0.561189
Seymchan_LuHf_Whitlockite - 05.csv	0.039259456	2.83649012	0.11135906	0.51824061	0.042331115	0.480636
Seymchan_LuHf_Whitlockite - 06.csv	0.040194219	2.962658771	0.119081755	0.51767386	0.039820107	0.522537
Seymchan_LuHf_Whitlockite - 07.csv	0.039455108	1.958721863	0.077281584	0.46281773	0.033576949	0.543841
Seymchan_LuHf_Whitlockite - 08.csv	0.040297151	2.039574672	0.082189049	0.48167867	0.036411709	0.533078
Seymchan_LuHf_Whitlockite - 09.csv	0.042300167	1.977769075	0.083659961	0.4781721	0.042103128	0.48041
Seymchan_LuHf_Whitlockite - 10.csv	0.043026305	2.00028393	0.086064827	0.45034904	0.03695215	0.524377
Seymchan_LuHf_Whitlockite - 11.csv	0.038091442	2.04455418	0.077880017	0.45950814	0.032210558	0.543403
Seymchan_LuHf_Whitlockite - 12.csv	0.039785709	2.023193091	0.080494172	0.47695145	0.039627471	0.478856
Seymchan_LuHf_Whitlockite - 13.csv	0.060050106	1.940880357	0.116550072	0.44821082	0.053406763	0.503964
Seymchan_LuHf_Whitlockite - 14.csv	0.057582475	2.109293393	0.121458335	0.52372696	0.060947581	0.49481
Springwater_LuHf_257 - 1.csv	0.223892853	48.4336764	10.84395398	4.68729094	1.182468154	0.887509
Springwater_LuHf_257 - 2.csv	0.257469621	57.09142538	14.69930767	4.88409186	1.413890261	0.889394
Springwater_LuHf_257 - 3.csv	0.215903356	2.650765613	0.572309192	0.54997575	0.217115856	0.546904
Springwater_LuHf_257 - 4.csv	0.181459787	39.686678	7.201536137	3.70971583	0.785088259	0.857438
Springwater_LuHf_257 - 5.csv	0.203287783	44.38488727	9.022905348	4.29320227	1.006307922	0.867285
Springwater_LuHf_257 - 6.csv	0.219523978	27.64506787	6.068755266	2.71772769	0.73905792	0.807253

APPENDIX 3: ADDITIONAL LU–HF ISOCHRONS

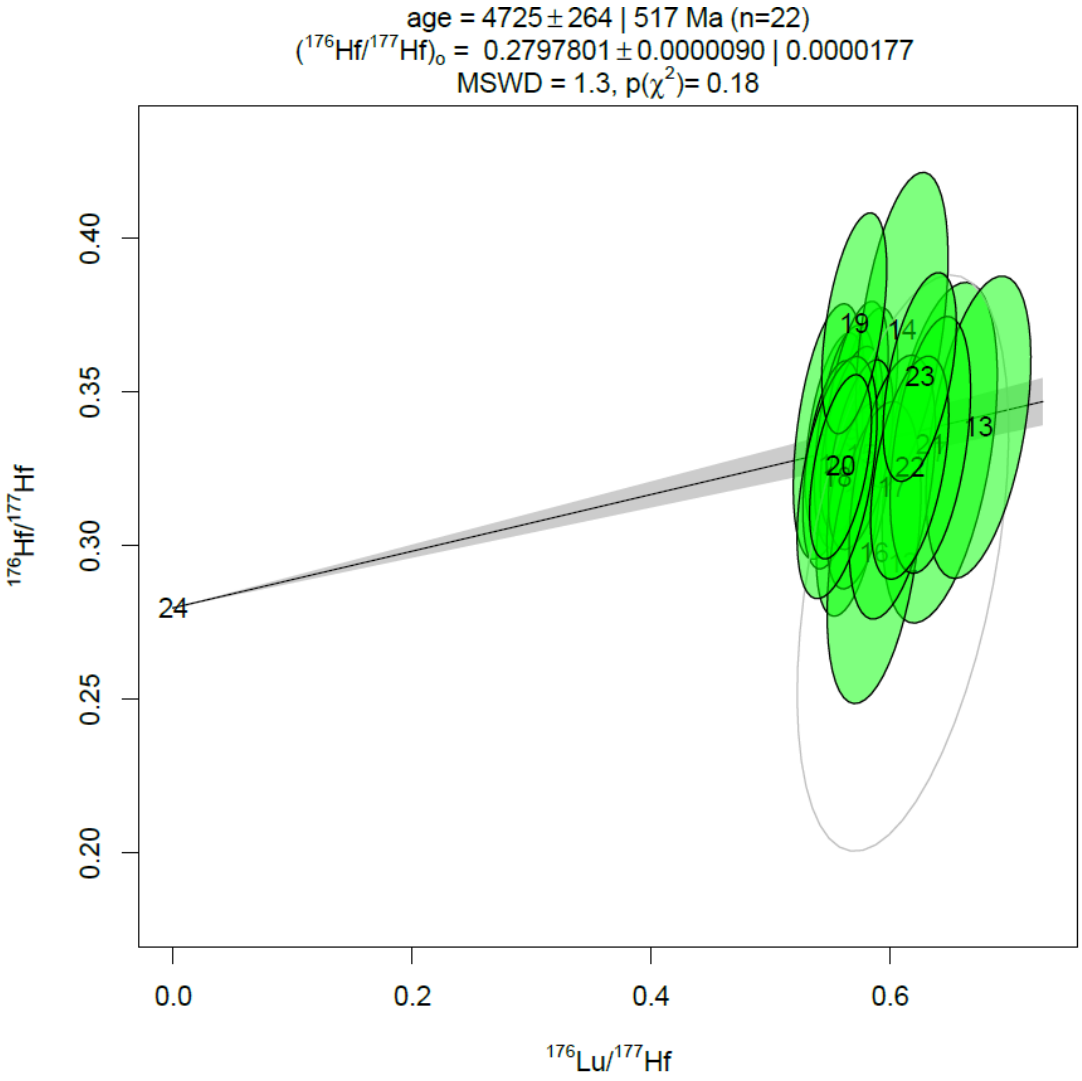

Fukang Isochron

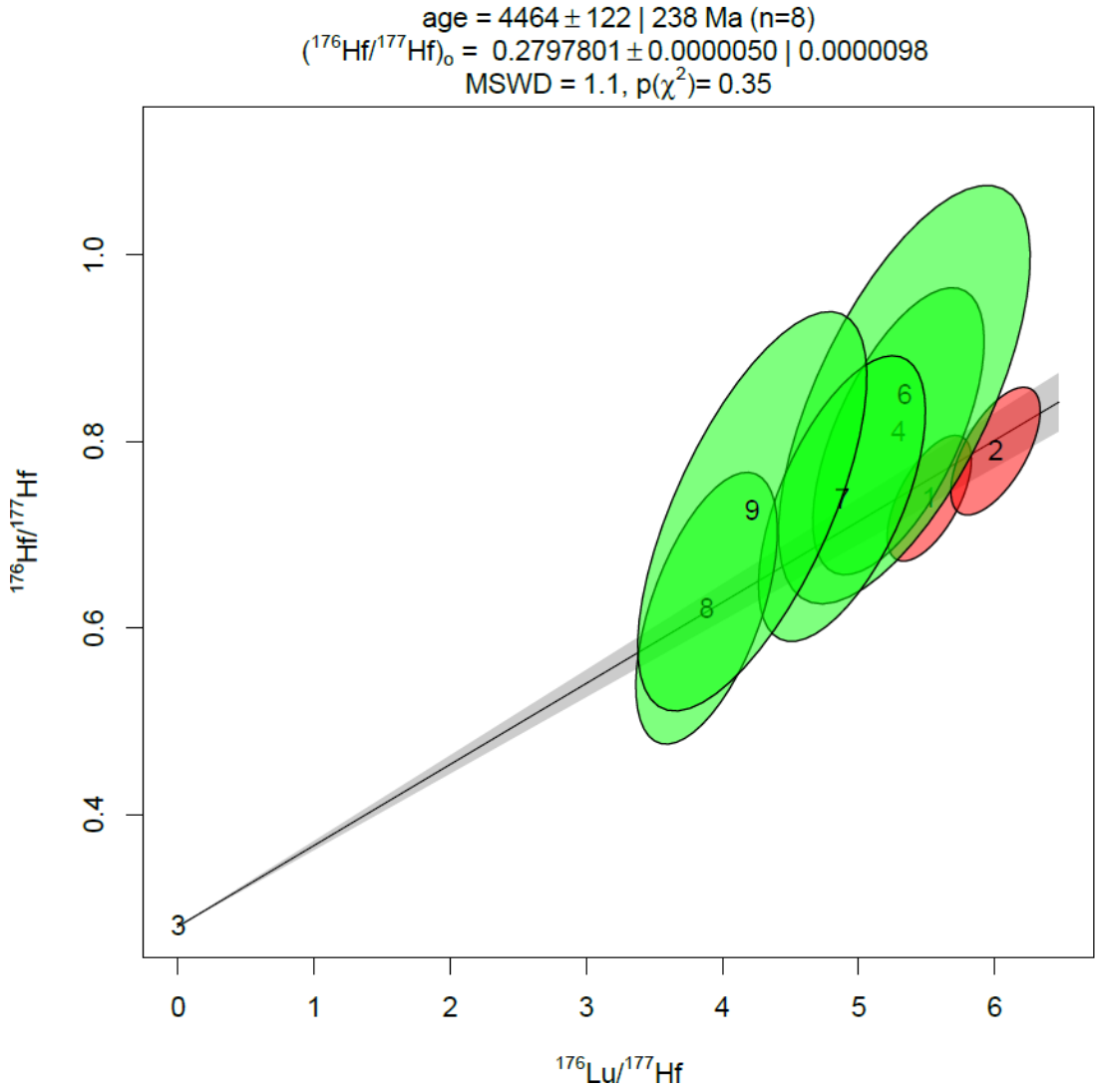

Glorieta Isochron